Fall 2015

Computational approaches for voltage stability monitoring and control in power systems

Kangombe Joseph Makasa

COMPUTATIONAL APPROACHES FOR VOLTAGE STABILITY MONITORING
AND CONTROL IN POWER SYSTEMS

by

KANGOMBE JOSEPH MAKASA

A DISSERTATION

Presented to the Faculty of the Graduate School of the

MISSOURI UNIVERSITY OF SCIENCE AND TECHNOLOGY

In Partial Fulfillment of the Requirements for the Degree

DOCTOR OF PHILOSOPHY

in

ELECTRICAL ENGINEERING

2015

Approved by

Dr. Kelvin T. Erickson, Advisor
Dr. Mehdi Ferdowsi
Dr. Jonathan Kimball
Dr. Mariesa Crow
Dr. Cihan Dagli

ABSTRACT

The electric power grid is a complex, non-linear, non-stationary system comprising of thousands of components such as generators, transformers, transmission lines and advanced power electronics based control devices, and customer loads. The complexity of the grid has been further increased by the introduction of smart grid technologies. Smart grid technology adds to the traditional power grids advanced methods of communication, computation and control as well as increased use of renewable energy sources such as wind and solar farms and a higher penetration of plug-in electric vehicles among others. The smart grid has resulted in much more distributed generation, bi-directional powerflows between customers and the grid, and the semi-autonomous control of subsystems. Due to this added complexity of the grid and the need to maintain reliable, quality, efficient, economical, and environmentally friendly power supply, advanced monitoring and control technologies are needed for real-time operation of various systems that integrate into the transmission and distribution network.

In this dissertation, the development of computational intelligence methods for on-line monitoring of voltage stability in a power system is presented. In order to carry out on-line assessment of voltage stability, data from Phasor Measurement Units (PMUs) is utilized. An intelligent algorithm for optimal location of PMUs for voltage stability monitoring is developed. PMU information is used for estimation of voltage stability load index in a power system with plug-in electric vehicle and wind farm included. The estimated voltage stability index is applied in the development of an adaptive dynamic programming based optimal secondary voltage controller to coordinate the reactive power capability of two FACTS devices.

ACKNOWLEDGMENTS

I would like to thank my advisor, Dr. Kelvin T. Erickson for his guidance and support during the time I was working on this dissertation. Without his help, this dissertation would not have been successfully completed. I thank Dr. Erickson for his efforts and time in correcting this dissertation.

Thanks also to members of my advisory committee for their effort and time in reviewing my dissertation. I would like to thank Dr. Medhi Ferdowsi, Dr. Jonathan Kimball, Dr. Mariesa Crow, and Dr. Cihan Dagli for their support and suggestions during the time I was working on this dissertation.

I am also grateful to members of my previous committee. I wish to thank Dr. Ganesh Kumar Venayagamoorthy, Dr. Donald C. Wunsch II, Dr. S. Balakrishnan, Dr. Keith Corzine, and Dr. Jagannathan Sarangapani for their efforts and support.

The financial support of the National Science Foundation (EFRI # 1238097 and ECCS # 1231820), Clemson University and ECE department at MS&T during the entire period of my studies is gratefully acknowledged.

Special thanks are due to the Department Chair for ECE, Dr. Daryl Beetner for his help in resolving a number of challenging hurdles that I faced during my studies. I am grateful for his guidance and support.

Thanks also to my family who have patiently endured long periods of my absence while I have been working on my dissertation. Special thanks to my wife Carol Makasa for her support and encouragement throughout my studies.

Above all, I thank the Almighty God, for giving me strength and making it possible for me to accomplish this work.

TABLE OF CONTENTS

LIST OF ILLUSTRATIONS

LIST OF TABLES

NOMENCLATURE

Acronym/Symbol	Description
AC	Alternating current
ACD	Adaptive Critic Designs
AD-HDP	Action Dependent Heuristic Dynamic Programming
ADP	Adaptive Dynamic Programming
ESN	Echo State Network
FACTS	Flexible AC Transmission Systems
MLP	Multilayer Perceptron
MSE	Means Sqaure Error
p.u.	Per Unit
P	Active power
Q	Reactive power
V	Voltage
I	Current
θ	Voltage angle
δ	Generator angle
PF	Participation factor
PEV	Plug in Electric Vehicle
PI	Proportional Integral (Controller)
WF	Wind Farm
PMU	Phasor Measurement Unit
SVC	Static Var Compensator
AC	Alternating Current
STATCOM	Static Synchronous Compensator
VSLI	Voltage Stability Load Index

1. INTRODUCTION

1.1. BACKGROUND

The electric power grid is a highly complex, non-linear, non-stationary system consisting of different components that are spatially distributed over hundreds of miles or even more in some cases. Since the advent of the electric grid over a century ago, there have not been many changes in the way the system has been operated. Recently however, developments in Smart grid technologies hope to make the grid ultimately as flexible as the internet. The term "energy internet" has been used to describe the smart grid. The main changes involved with making the grid smart is the implementation of cyber technologies to the grid. Cyber-physical systems refer to the tight coupling between computational and physical resources [1, 2]. Developments in information technology will enable exchange of information between the main domains of the smart grid to enable intelligent decisions by computing applications so that the system is operated in a more energy efficient, environmentally friendly, reliable and cost effective manner. The smart grid proposes to increase the use of renewable energy sources, and more plug-in electric vehicles, thus contributing to reduction on the dependence on oil and reduced emissions [3]. However, these changes have resulted in not only new opportunities but challenges for modeling and control of the smart grid. Most smart grid technologies have added to the complexity and non-linearity of the grid. In order to assure reliability and power quality of the 21st century, new and advanced intelligence based methods will be required for monitoring and control of the smart grid.

Measurement based intelligent methods of monitoring developed based on phasor measurement units and other fast communication devices, and new techniques based on computational intelligence are very attractive for improved stability control and have much potential to realize a truly smart grid. Measurements of system states in transmission system such as bus voltage magnitudes and angles can be obtained in real-time using phasor Measurement Units (PMUs), and facilitate implementation of control strategies using Wide Area Control Systems [4]. The bi-directional powerflows between customers and the distribution network provide means for rapid control of voltage in the distribution network. Information exchange with the customer through smart meters

empowers customers with the ability to participate in electricity markets and thus pose a different challenge during peak demands when the system is more prone to experience instability. In this study intelligent techniques have been developed for monitoring voltage stability in the smart grid. The study considers the optimal placement of phasor measurement units for complete system observation for voltage stability monitoring and control. The information captured with PMUs is used for computing a voltage stability index.

1.2. RESEARCH OBJECTIVES

The specific objectives of this dissertation are:

- Develop an intelligent approach for monitoring voltage stability load index.
- Use computational intelligence methods (neural networks) to estimate the Voltage Stability Load Index in a power system using PMU measurements
- Evaluate the performance of the VSLI monitoring technique for islanded power systems.
- Apply the VSLI technique for monitoring voltage stability in a power system with including wind farm and FACTS devices.
- Study the effect of SmartParks charging and discharging modes on the voltage stability of the smart grid.
- Demonstrate the scalability of the VSLI approach for monitoring voltage stability using echo state networks on the IEEE 14 bus, IEEE39 bus, and IEEE 68 bus test systems.
- Development of an Adaptive Dynamic Programming controller for optimal voltage control in power system is presented.

1.3. RESEARCH CONTRIBUTIONS

The contributions in this dissertation are in four main areas:

- Development of an intelligent technique for estimation Voltage Stability Load Index in a power system.

- Development of an algorithm for optimal PMU placement to ensure complete observability under normal and islanded operating conditions.
- Demonstration of the scalability of the VSLI approach in voltage stability monitoring and its performance in a power system.
- Development of adaptive dynamic controller based on VSLI information for voltage stability control in smart grids.

1.4. ORGANIZATION OF THE DISSERTATION

The work presented in this dissertation is organized in seven sections as follows: Section 2 is an introduction to voltage stability assessment and computational approaches. The impact of smart grid technologies on traditional power systems is discussed. Classical computation methods used for monitoring voltage stability are compared with computational approaches and the advantages of the later approaches are discussed.

Section 3 presents the development of Voltage Stability Load Index and estimation using a multilayer perceptron. An application of the technique in a power system with plug-in electric vehicles is discussed. A comparative study of the performance Echo State Networks (ESNs) and multilayer perceptron (MLP) for estimation of VSLI is presented is section 4.

In Section 5 Phasor Measurement Unit (PMU) information is used to estimate voltage stability index in a power system during normal and islanding operating conditions. The assessment of the scalability of the computational approach developed in this dissertation as the power system becomes realistically sized is demonstrated.

Finally section 6 presents the development an adaptive dynamic controller based computational methods for and adaptive dynamic control is developed and Section 7 is a summary of the main conclusions of the dissertation.

1.5. SUMMARY

Advancements in power systems due to the advent of smart grid technologies has brought about new opportunities for improved communications, computations, and

control techniques as well as challenges for control of voltage stability. Particularly the development of phasor measurement units makes it possible for voltage phasor information in the power system to be available at fast enough speeds for real-time applications of monitoring and control.

This dissertation presents development work for a novel intelligent technique for monitoring of voltage stability in real-time using phasor measurement unit information. The dissertation also presents the application of the voltage stability load index for development of an adaptive dynamic controller for secondary voltage control.

2. BACKGROUND AND LITERATURE SURVEY

2.1. INTRODUCTION

The advent of smart grid technologies in modern power systems has brought about new opportunities for use of cleaner renewable energy sources on one hand, and also new monitoring and control requirements on the other. Increased penetration of renewable energy sources such as wind farms in the smart grid is desirable because of many reasons: Wind is an abundant, low cost energy source; it is clean and inexhaustible. However, wind turbines can cause voltage stability problems due to their reactive power consumption [5]. The use of more Plug-in Electric Vehicles (PEVs) has many benefits. Among other benefits PEVs can serve as a source of additional power during critical peak periods. Reference [6] presents a study that shows the potential for PEVs to help in improvement of system voltage stability in a similar way a STATCOM can provide reactive power support. Voltage stability monitoring in a system with these technologies is thus of great importance in order to ensure improved control and coordination with other reactive power devices in the system such as FACTs devices. This dissertation develops intelligent algorithms for monitoring and control of voltage stability in electric grids.

IEEE Smart grid describes "Smart grid" to be the next generation electrical power system that is typified by the increased use of communications and information technology in the generation, delivery and consumption of electrical energy. The Smart grid will promote among other things customer participation through exchange of information that will allow consumers to make decisions on usage, and in some cases selling electricity to the grid in the most efficient and economic manner. Plug-in electric vehicles will be able to charge and discharge electrical energy with the aim of making use of the extra capacity of plug-in electric vehicles in improving the system reliability.

A Smart grid or sometimes referred to as an intelligent grid, is an electric grid that attempts to intelligently respond to the behavior and actions of all electricity sources and loads connected to it, in a manner that enables the grid to deliver reliable, economic and sustainable electric services. According to the Energy Independence and Security Act of 2007, a smart grid must:

- Have a self-healing capability
- Be fault tolerant by resisting attacks
- Allow the integration of a wide range of energy generation and storage options including plug-in electric vehicles
- Allow for dynamic optimization of grid operations and resources
- Allow for incorporation of demand response, demand-side resources and energy-efficient resources
- Allow electricity clients to actively participate in the grid operations by providing timely information and control options
- Be more environmentally responsive through reduction of emissions
- Improve reliability, power quality, security and efficiency of electric infrastructure.

The above list entails that in order for the electric grid to be truly a Smart grid, intelligence at various levels both distributed and coordinated is inevitable in facilitating processing of field data, fast and adaptable control of power system elements.

The increased penetration of renewable sources of energy and use of more plug-in electric vehicles necessitates the need for coordinating these energy sources with existing traditional energy sources so as to achieve optimal use of infrastructure and ensure higher reliability. Plug-in electric vehicles coordinated with wind farms can act as a sources of improving performance of wind farms. Coordination of plug-in electric vehicles with existing Flexible AC Transmission devices can result in improved supply of reactive power and thus better voltage control [7]. During peak loads plug-in electric vehicles in the discharge mode can help stabilize the power grid thus improving reliability and self-healing capabilities of the grid.

2.2. VOLTAGE STABILITY AND ASSESSMENT

Voltage Stability can be defined as the ability of the power system to maintain acceptable levels of voltage at all system buses during normal operation and regain an acceptable operating point after being subjected to a disturbance. Voltage stability is classified as "small signal" voltage stability or "large signal" or transient voltage stability depending on the nature of system disturbance being considered. Small signal voltage stability refers to the system remaining voltage stable following relatively small changes in operating conditions such as the natural increase in load demand, or change in power output of a wind farm, whereas large signal voltage stability considers contingencies that result in major events taking place in the system such as loss of a transmission line or generating unit [8,9]. In this dissertation both small signal and transient voltage stability have been studied.

The stability of a power system however is impacted by the new smart grid technologies that are introduced to traditional power grids. In this dissertation the impact of smart grid technologies on power system voltage stability has been considered. In Figure 2.1 key aspects of the smart grid that play important roles in voltage stability of a power system are depicted [7].

Renewable energy sources and energy storage devices have a great impact on the voltage stability of the power system. References [10-13] have investigated the impacts of renewable sources namely, solar farms and wind farms on system stability. The intermittent nature of renewable sources cause voltage fluctuations in the system and may result in power oscillations. Smart grid technologies offer new solutions for monitoring and controlling the grid's transmission network. Phasor Measurement Units are capable of taking measured samples of voltage and current, that are time synchronized via global positioning system to the Universal Time, in as many as sixty time frames per second, giving a snapshot of the smart grid in real time [14]. Through smart grid communication technologies measurements are obtained and made available much quicker than in traditional power systems, and thus the dynamics of the system can be observed and
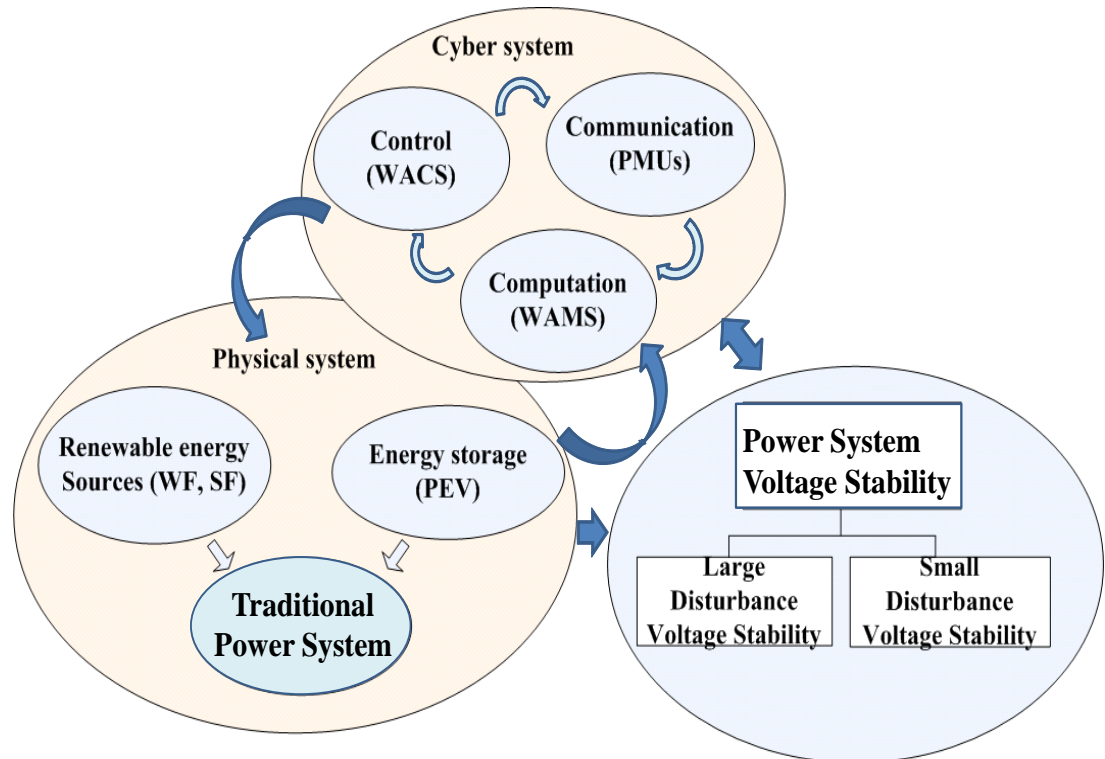
Fig. 2.1 Power System Voltage Stability in a Smart Grid Environment

controlled in timely manner and with high precision. Voltage Stability phenomena in a smart grid can occur in time frames ranging from a few seconds to minutes thus, with smart grid technologies offering very fast measurements the both voltage stability monitoring and control can be enhanced in the power system [15,16].

Smart grid technologies offer new means of controlling the transmission system in an intelligent manner [4]. By using advanced intelligent controllers such as Adaptive Programming based controllers, the ability of the system to maintain voltage stability is enhanced and the system can be operated with much greater voltage stability margin. The combination of communication and computation techniques offers the smart grid better chances of maintaining system voltage stability during normal operations or during transient conditions. This offers an automated way of monitoring and controlling the grid. In events of severe disturbances computational techniques utilizing available system measurements can be used to route power from other sources [7]. The amount of reactive power available in the network can be rapidly provided from available sources as well as

reducing on reactive power demand so as to limit the effects of a voltage stability incidence. This is referred to as the self-healing capability of the smart grid.

Finally voltage stability of the power system will be greatly influenced by plug-in electric vehicles that will help in balancing the energy on the grid by serving as distributed sources of stored energy, this concept is referred to as "vehicle to grid" (V2G). Reference [6] shows that plug-in electric vehicles connected to the grid can act as a virtual STATCOM and thereby contribute to enhancing of system voltage stability. During critical peak periods, the energy stored in plug-in electric vehicles is injected back into the grid thus averting voltage instability. By carefully coordinating plug-in electric vehicles with existing reactive power sources, the size and amounts of expensive FACTs devices needed in the system can be reduced and thus providing a more cost effective means of maintaining voltage stability.

2.3. PRIMARY VOLTAGE CONTROL

Primary Voltage Control (PVC) refers to the control of voltage at a local bus using a controller installed at that bus. Examples of primary voltage control in power systems are Automatic Voltage Regulators (AVRs) installed at the synchronous machines to control the terminal voltage of the generator at a specified set point. Generally PI regulators that use measured terminal voltage of the machine as the feedback signal to regulate the generator field voltage are used for primary voltage control. Figure 2.2 shows a PVC loop for a synchronous generator for the IEEE 68 bus system [17-19].
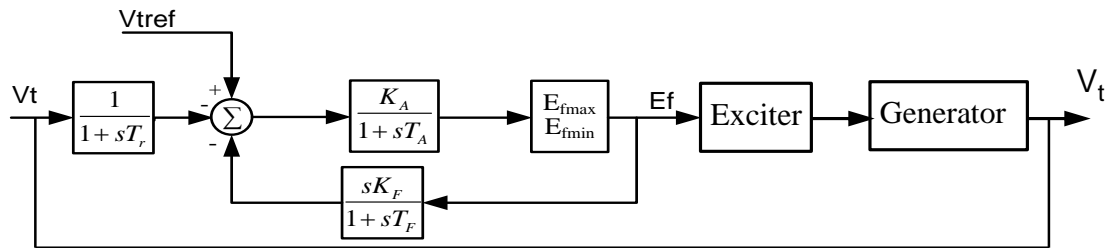
Fig. 2.2 Primary voltage control: Generator AVR system with a PI controller.

Other examples of primary voltage control include Load Tap Changing (LTC) transformer voltage control that use measured local voltage to regulate the voltage of the

local bus. Flexible AC Devices such as Static Var Compensators (SVCs) and Static Synchronous Compensators (STATCOM) installed in the distribution and transmission systems are also used for control of voltage at the substation bus at which these devices are installed [20].

2.4. SECONDARY VOLTAGE

While primary voltage control focuses on control of voltage at the bus at which the control equipment such as an AVR, LTC, SVC nor STATCOM is installed, secondary voltage control aims to control the voltage profile of an area or region of the power system. Feedback voltage signals not only from the local bus, but also from buses in the area that are remote to the voltage control device. Such remote buses that are controlled by a device located remotely are referred to as pilot buses. Thus secondary voltage control allows coordinating of reactive power resources to control the voltage profile of an area. The use of a FACTs device for secondary voltage control is shown in Figure 2.3 [21-22]. In Figure 2.3, measurement of voltage magnitudes and angles at buses 35, 39, and 50 are used to provide auxiliary voltage control signals for both STATCOMs.
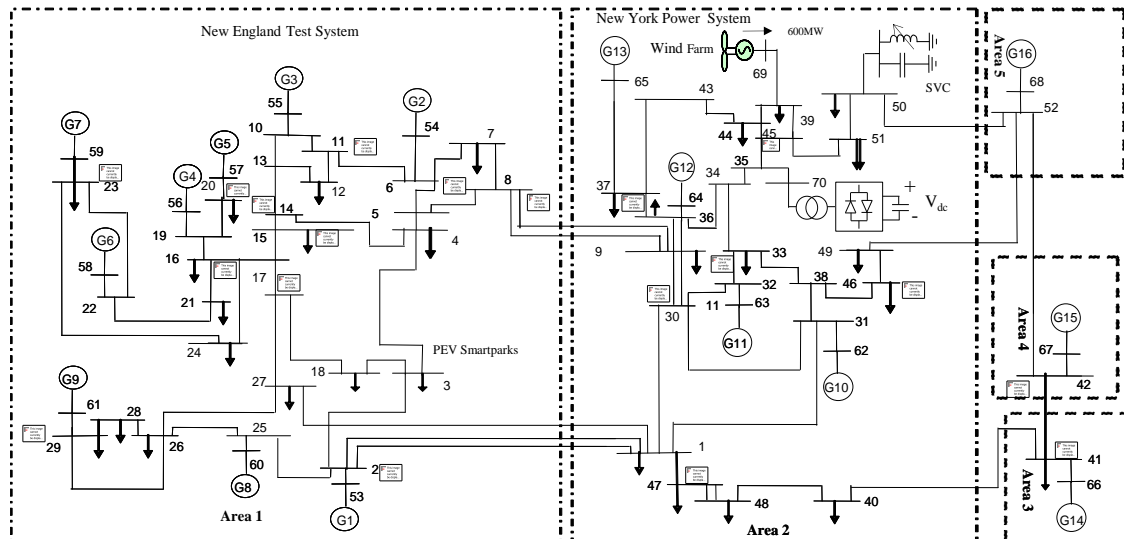
Fig. 2.3 Power System Secondary Voltage Control with a FACTs device

Secondary voltage control also allows power system equipment in the area to operate at their maximum efficiencies, since reactive power resources are better utilized and the voltage profile of the area is improved.

2.5. POWER SYSTEM ISLANDING

Power system islanding entails the separation of the power system into smaller groups of synchronous generators and buses operating at reduced capacity. In the controlled self-healing islanding approach the aim is to separate the system into groups of coherent machines and buses that avoids system-wide catastrophic failure events [23]. Controlled islanding can result in significant benefit to the corrective actions that follow system islanding. The islands are determined in advance using off-line studies and are assumed to be independent of the size of the disturbance. Following islanding, optimal power flow can be used to obtain generation-load balance in each of the resulting islands. The islands with excessive generation compared to the load usually will curtail generation in order to match the total generation within the Island with the demand. On the other hand the islands with higher demand that the available generation go through the process of load shedding in a controlled manner, starting with the least critical loads until generation-load criteria is met [24-26]. Figure 2.4 illustrates the case of the IEEE68 bus system divided into five islands.

-------- Islands boundary
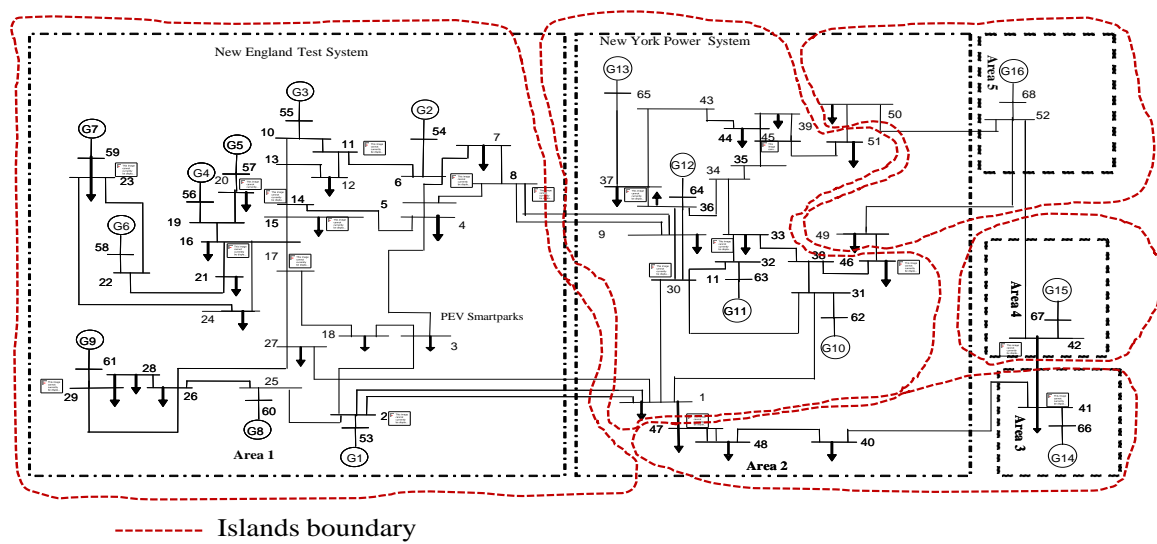
Fig. 2.4 IEEE 68 bus power system divided into five islands

2.6. PHASOR MEASUREMENT UNITS AND OPTIMAL PLACEMENT

New smart grid technologies for on-line measurement of the system state, known as Wide Area Monitoring Systems implemented using Phasor Measurement Units (PMUs) are used to capture the snap shot of the state of the entire power system system in the time frame of a few milliseconds [6-7].

Historically, power system state estimation algorithms used measurements of line flows, both active and reactive power (P and Q), to estimate the bus voltage angles (θ in radians) and magnitudes (V in per unit). The measurements were unfortunately not time synchronized, and compromises were made in estimating system sate from the various power flow measurements. The measurements of Supervisory Control and Data Acquisition (SCADA) system composed of remote terminal units were used for obtaining system state. Data acquisition in this case took too long, and in most cases the state of the system had already changed before the algorithm computed the estimated system state of bus voltages and angles [7]. The advent of phasor measurement units has made it possible for direct states to be obtained as measurements at a sampling rate in the order of a few microseconds.

In the smart grid the transmission network, powerflow, and voltage control strategies make use of the communication and control devices such as Wide Area Monitoring Systems (WAMS), PMUs, and Wide Area Monitoring Systems (WACS) [9]. Electrical flow between the distribution and customer loads can be bi-directional as opposed to the general practice of one direction flow in traditional power networks. The cyber domain of the smart grid consist of communications which have increasingly less latency, and this speed of communication has a great impact on system stability.

Smart grid technologies can influence the system stability in many ways, for example with improvement communication achieved with PMUs, accurate actual measurements of the system are available at control centers in a very short time frame of few milliseconds for decision making to avert potentially unstable situations. Intelligence based controllers acting on the measurements can provide control actions fast enough to prevent instability. The types of actions might be isolating a section of the system that is

under an emergency, through the process of defensive islanding thus preventing system-wide black out. Actions of smart grid actors and applications that affect voltage stability are the direct measurements of voltage phasor measurements using PMUs that enable real-time monitoring and control. Feedback control using the output of computing domain of the smart grid results in faster control actions such as adjusting the reference of reactive power support devices or control of SmartPark converters that allows the SmartPark to operate as a virtual STATCOM [6].

Optimal PMU location for a given application is the process of determining the smallest number of PMUs and their locations in the power system in such a manner that the system is completely observable. Optimal PMU placement aims to use the smallest number of PMUs for a given application without sacrificing critical information, ensuring power system observability, increasing measurement redundancy, monitoring voltage stability, and increasing the state estimator accuracy among other applications.

Several techniques for optimal PMU placement have been studied and reported in the literature. Among the algorithms that have been used for optimal PMU locations are: the bisecting search method, simulated annealing, integer programming, and the genetic algorithm [27].

2.7. COMPUTATIONAL APPROACHES

2.7.1. Classical Computational Approaches. Classical computation methods employed for voltage stability analysis can be classified into two main approaches: static analysis methods and time domain methods. The former methods assume that the problem of voltage stability can be treated as a static phenomenon; such methods have been used in identifying voltage-weak areas and to measure proximity to instability [15, 28]. On the other hand, time domain simulations, in which appropriate modeling is included, capture the actual events and their chronology that lead to instability. References [29, 30] review the main methods that are used for voltage stability analysis in traditional power systems. The references also describe the use of PV and QV curves plotted from load flows by varying a parameter for demand and solving the load flow equations for values of P, Q and V. Such P-V and Q-V curves can provide insight into the distance from the stability limit for a given operating point. Some drawbacks of using P-

V and Q-V curves for voltage stability analysis are that the method generally requires executing a large number of load flows, which is thus time consuming, and P-V and Q-V curves do not readily provide information useful in gaining insight into causes of stability problems. Voltage stability analysis using PV and QV curves is illustrated in Figure 2.5 and 2.6 respectively.
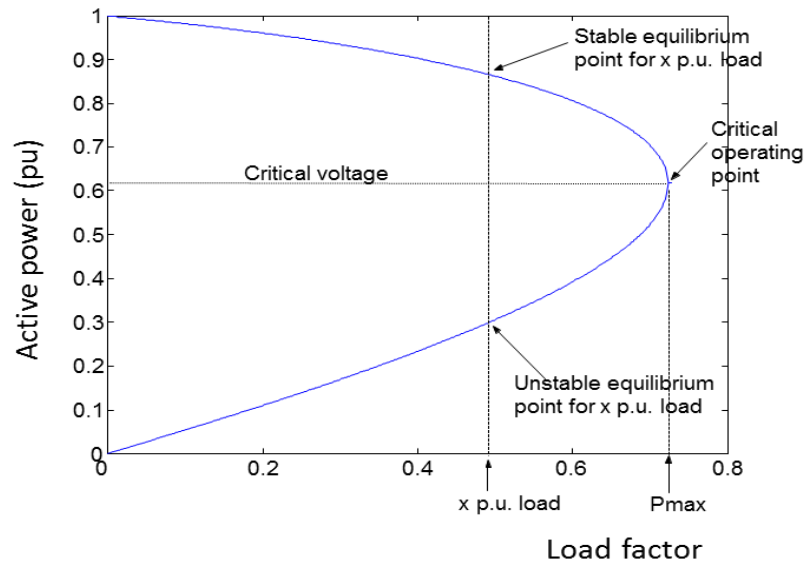
Fig. 2.5 PV curve at a load bus
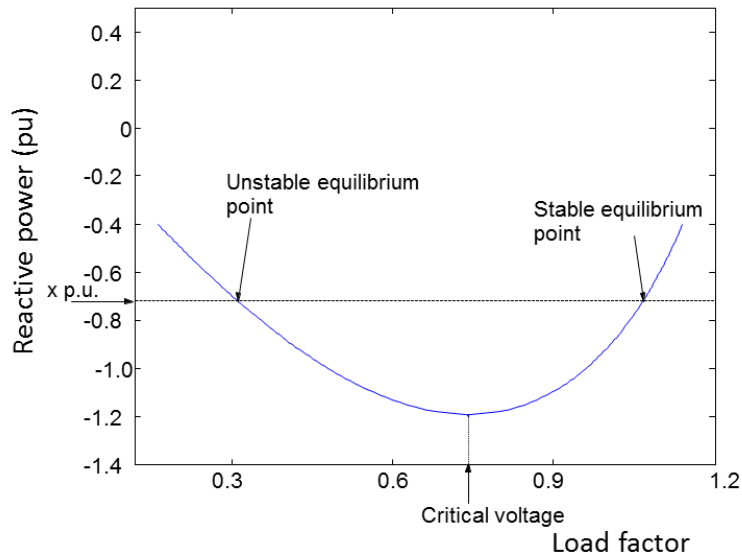
Fig. 2.6 QV curve at a load bus

In addition, the procedure focuses on stressing individual buses independently, which may result in unrealistically distorting the stability information of the system [28]. The main draw-backs of the forgoing computation methods to meet the demands of a power system are time requirements for analysis. Static methods based on load flow analysis are time consuming and therefore have limitations for real-time application. The methods also really on static models of the power system at specified operating points. Time domain simulations on the other hand require detailed mathematical models of the power system, and thus are computationally burdensome if the voltage stability of the power system is to be accurately analyzed.

Traditional methods of modeling and control, and optimization of power systems are in many cases based on linear, static models of power systems. PI controllers tuned to operate around a specified point have satisfactory performance around the specified operating points. When system conditions change the performance of such linear controllers degrades. Intelligent and adaptable methods however, have the potential to provide optimal performance in dynamical environments. Computational methods making use of real-time measurements can be effectively used in monitoring system operation conditions, predicting system variables and performing of control functions that ensure an efficient and robust system.

2.7.2. Classical Neural Networks. In this dissertation novel measurement based intelligent approaches for monitoring (using echo state networks) and adaptive control for power system voltage stability are presented. Computational intelligence is the study of adaptive mechanisms to enable or facilitate intelligent behavior in complex and changing environments. These mechanisms include paradigms that exhibit an ability to learn or adapt to new situations, to generalize, abstract, discover and associate [31]. The main computational Intelligence paradigms include neural networks, swarm intelligence, evolutionary computing, immune systems and fuzzy systems.

A neural network has been defined as a massively parallel distributed processor made of simple processing units, and has the propensity for acquiring experiential knowledge and making it available for use. Neural networks aim mimic biological neurons and resemble the human brain in the three distinct aspects:

- Acquiring knowledge from the environment through a learning process – training,

- Interneuron connection strengths known as synaptic weights, are used to store acquired knowledge and,

- Capable of solving a problem using the knowledge acquired. This process is referred to as inference.

A wide range of neural network architectures have been developed for a variety of applications and purposes. Although the different architectures of neural networks may differ in their structure, implementation, and principle of operation, they all share the common features discussed above. Moreover, connection weights (synaptic strengths) of neural networks are adaptive, meaning that the synaptic strengths change during the learning process. Since the weights associated with any of the neurons in the structure can be adapted, neural networks are said to have distributed memory.

In this dissertation two kind of neural networks have been used for monitoring VSLI in a power system. The echo state neural network (ESN) is a recurrent neural network and consists of a rich dynamic reservoir of neurons that are sparsely connected. Figure 2.7 shows a diagram of the general structure of a multilayer perceptron consisting of input layer and hidden layer and output layer neurons.
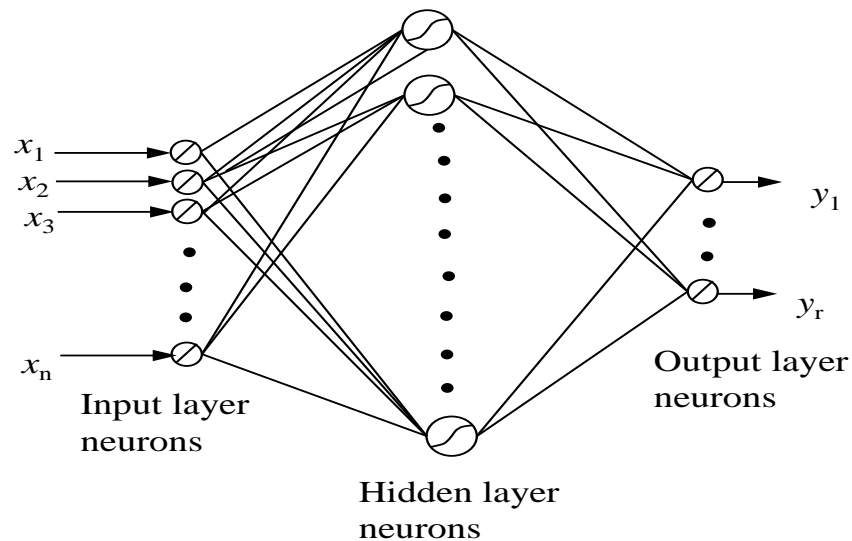
Fig.2.7. The general structure of a multilayer perceptron with n neurons in the input   layer, m neurons in the hidden layer and r output layer neurons

The multilayer perceptron, which is a feedfoward neural network, which has been successfully applied for Dynamic Security Assessment (DSA) and FACTs devices controller implementation [70].

The structure of an Echo State Network (recurrent neural networks) with a rich dynamics reservoir is shown in Figure 2.8. The ESN has memory since it has feedback between the output and dynamic reservoir.

K input units   *N* internal units   *L* output units
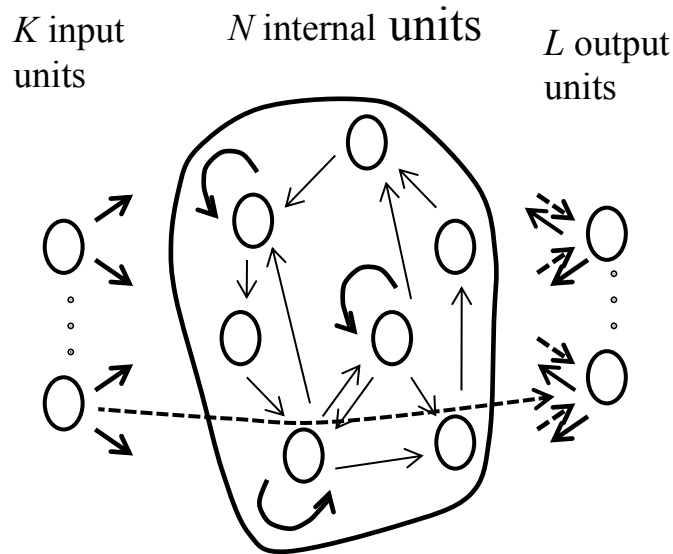
Fig.2.8. The general structure of an Echo State Network with K inputs, N units in the dynamic reservoir, and L output units

2.7.3. Adaptive Critic Designs. Adaptive Critic Designs control techniques are designs that solve the classical non-linear optimal control problem by using the combined concepts of approximate dynamic programming and reinforcement learning [33,34]. The adaptive critic design approach determines optimal control laws for a system by successively adapting two neural networks called the Action neural network and the Critic neural network. The action dispenses the control action for the plant while the critic network learns the desired performance index for a function associated with the performance index. The two networks approximate the Hamilton-Jacobi-Bellman equation associated with optimal control theory [24].

Reinforcement learning refers to the problem that an agent that learns behavior through trial and error interactions with the plant. Reinforcement learning involves a

reward or punishment depending on whether the agent is successful or not. Problems of reinforcement learning can be solved using two main strategies namely search in the space of behaviors to find the best behavior performing well in the environment or statistical techniques and dynamic programming methods to estimate the utility of taking actions in states of the plant.

Dynamic programming is an approach developed to solve sequential, or multi-stage, decision problems. Dynamic programming relies on the principles of optimality given by Bellman:

"An optimal policy has the property that whatever the initial state and initial decisions the remaining decisions must be optimal with respect to the state resulting from the first decision."

The family of adaptive critic designs was proposed by Werbos in 1977 consists of three main types of adaptive critic designs varying in both complexity and power. The three main families of ACDs are: Heuristic Dynamic Programming (HDP), Dual Heuristic Programming (DHP), or Global Dual Heuristic Programming (GDHDP). In HDP the ACD learns to approximate the cost-to-go function J, while in the HDP family the derivative of the cost-to-go is approximated. The GDHDP adaptive critic design approximates both the cost-to-go and its derivative. The Action Dependent forms of each type of ACD have no model of reality between the action network and the critic network [33,35].

Adaptive Critic Designs have been demonstrated successfully for a number of challenging non-linear control problems. The potential application areas include among others: power system control and optimization, FACTS devices control, and distributed parameter system (DPS) applications such as chemical reactor control, ecology management, and flight control.

The Action Dependent Heuristic Dynamic Programming (ADHDP) is used in this dissertation for secondary voltage control using STATCOMs. The design of the ADHDP controller used in this dissertation is shown in Figure 2.9. The flowcharts used in training the ADHDP based controller in this dissertation are shown in Figures 2.10 and 2.11.
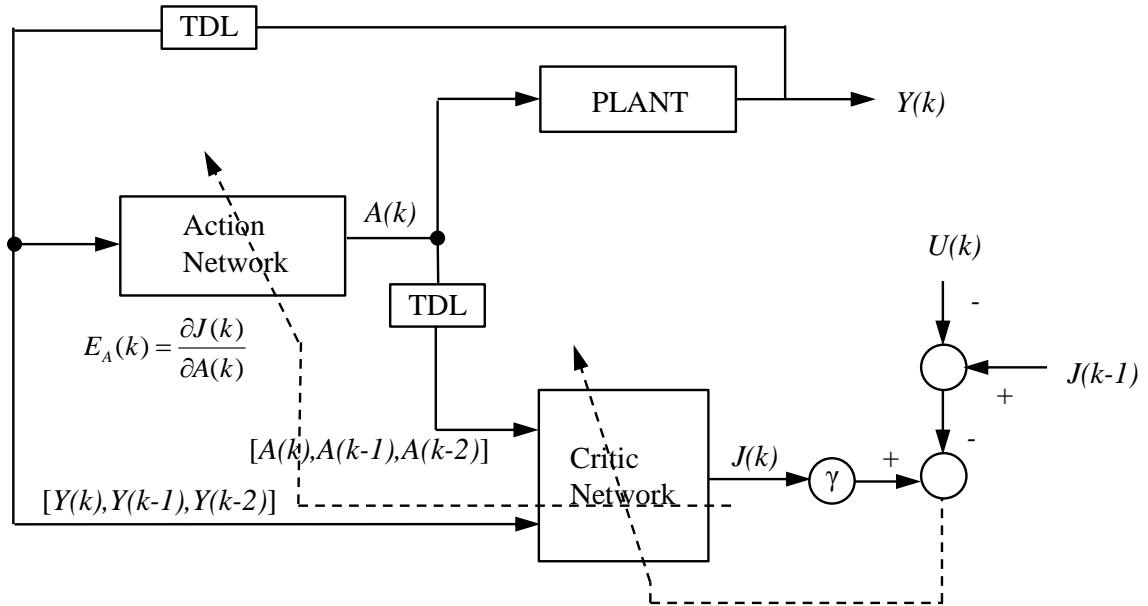
Fig.2.9. Structure of the ADHDP based secondary voltage controller

2.8. DFIG WINDFARMS

Doubly Fed-Induction Generator (DFIG) wind turbines are the most commonly used wind turbine generator. DFIGs consist of a rotor supplied with three symmetrical a.c. power at variable frequency and a stator that is supplied at the power system frequency (typically 60Hz and 50Hz a.c. power supply) [28].

Two back to back convertors are used to supply the rotor, with the rotor side convertor used for controlling the speed while the grid side convertor is used to keep the D.C. voltage constant. The advantages of using DFIG wind turbines as compared with variable speed wind turbines is that only a fraction of the power passes through the converters (typically 30 %) thus lower rated and thus cheaper convertors can be used in the construction of the wind turbine. During low system voltages DFIGs can draw a large amount of reactive power and further increase the possibility of voltage instability [29, 30].
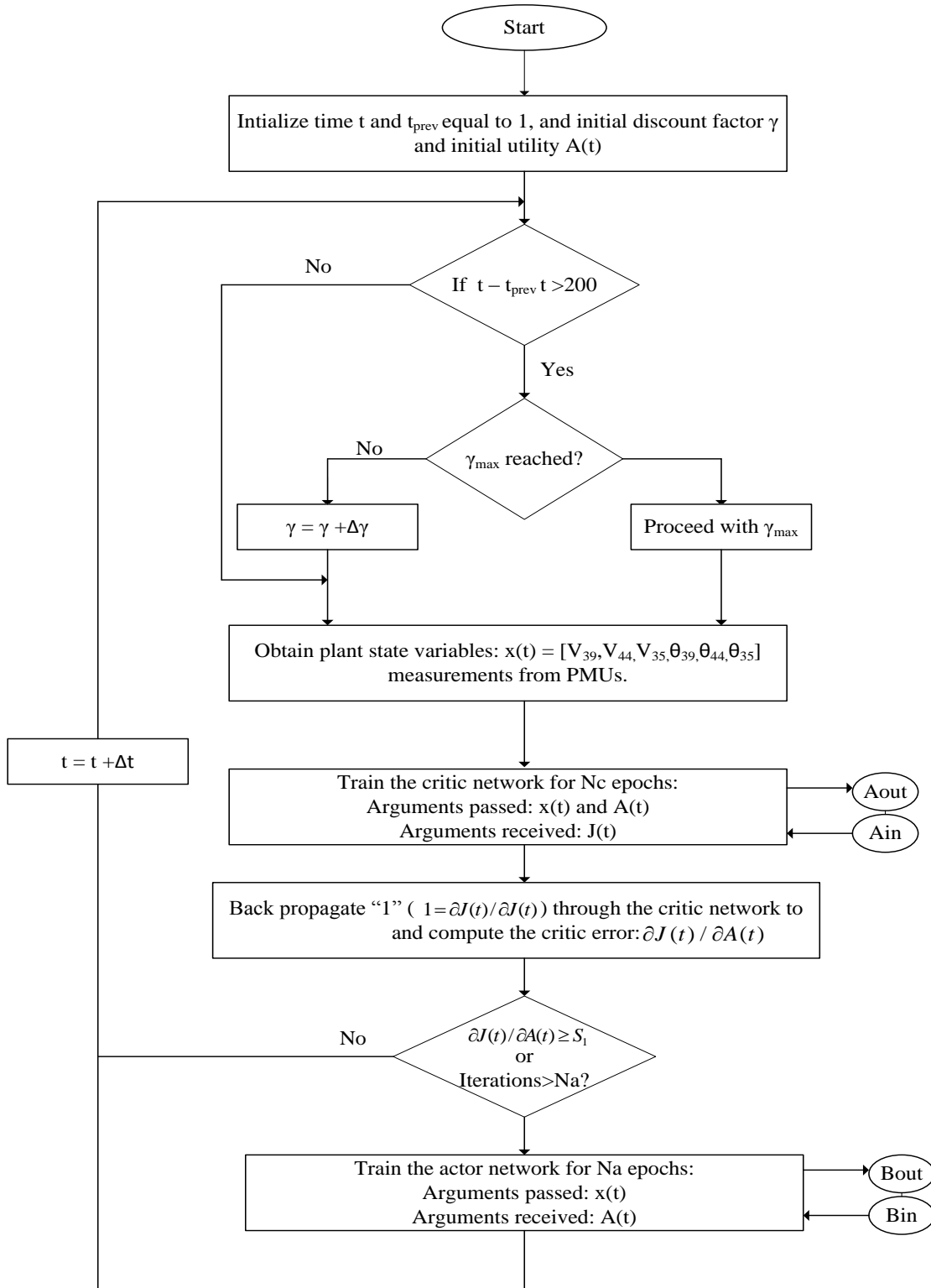
Fig 2.10 ADHDP training flowchart showing the alternate critic and actor training cycles.
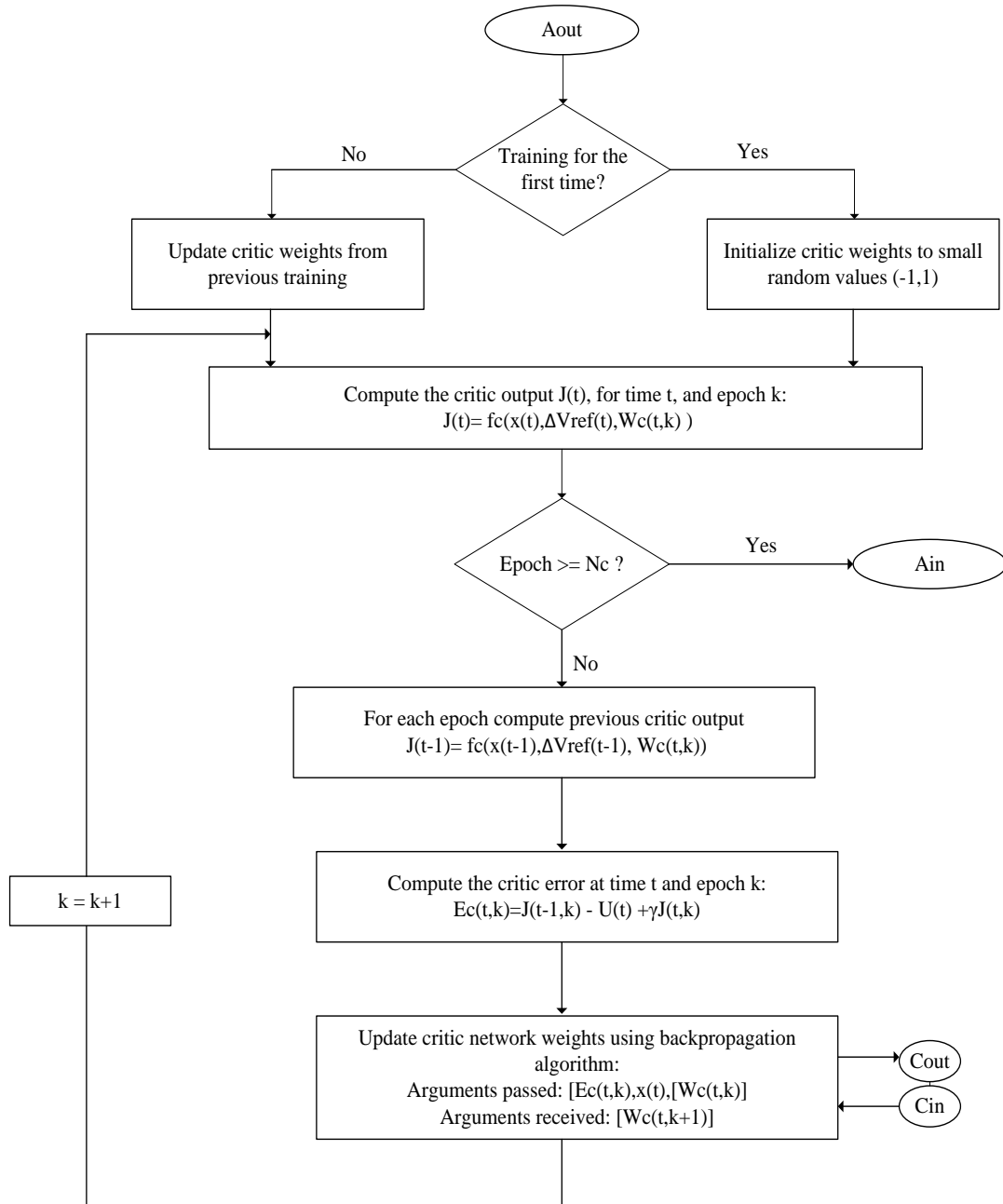
Fig 2.11 ADHDP training flowchart showing the critic and training.

2.9. SMARTPARKS

Smartparks consistsing of plug-in Electric Vehicles (PEVs) in the power systems have resulted in new challenges for both analysis and control of system stability [58,59]. The amount of PEV load at any instant of time depends on the number of vehicles connected to the grid and state of charge of the battery. PEVs can both provide active power to the system when the battery is discharged or draw power from the system during charging operation. When PEVs discharge energy into the grid, they serve as an additional source of power and hence help to improve the stability margin of the grid. Particularly additional reactive power support can be realized from PEVs that improves voltage stability of the system [42].

3. VOLTAGE STABILITY LOAD INDEX AND ESTIMATION USING MLP

3.1. INTRODUCTION

Power system voltage stability has become an issue of great concern for both power system planning and operation in recent years, as a result of a number of major black outs that have been experienced in many countries due to voltage stability problems [12, 18]. This has been mainly due to power systems being operated closer to their stability limits because of increased demand for electricity [12]. Many studies have been carried out to determine voltage stability indices in order to take necessary action to preclude eminent instability and thereby improving voltage stability in a power system. References [25, 26] present comparative studies and analysis of six different voltage stability indices, while [27] introduces the voltage stability L-index to be a simple but effective means of measuring the distance of a power system to its stability limit. The disadvantage of using the L-index, is that its calculation depends upon the no-load voltage phasor at the load bus for a given topology of the system. Since the no-load voltage is dependent upon the system topology and operating point, it varies as the system topology or operating point changes. In practice it is difficult to obtain no-load voltage at a bus. The proposed Multilayer Perceptron (MLP) approach capable of estimating the L-index without directly obtaining the no-load voltage overcomes this limitation and facilitates on-line determination and use of the L-index.

The electric power grid is rapidly growing and demanding new technologies for efficient and rapid control in order to ensure reliable and secure power networks [6]. Reference [28] carries out a study of the impact of Plug-in Electric Vehicles (PEVs) parking lots (SmartParks) on the stability of a power system. In particular, the study shows voltage characteristics following changes in power demand of PEVs. When PEVs discharge into the power network, system voltage support is enhanced, while charging action is accompanied by voltage drop in the load area. The method for estimation of voltage stability L-index developed in this study is applied for monitoring voltage stability in a power system with SmartParks included.

3.2. FORMULATION OF VSLI

The voltage stability load index used in this dissertation is calculated from PMU measurements of voltage magnitudes and angles at load buses. PMUs can provide real-time measurements of voltage phasors and incident current phasors. This information can be adequately used to detect voltage stability margin directly from the measurements and in real-time [40, 41]. The minimum number of PMUs that make the system observable are placed at pre-determined buses to take direct measurements while voltage phasor information at the remaining buses is calculated from these measurements and known system transmission line impedances.

The mathematical formulation of VSLI used in this dissertation is presented in Appendix A [42]. The voltage stability load index used is derived from voltage equations of the Thevenin equivalent representation of the system at the load bus (Figure 3.1). The voltage stability load index in terms of voltage phasors at the load bus can be derived as the following:

$$VSLI = \frac{4[V_0 V_L \cos(\theta_0 - \theta_L) - V_L^2 \cos^2(\theta_0 - \theta_L)]}{V_0^2} \qquad (1)$$
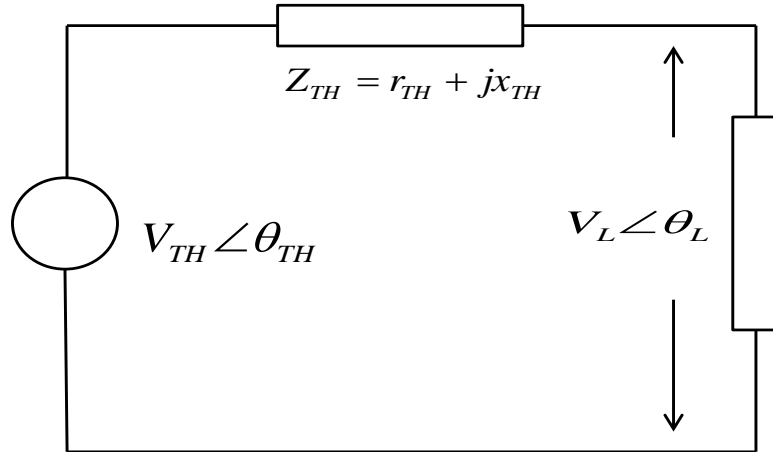
Fig.3.1. Thevenin equivalent representation at a load bus

Where V_0 and V_L are the no-load and load voltage magnitudes at the load bus and θ_0 and θ_L are the no-load and load voltage phase angle measurements respectively. The value of voltage stability load index varies from zero at no-load to one at the point of voltage stability limit or collapse. The point of voltage stability limit corresponding to VSLI value of one is the point at which the load factor is maximum (Figure. 3.2).
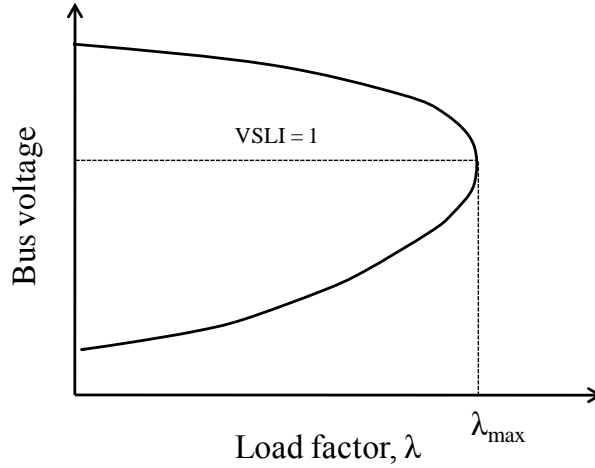
Fig. 3.2. P-V curve at a load bus showing VSLI of one at the maximum load factor.

3.3. VOLTAGE STABILITY LOAD INDEX ESTIMATION

Reference [42] presents the formulation of a voltage stability load index at a load bus using voltage equations (appendix A). The technique uses measurements of voltage phasors and no-load voltage at the bus to calculate the voltage stability *L*-index. The complete mathematical derivation of the Voltage Stability *L*-index in (1) is presented in Appendix A. The index gives the distance of the bus to the voltage stability limit.

3.4. VSLI ESTIMATION USING A MULTILAYER PERCEPTRON

A feed forward multilayer perceptron neural network can be used to estimate voltage stability *L*-index at a bus. Equations (11) to (15) in Appendix A show that voltage stability *L*-index is a function of real power (*P*), reactive power (*Q*), and voltage magnitude (*V*) and phase (*θ*) at the bus. The quantities are selected as input variables in the estimation of *L*-index using the MLP neural network as shown in Figure 3.3. The MLP consists of four neurons in the input layer, 35 neurons in the hidden layer and a single neuron in the output layer.

The inputs to the neural network are active and reactive power (P, Q) and voltage magnitude and angle (V, θ) measurements at the concerned load bus. The output of the neural network is the estimated voltage stability L-index at the load bus. Activation functions in the input and output layers are linear activation functions while the hidden layer uses sigmoidal activation functions.
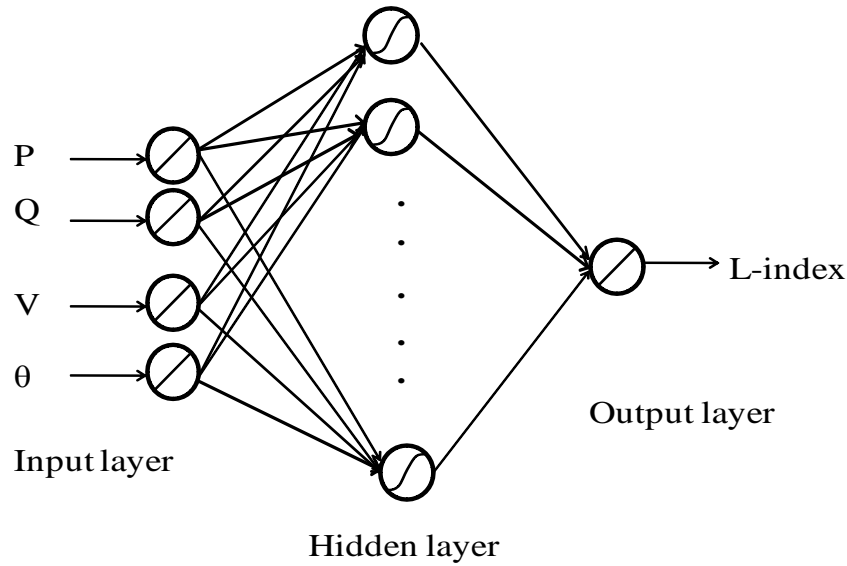
Figure 3.3. Multilayer perceptron structure for *L*-index estimation.

The process followed in development of the MLP, described in section 2, involved two phases shown in a flowchart in Figure 3.4. In the development phase, training data was obtained, with no plug-in electric vehicles connected. Values of real power and reactive power at non generator buses as well as voltages at the load buses were taken with the load at bus 7 and bus 10 varied simultaneously from 0.8 to 1.2 load factor in small steps to obtain one hundred sets of data. Voltages at bus 7 and bus 10 were used to calculate voltage stability L-indices for bus 7 and 10 respectively were used in the MLP training process as target values for corresponding sets of real and reactive power. Sixty input output patterns were selected at random and used as training data. Particle swarm optimization training algorithm [32] was used to train the multilayer peceptron. Training was carried out for the number of iterations that resulted in acceptable mean square error. Training data input output sets used are shown in appendix B.
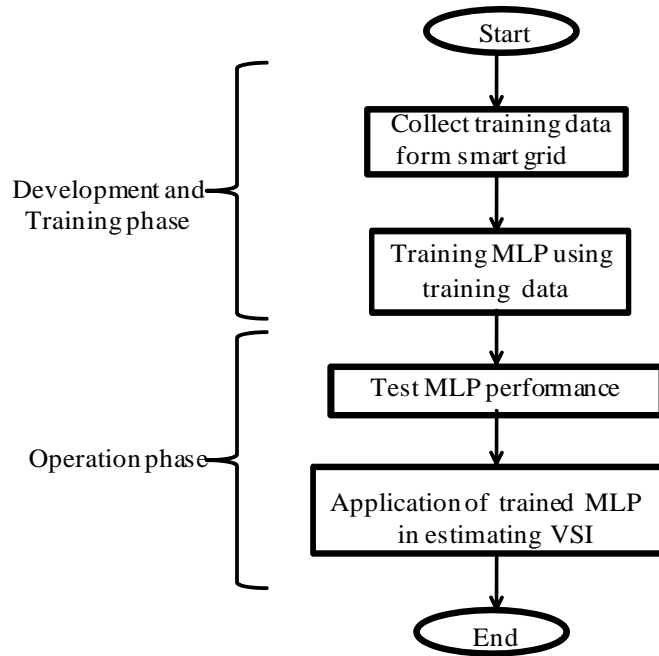
Figure 3.4. Development and operation phases for VSLI.

In the second phase, the operation phase, the trained MLP was applied in the estimation of voltage stability L-index in the system. First, 40 input patterns are used to test the accuracy of the neural network in estimating voltage stability L-index. After

successfully training and validating the MLP neural network was used for estimation of voltage stability L-index of the test system with Smart Parks included. Evaluation of L-index was carried out with all five transmission lines in the system available, and then the contingency of the outage of one transmission line was also evaluated.

3.5. RESULTS AND DISCUSSION

Figure 3.5 shows the 10 bus voltage stability test system with plug-in electric vehicle parking lot models included. The power system consists of two generators, G1 and G2 supplying the load area through five long (200km) parallel transmission lines, and one local generator, G3 providing voltage support in the load area. Bus 10 is a voltage controlled bus using an on-load transformer tap changer. System parameters and loading conditions of the system used in this dissertation are those given in Appendix E of reference [9]. The original system with 10 buses was modified by adding two SmartPark buses 11 and 12.
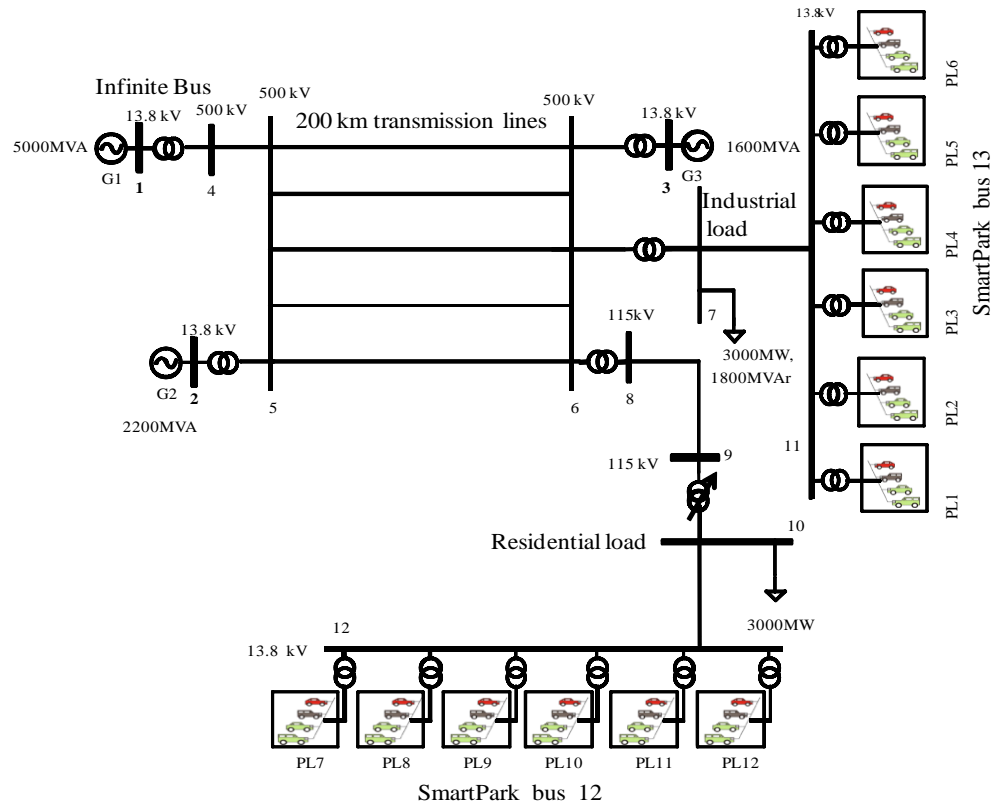
Figure 3.5 Power System with plug-in electric vehicle parking lots (SmartParks).

The nominal (industrial) load at bus 7, load is 3000MW, 1800MVAr modeled as a constant power load, while load (residential) at bus 10 is 3000MW modeled as constant power load. Plug-in electric vehicle parking lots represent six SmartParks at bus 11 and 12 with capacity +/-180 MW each. Bus 7 is a load bus located in an industrial area and bus 10 is a load bus in a residential area.

As described in the preceding section, the process of developing and implementing an MLP for estimation of voltage stability *L*-index involved two phases; development phase and the operation phase. In the development phase the MLP is trained for accurate estimation of voltage *L*-index. Performance of the MLP is then validated using patterns of input output data sets to test its performance.

The first set of results for the development phase that show that the MLP was successfully trained for estimating voltage index to a high degree of accuracy. On-line application of the trained MLP is then carried out by applying the MLP to estimate the voltage stability *L*-index of the power system with SmartParks. Voltage index target and MLP output values used in the testing phase are shown in Tables 3.1 and 3.2. The table shows that the MLP output values are very close to the target values at both bus 7 and 10.

Figures 3.6 and 3.7 show plots of bus voltage and *L*-index against real power and reactive power at bus 7. In Fig. 3.6 increasing load demand at the load buses results in increasing voltage *L*-index and thus approaching the limit. Voltage decreases with increasing load. After 3200 MW bus 10 is the critical bus. Testing results have validated the MLP in accurately estimating voltage stability *L*-index of the power system. MSE obtained using an MLP: 8.75×10^{-5}.

The trained neural network is used to estimate the voltage stability *L*-index of the 10 bus test system with SmartParks included at bus 11 and 12. In Figures 3.8 and 3.9, negative values of power represent charging of electric vehicles where real power flow is from the grid to the SmartPark and positive values of power represent discharging action where power flow is from the SmartPark to the grid. Plots of the voltage stability *L*-index output of the MLP for a 24 hour period at bus 7 and bus 10 are shown in Figure 3.10 and 3.11 respectively.

Table 3.1. Bus 7 Load Flow and Calculated and Estimated Voltage Stability L-index

Bus 7 Voltage		P(MW)	Q(MVar)	L-index (Calculated)	L-index (estimated)
(pu)	(deg)				
1.0470	-27.49	2960	-197.4	0.6311	0.6251
1.0444	-27.71	2971	-180.7	0.6381	0.6319
1.0417	-27.93	2982	-164.2	0.6450	0.6388
1.0365	-28.36	3004	-131.6	0.6587	0.6531
1.0339	-28.57	3014	-115.6	0.6654	0.6603
1.0313	-28.78	3025	-99.66	0.6720	0.6677
1.0287	-28.99	3035	-83.92	0.6786	0.6750
1.0235	-29.41	3055	-52.91	0.6915	0.6896
1.0209	-29.61	3064	-37.63	0.6978	0.6967
1.0183	-29.82	3074	-22.51	0.7041	0.7039
1.0157	-30.02	3083	-7.536	0.7103	0.7108
1.0106	-30.42	3101	21.95	0.7224	0.7242
1.0081	-30.62	3110	36.48	0.7284	0.7308
1.0055	-30.81	3118	50.85	0.7342	0.7370
1.0030	-31	3126	65.08	0.7399	0.7431
1.0004	-31.2	3135	79.16	0.7457	0.7492
0.9979	-31.39	3143	93.1	0.7513	0.7549
0.9954	-31.58	3151	106.9	0.7568	0.7605
0.9929	-31.76	3158	120.5	0.7622	0.7658
0.9903	-31.95	3166	134.1	0.7676	0.7711
0.9878	-32.14	3173	147.4	0.7730	0.7762
0.9853	-32.32	3181	160.7	0.7781	0.7811
0.9829	-32.5	3188	173.8	0.7833	0.7857
0.9804	-32.68	3195	186.7	0.7883	0.7903
0.9779	-32.86	3202	199.6	0.7933	0.7946

Two different operating conditions of the power system have been considered: the first case considers the system fully operational with no fault. In the second case the contingency with one of the five parallel transmission lines out of service is considered. The MLP estimated L-index outputs for these two cases are shown in Figures 3.8 and 3.9. At both bus 7 and bus 10, when the SmartParks are discharging, i.e. positive power, the voltage indices at the buses are lower.

Table 3.2. Bus 10 Load Flow and Calculated and Estimated Voltage Stability L-index

Bus 10 Voltage		P(MW)	Q(MVar)	L-index (Calculated)	L-index (estimated)
(pu)	(deg)				
1.0530	-33.81	2980	-963.9	0.5716	0.5704
1.0503	-34.08	2991	-959	0.5819	0.5810
1.0450	-34.62	3013	-949.3	0.6022	0.6021
1.0423	-34.89	3024	-944.4	0.6122	0.6124
1.0396	-35.15	3035	-939.6	0.6218	0.6221
1.0343	-35.68	3055	-930	0.6411	0.6417
1.0317	-35.94	3065	-925.3	0.6504	0.6511
1.0290	-36.19	3074	-920.5	0.6595	0.6603
1.0237	-36.7	3093	-911.1	0.6774	0.6784
1.0211	-36.96	3102	-906.4	0.6863	0.6873
1.0184	-37.21	3111	-901.8	0.6949	0.6959
1.0158	-37.46	3120	-897.1	0.7034	0.7045
1.0105	-37.95	3137	-887.9	0.7199	0.7212
1.0079	-38.19	3145	-883.3	0.7279	0.7292
1.0053	-38.44	3153	-878.7	0.7359	0.7374
1.0027	-38.68	3161	-874.2	0.7436	0.7452
0.9975	-39.16	3176	-865.1	0.7588	0.7604
0.9949	-39.39	3183	-860.7	0.7661	0.7675
0.9923	-39.63	3190	-856.2	0.7733	0.7749
0.9897	-39.86	3197	-851.8	0.7804	0.7817
0.9846	-40.32	3210	-842.9	0.7941	0.7951
0.9820	-40.55	3217	-838.6	0.8008	0.8016
0.9794	-40.78	3223	-834.2	0.8073	0.8080
0.9718	-41.45	3241	-821.3	0.8261	0.8255
0.9693	-41.67	3246	-817	0.8321	0.8312
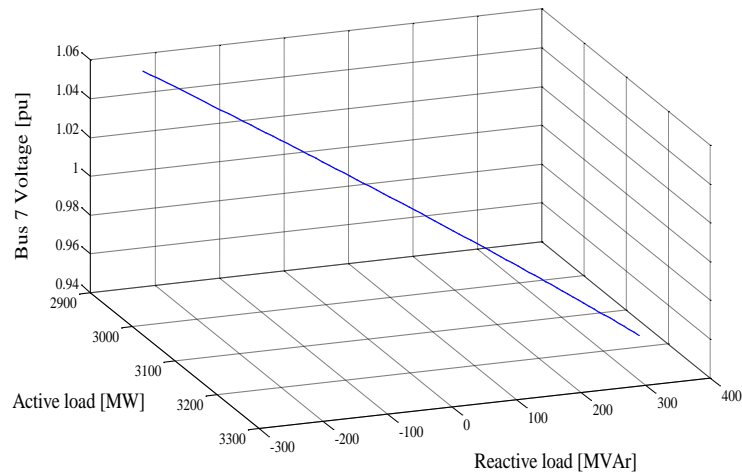
Figure 3.6. Plot of Bus voltage against real and reactive load for bus 7.
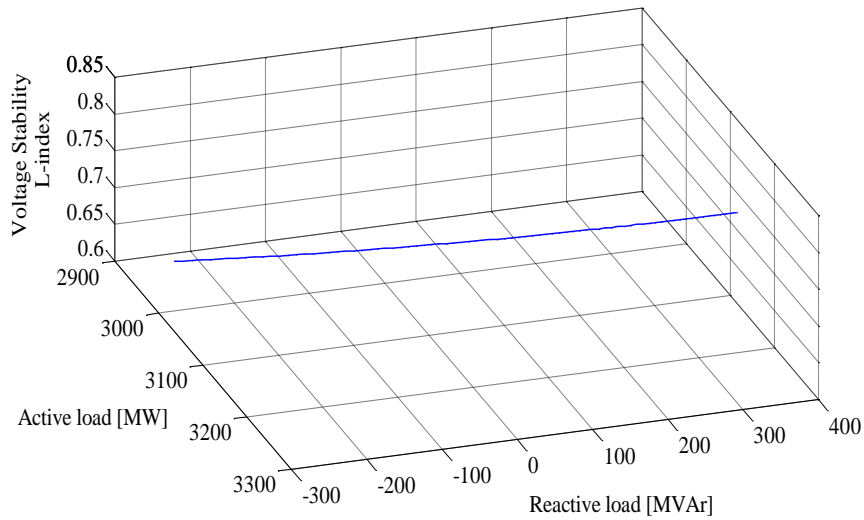
Figure 3.7. Plot of Bus voltage against real and reactive load for bus 10.

This is when the SmartPark is providing power to the grid, hence helping to increase the system stability margin. The parking lot is supplying additional power to the system (generating). When the SmartPark is charging on the other hand, voltage stability index values are higher, indicating the system is less stable.
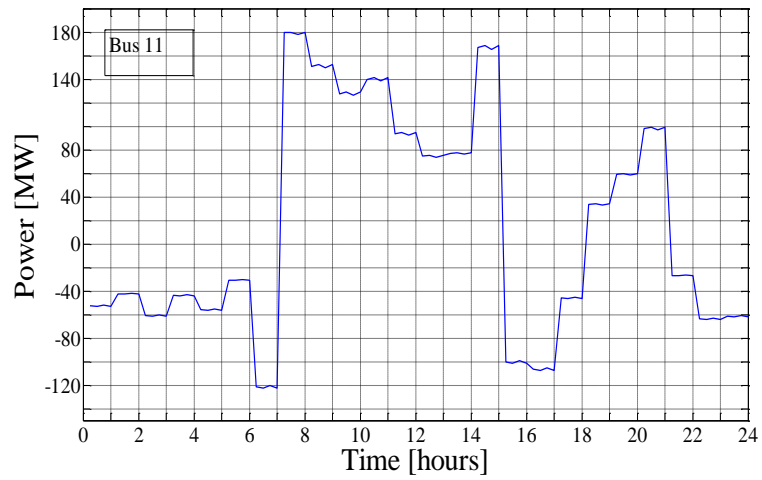
Figure 3.8. Smartpark power variation at bus 11.
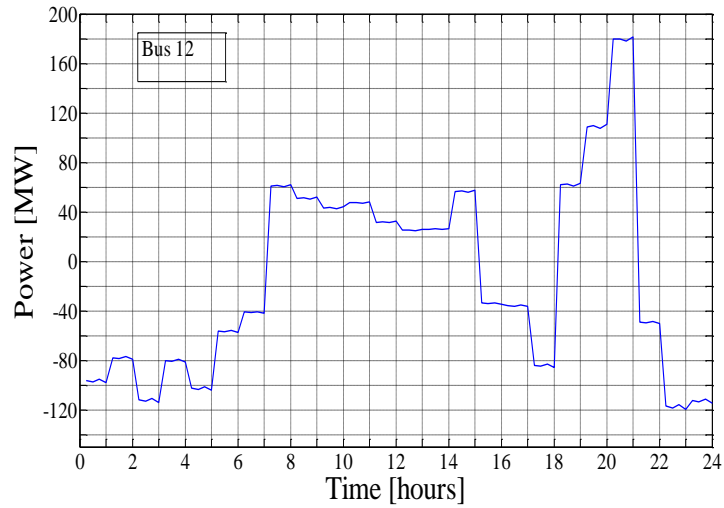
Figure 3.9. Smartpark power variation at bus 12.

The system stability margin varies according to the operation of the SmartPark operation, of charging and discharging. The results also show that the system has lower values of voltage stability L-index, and hence more stable, with all five transmission lines in service.

With one line is out of service, higher values of voltage stability *L*-index indicate that the system is less stable. This can be seen in the graphs of Figures 3.8 and 3.9, where

the graphs of *L*-index corresponding to the system with all five transmission lines in service as lower *L*-index values than that corresponding to the system with one of the five transmission line out of service.
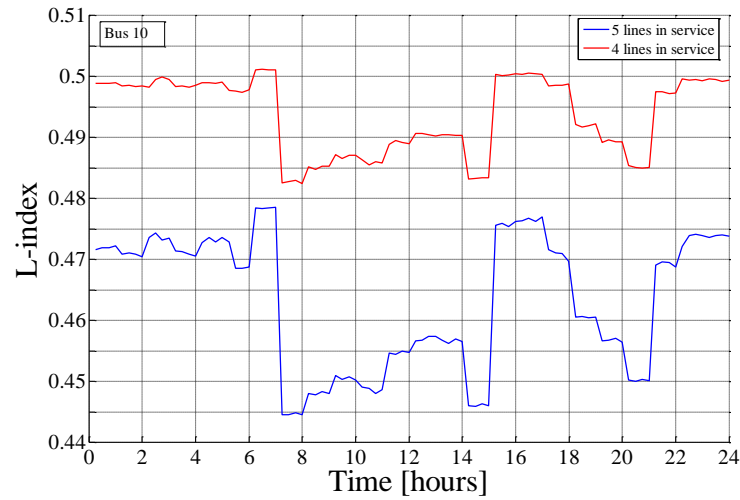
Figure 3.10. Estimated voltage stability L-indices at bus 10 with Smartparks included
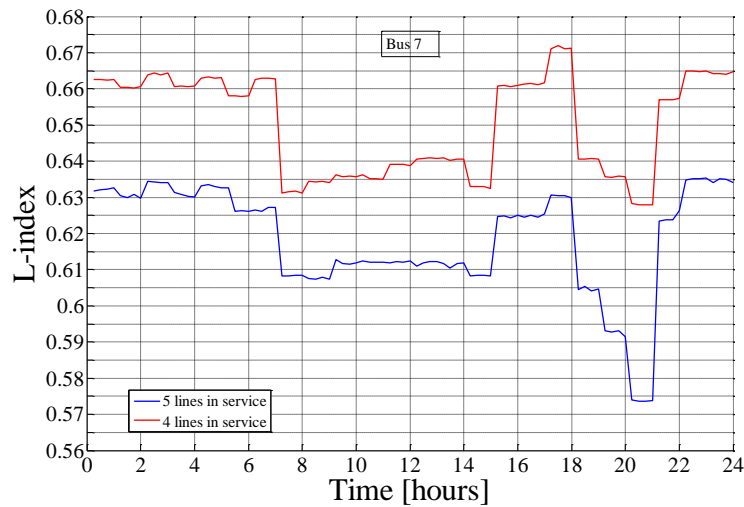
Figure 3.11. Estimated voltage stability L-indices at bus 7 with Smartparks included

3.6. SUMMARY

A multilayer perceptron feedfoward neural network based approach for estimation of the voltage stability *L*-index in a power system with SmartParks has been presented.

The presented neural network approach is independent of the no-load voltage at given load bus. Real power, reactive power and voltage at load bus are sufficient measurements to estimate the *L*-index. Results show that the MLP approach is able to estimate accurately the *L*-index even with changes in topology and operating conditions.

4. VSLI ESTIMATION USING ECHO STATE NETWORKS

4.1. INTRODUCTION

The development of an echo state network (ESN) for estimation of voltage stability index in a smart grid is presented. Assessment of the performance of the ESN neural networks in estimation of voltages stability load index (L-index) in a smart grid with plug-in electric vehicles has been made and comparison made with the performance of the MLP described in section 3.

4.2. DEVELOPMENT OF THE ESN FOR VSI ESTIMATION

4.2.1. Echo State Networks. The general structure of an Echo State Network (ESN) is shown in Figure 4.1 below. The network consists of K input neurons, N neurons internal neurons and L output neurons.
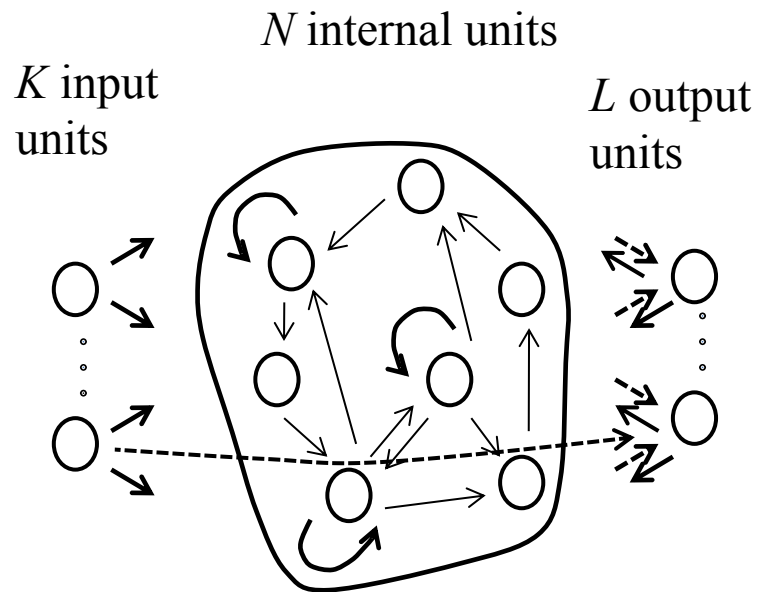
Fig.4.1. General Structure of an Echo State Network.

An Echo State network consisting of a Dynamic Reservoir (DR) with input, internal and feedback weight matrices (W_{in}, W and W_{back}) respectively with the Echo State property was procured following the steps described in [31]. Ten input neural networks and two output neural networks with linear functions were used, while internal units consisted of sigmoid functions. Three cases were considered for 20, 50 and 100 internal units.

The untrained network was driven with the training data set consisting of real and reactive power values at five buses including load buses and three nearest buses as input data with the desired output data calculated L-index at bus 8 and bus 11. Internal states were calculated using equation 2.

$$x(n+1) = f(u(n+1)W^{in} + x(n)W + d(n)W^{back}) \qquad (2)$$

The network state x(n) and output d(n) were collected into a state collecting teacher matrix M and teacher collecting matrix T neglecting the first few term T allow for washout since the initial state x(0) and output d(0) are not defined and are both set to zero.

Output weights, W^{out} are computed by multiplying the pseudoinverse of the state collecting matrix M by the teacher forcing matrix T as given by the equation:

$$W^{out} = M^{-1}T \qquad (3)$$

Finally utilizing the trained output weight matrix and the DR the network is used for estimating the desired output when presented using equation (2) and (4):

$$y(n+1) = f(u(n+1)W^{out}, x(n+1), y(n)) \qquad (4)$$

The neural network used for estimating VSLI is a kind of recurrent neural network known as the echo state network. The ESN consisting of *K* input neurons, *N* internal neurons and *L* output neurons is shown in Figure 4.2. The inputs are PMU measurements of voltage magnitude and phase angle at each bus equipped with a PMU.

An ESN consisting of a dynamic reservoir with input, internal and feedback weight matrices (Win and W) respectively with the echo state property was developed following the steps described in [32]. The ESN outputs are the estimated values of VSLI at each load bus. The input and output layer neurons have linear functions; while dynamic reservoir neurons have sigmoid functions. The untrained network was driven with the training data set consisting of PMU measurements of voltage magnitudes and phase angles at each bus equipped with a PMU. The target outputs are calculated VSLI at all load buses (Figure 4.2). The ESN internal states are calculated using (2).
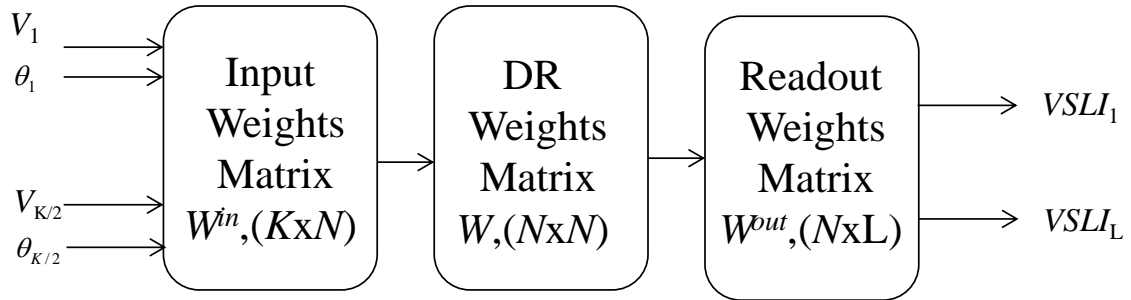
Fig. 4.2. Structure of ESN for VSLI estimation.

4.2.2. Development of ESN for VSLI Estimation. The process followed in the development of an ESN involved two phases shown in a flowchart in Figure. 4.3. The test system showed in Figure 3.5 is utilized in the development of the VSLI estimation. In the training phase, training data is obtained, with no plug-in electric vehicles connected. Values of real power and reactive power at non generator buses as well as voltages at the load buses are obtained with the load at bus 8 and 11 varied simultaneously from 0.8 to 1.2 load factor in small steps to obtain one hundred sets of data. Voltages at bus 8 and 11 were used to calculate voltage stability L-indices for bus 8 and 11 respectively used in the ESN training process as target values for corresponding sets of real and reactive power. Sixty input-output patterns were selected at random and used as training data.
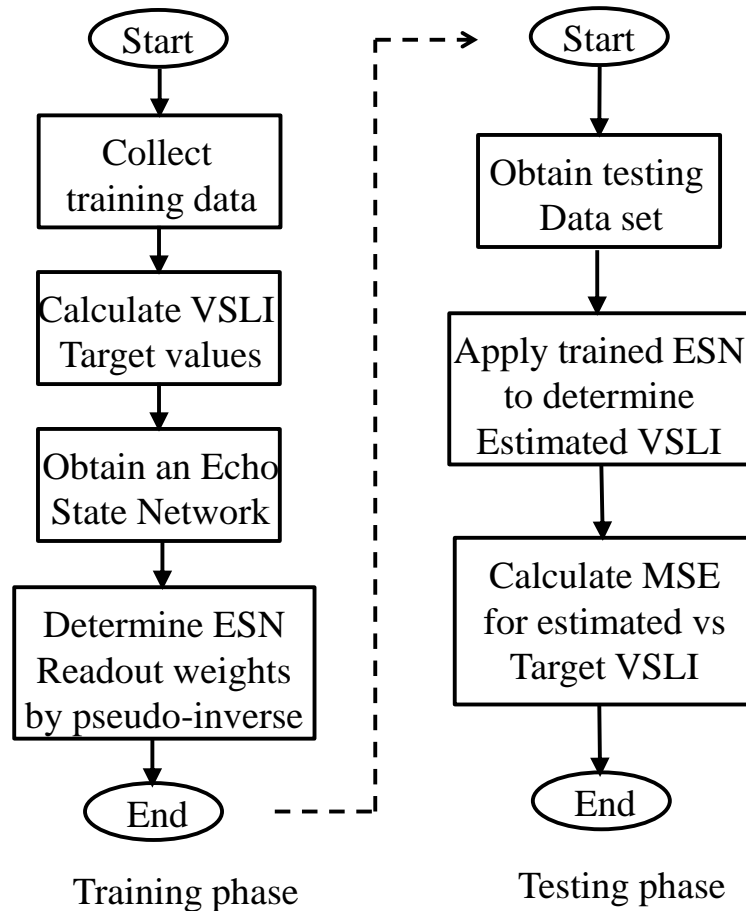
Figure 4.3. Development and operation phases for VSLI using an Echo State Network.

In the second phase, the operation phase, the trained ESN was applied in the prediction of voltage stability L-index in the system. First, 40 input patterns are used to test the accuracy of the neural network in predicting voltage stability L-index. After successfully training and validating the ESN neural network was used for estimation of voltage stability L-index of the test system with plug-in electric vehicles included. Evaluation of L-index was done with all five transmission lines in the system available, and then with the contingency of the outage of one transmission line was also evaluated.

In the case of the IEEE 14 bus system development phase, training data was obtained varying the load factor, λ at each load bus in the range 0 to 0.7. In order to

ensure variability of load, random values of load factor were used at each bus for each training set. Generator output was increased in proportion to the total system load increase. The load at each bus, PLi and generator output PGi are given by (10) and (11) respectively, and PL0i and PG0i are base case values of real power at load buses and generator buses, respectively.

$$P_{Li} = P_{L0i} * (1 + \lambda_i) \qquad (10)$$

$$P_{Gi} = P_{G0i} * (1 + \lambda_i) \qquad (11)$$

PMU measurements of voltage magnitudes and phase angles are obtained as input data for VSLI estimation for each load factor. A total of 250 inputs and output training data sets were obtained.

The ESN structure developed for VSLI estimation in this dissertation is shown in Figure 4.4. The approach uses, $m+1$ number of ESNs where m is the number of islands in the system obtained using a defensive islanding method [49, 52]. Each ESN consists of a dynamic reservoir with input, internal and feedback weight matrices (W^{in}, W, and W^{out}) respectively with the echo state property was developed following the steps described in [53]. The output of the network is in position 1 (Figure 4.4) when the system is in the normal operating mode or position 2 during islanded system operation. The outputs of each ESN are estimated values of VSLI at load buses for whole system when switch is in position 1 or for each island when switch is in positions 2.

The echo state network is used in this dissertation for estimating VSLI for the following reasons: Firstly, ESNs are recurrent neural networks with feedback connection between the readout units and the dynamic reservoir units; as such ESNs have memory and perform better in dynamic nonlinear systems. Secondly, the readout weights of the ESN NN are calculated rather that trained iteratively, thus the time needed to obtain readout weights is much smaller when compared to time taken for training a Feedforward NN such as an MLP.
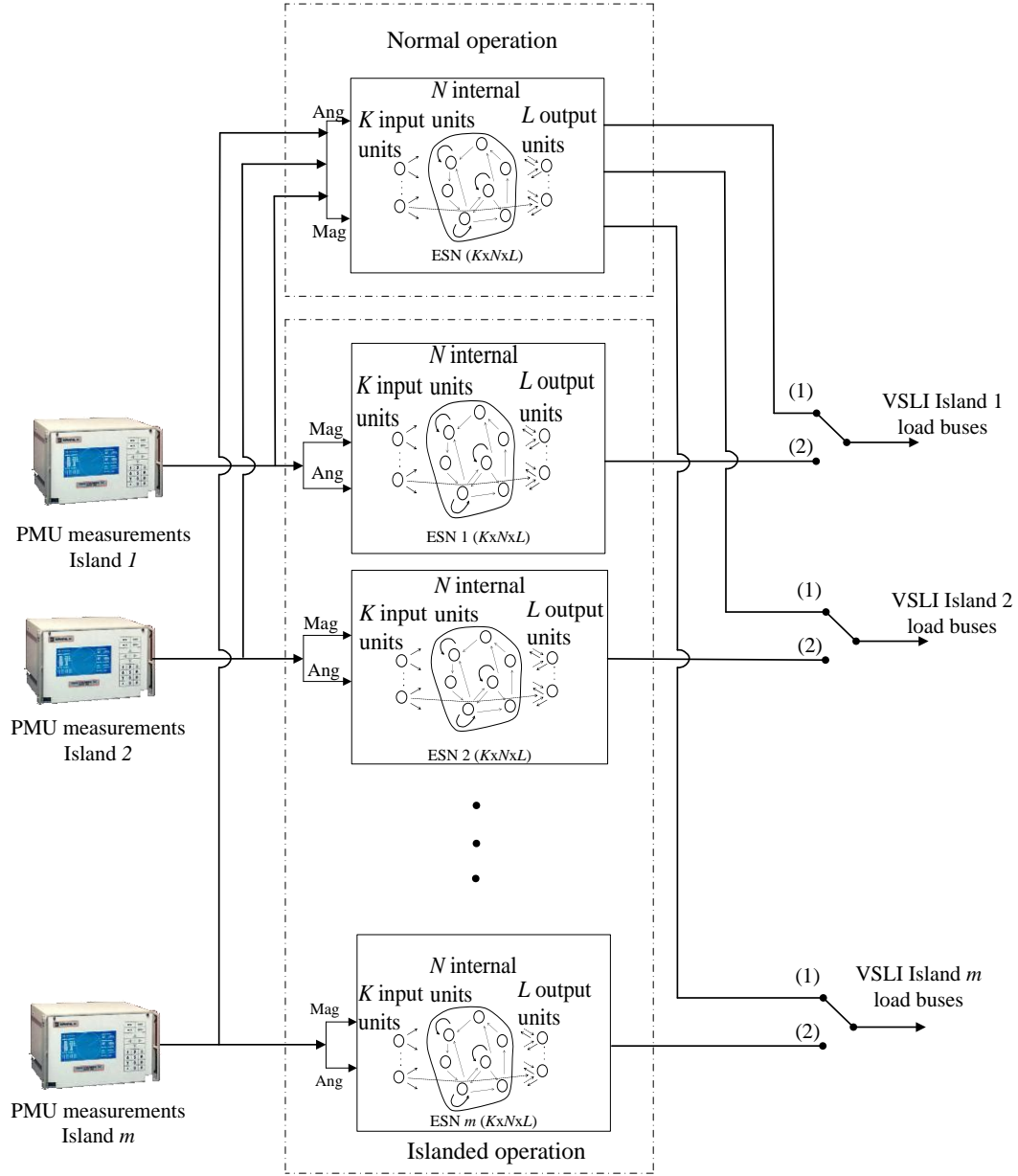
Fig.4.4. Structure of ESN for VSLI estimation under normal and islanded operating conditions.

4.3. TEST SYSTEM

The test system is the 11 bus voltage stability test system with plug-in electric vehicle models included shown in Figure 3.5. The power system consists of two generators, G1 and G2 supplying the load area through five long parallel transmission

lines, and one local generator, G3 providing voltage support in the load area. Bus 11 is a voltage controlled bus using an on-load transformer tap changer. System parameters and loading conditions of the system used in this dissertation are those given in appendix E of reference [9].

The nominal load at bus 8, industrial load is 3000MW, 1800MVAr modeled as a constant power load, while load at bus 11, represents residential load at 3000MW modeled as constant power load. Plug-in electric vehicle parking lots represent six parking lots at each load bus with capacity +/-180 MW each. Bus 8 is a load bus located in an industrial area and bus 11 is a load bus in a residential area.

4.4. RESULTS AND DISCUSSION

As described in the preceding section, the process of developing and implementing an ESN for estimation of voltage stability L-index involved the development phase and the operation phase. In the development phase the ESN NN is trained for accurate prediction of voltage L-index. The performance of the ESN in estimation of VSLI is then validated using randomly selected patterns of input output data sets different from the training data set. The first set of results for the development phase that show that the ESN NN is successfully trained for predicting voltage index to a high degree of accuracy. On-line application of the trained ESN is then done by applying the ESN to predicting voltage stability L-index of the power system with plug-in electric vehicles. Voltage index target and ESN output values used in the testing phase are shown in Table 4.1. The table shows that the ESN output values are very close to the target values at both bus 8 and 11.

Plots of voltage stability L-index at bus 8 and 11 are shown in Figure 4.5 below. Figure 4.5 shows calculated and estimated voltage stability L-index for the case of the MLP and the ESN. The estimated L-index approximates the target L-index more closely in the case of the ESN than the MLP. The MSE obtained using the MLP was 8.75×10^{-5}, the MSE obtained with the ESN is 1.075×10^{-9}.
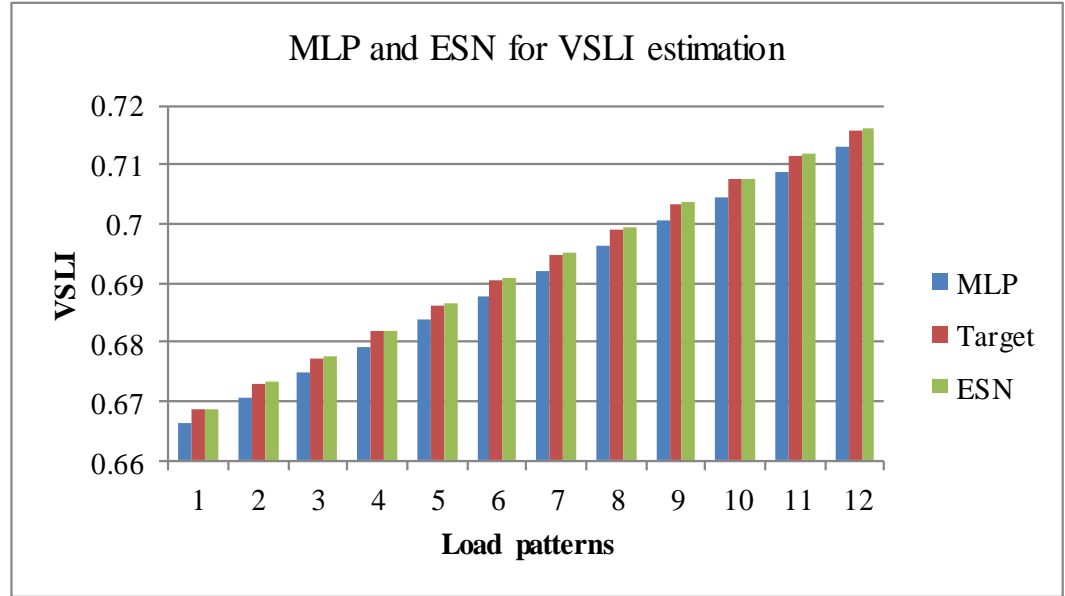
Fig.4.5. MLP and ESN for VSLI Estimation: VSLI Estimation is obtained using a multilayer perceptron and an ESN in order to compare the performance of the two neural networks in estimate the calculated VSLI target

The trained neural network is applied to predicting of voltage stability L-index of the 11 bus test system with plug-in electric vehicles included at bus 8 and 11. Values of L-index are obtained over a period of 24 hours with both parking lots at bus 8 (located in an industrial area) and bus 11, located in a residential area. Graphs showing typical power demand in a 24 hour period for the two parking lots used in this dissertation are shown in Figures. 4.6 and 4.7. Graphs of Figures 4.6 and 4.7 show that the performance of the ESN for estimating VSLI in the power system has higher accuracy in the MSE than that of the MLP. The graph of L-index estimated using the ESN closely matches the calculated L-index. The calculated MSE using the ESN is 2.018×10^{-12} while the MSE for the multilayer perceptron is 6.34×10^{-4}.

Table 4.1. Voltage Stability L-index Prediction at buses 8 and 11

Target		Output	
Bus 8	Bus 11	Bus 8	Bus 11
0.5404	0.4047	0.5428	0.4075
0.8001	0.5076	0.8021	0.5075
0.7332	0.5042	0.7350	0.4989
0.7575	0.5017	0.7562	0.5008
0.6051	0.4818	0.6096	0.4734
0.5765	0.4466	0.5765	0.4492
0.7231	0.5025	0.7265	0.4969
0.5765	0.4466	0.5765	0.4492
0.7575	0.5017	0.7562	0.5008
0.6465	0.4927	0.6457	0.4921
0.7434	0.5064	0.7450	0.5013
0.6580	0.4936	0.6532	0.4964
0.6346	0.4768	0.6301	0.4784
0.5702	0.4414	0.5714	0.4445
0.5469	0.4127	0.5451	0.4195
0.5702	0.4414	0.5714	0.4445
0.5296	0.3913	0.5271	0.3892
0.7750	0.5037	0.7746	0.5036
0.7926	0.5073	0.7932	0.5074
0.6269	0.4825	0.6273	0.4792
0.5909	0.4670	0.5959	0.4618
0.7678	0.5051	0.7677	0.5029
0.6011	0.4788	0.6082	0.4690
0.7926	0.5073	0.7932	0.5074
0.5702	0.4414	0.5714	0.4445

4.5. SUMMARY

The development of an Echo State Network (ESN) based approach for estimation of VSLI has been presented. Simulation results of application of the ESN approach to a standard 10 bus system have been presented. A comparative study of the performance of the ESN and MLP for the estimation voltage stability loads index in smart grid.
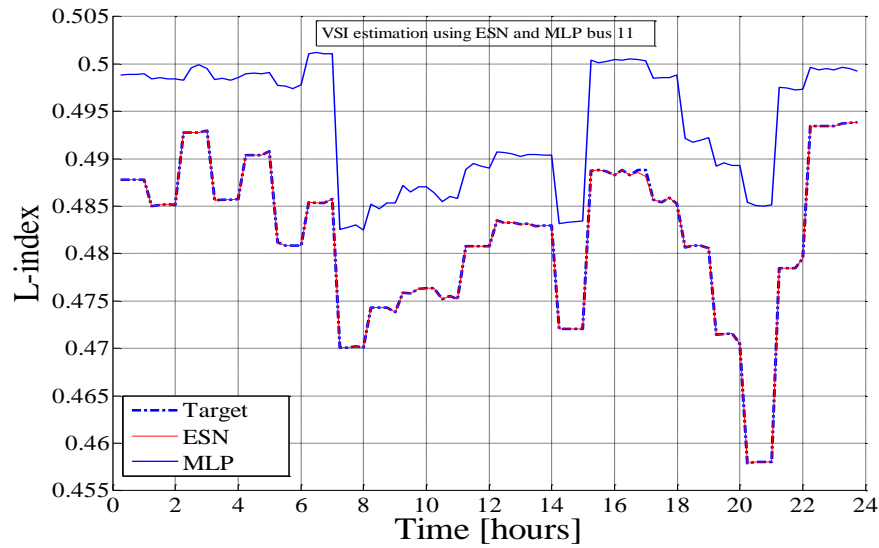
Fig. 4.6. Estimated voltage stability L-indices at bus 11
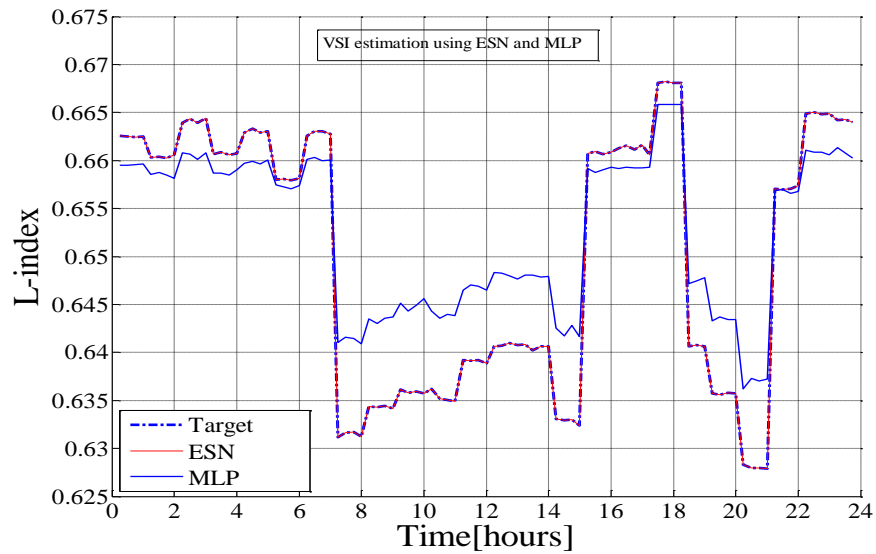
Fig. 4.7. Estimated voltage stability L-indices at bus 8

The development of the MLP and ESN and compared the accuracy in estimating voltage stability indices at two load buses has been presented. Simulation results have demonstrated the application of the neural network in predicting voltage stability index in a power system with parking lot electric vehicles. In this section results show that the trained ESN performs better than the MLP in the estimation voltage stability index.

5. ONLINE VOLTAGE STABILITY LOAD INDEX ESTIMATION BASED ON PMU MEASUREMENTS

5.1. INTRODUCTION

In this section the VSLI algorithm is implemented using synchrophasor measurements as input information for the neural network. Reference [47] introduces a method of using multilayer perceptrons to predict the voltage stability margin of a power system based on continuation power flow using synchrophasor measurements of voltage magnitudes and phase angles. In this dissertation synchropahsor measurements are used to estimate VSLI as measure of the closeness of each load bus to voltage instability. The VSLI estimation approach is not dependent on the loadflow solution of the system that relies on having detailed system parameters and iterative calculations to determine the measure of instability. The voltage stability margin gives the distance of the power system to the critical load at which the system becomes voltage unstable in a specified load direction. However for local monitoring it is helpful to have voltage stability index at individual load buses in the system [48].

The estimation of the VSLI is carried out by an Echo State Network (ESN). A real-time model of the IEEE 14-bus test system simulated using the Real-Time Digital Simulator (RTDS) has been used to investigate the ESN based approach. Phasor Measurement Units (PMUs) are placed at pre-determined buses that ensure that the system is fully observable for voltage stability monitoring. Placement of PMUs for voltage stability monitoring is done is such a way as to ensure that voltage phasors at all load buses are either direct measurements form PMUs or calculated at first level of observability. The method for optimal PMU placement developed in this study ensures that the power system is fully observable during normal operation and under islanded conditions. Reference [40] presents a technique for splitting the system into smaller islands followed by load shedding for the purpose of preventing wide spread system failure and black out. During these instances monitoring and control of voltage stability remain critical for the system to survive the disturbance.

It is desired in a power system with smart grid technologies, that monitoring and control strategies to enable adaptation to different contingencies are implemented. In the

present study, the possibility of continuously monitoring VSLI of the system for normal operation and when the system is islanded is considered. The ESN based method that enables monitoring of VSLI during normal operating conditions and during islanding is presented. The primary contributions of this section are the following:

- An intelligent algorithm for optimal PMU placement in power system to ensure complete observability during normal operating conditions and when the system is islanded is developed and implemented on three test systems.

- Assessment of the scalability of the ESN based approach method using PMU information for monitoring voltage stability. The dissertation shows the performance of the technique as the system size is increased;

- Demonstrates that the ESN based approach for VSLI estimation can be used during power system islanding; and,

- Application of the new method for online voltage stability in a smart grid including wind generation and SmartParks.

5.2. OPTIMAL PMU PLACEMENT

Optimal placement of PMUs in power systems is done in a manner that ensures that all system bus voltages can be observed using the minimum possible number of PMUs. This is important from the economic and technical point of views. PMUs are used in power system for system monitoring, and state estimation that can facilitate on-line control and protection operations. However, during contingencies, the system may not be fully observable for example when measurements from one PMU are lost and there is not enough redundancy. Further, during emergencies, a power system may be operated in an islanded mode. In this case the system is separated into smaller islands at reduced load in order to avoid system wide failure or blackout. The algorithm for the optimal PMU placement that ensures that the system is fully observable during normal operating conditions and under conditions of islanding using the minimum number of PMUs is developed in this dissertation. Figure 5.1 shows the flowchart for optimal PMU placement using Genetic Algorithm (GA). Besides GA algorithm other methods are also applicable such as particle swarm optimization [50].
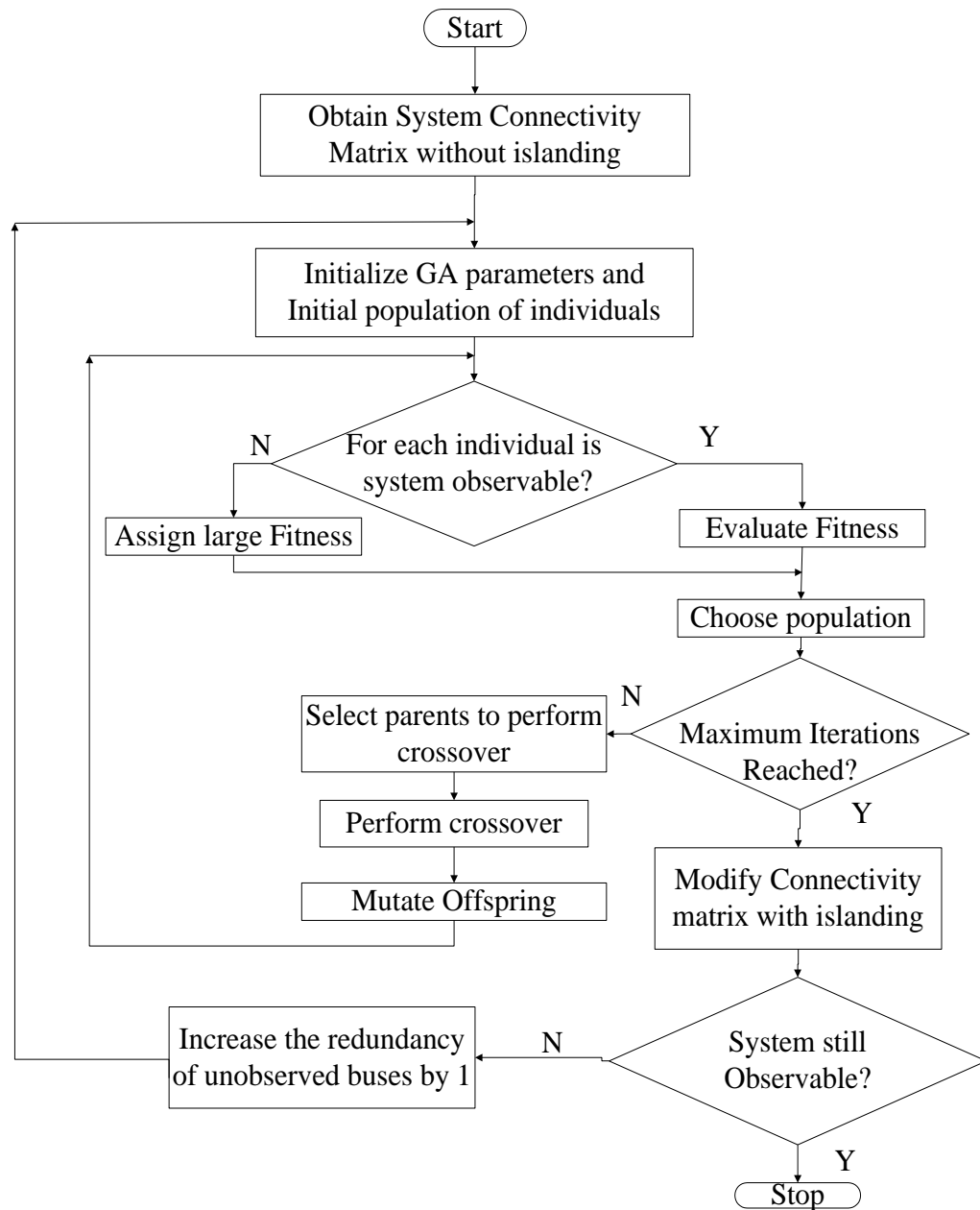
Fig. 5.1. Flowchart for optimal PMU placement consideration islanding using GA.

During islanding conditions optimal placement of PMUs is vital as it is necessary to monitor the separated islands and maintain voltage stability. The algorithm for the optimal PMU placement that ensures that the system is fully observable during normal operating conditions and under conditions of islanding using the minimum number of

PMUs is developed in this dissertation.

The procedure for determining optimal PMU locations in a power system considering islanding can be summarized in the following steps:

1. Obtain optimum PMU locations for normal operating conditions using GA.

2. Split system into the desired set of islands and modify the system connectivity matrix.

3. Use solution obtained in step 1 and test if islanded system (the islands are) is still observable.

4. If islanded system is also observable, the solution in step 1 is the required solution.

5. If islanded system is not observable with solution in step 1, identify buses not observed after islanding.

6. Increase redundancy at each bus that becomes unobservable after islanding by one.

7. Repeat steps 1 to 6 until the optimum solution that makes the system observable for both normal and islanded conditions is obtained.

The following rules have been used for optimal PMU placement [51]:

1. Assign a voltage measurement to a bus where a PMU is placed including a current measurement to each line incident at the bus (assuming that the number of channels of each PMU is at least one less than the maximum number of incident lines), the current in the remaining line can be obtained by Kirchhoff's current law.

2. Assign a pseudo-voltage measurement to each node reached by a node that has a PMU. The voltage measurement of such a bus is obtained from the known voltage of the bus with a PMU, line current and impedance of the line.

3. Assign a pseudo-current to each line connecting two buses whose voltages are known. The current is such a branch is readily obtained from the two known voltages and line impedance using Ohm's law.

4. Assign a pseudo-current measurement to an incident line where all other lines current measurements are known. The unknown current is obtained using Kirchhoff's current law.

Equations for evaluation of fitness function, F used with the GA algorithm to determine the optimal number and location of PMUs in the system are as follows:

$$F = \begin{cases} K \ \text{if not observable} \\ w_1 F_1 + w_2 F_2, \ \text{otherwise} \end{cases} \tag{2}$$

Where,

$$F_1 = x^T x \tag{3}$$

$$F_2 = (N - A_X)^T (N - A_X) \tag{4}$$

And K is a large value assigned to the fitness function if the current solution x does not make the system fully observable; w1 and w2 are two user defined weights that ensure that the two parts of the fitness function F1 and F2 are comparable. The elements of the binary vector x are defined as follows:

$$x_i = \begin{cases} 1 \ \text{if a PMU is place at bus } i \\ 0 \ \text{otherwise} \end{cases} \tag{5}$$

The connectivity matrix of the system, A is given by:

$$A = \begin{cases} 1 \ \text{if } i = j \\ 1 \ \text{if } i \text{ and } j \text{ are connected} \\ 0 \ \text{otherwise} \end{cases} \tag{6}$$

The vector *N* is chosen to give the desired level of measurement redundancy at a bus. For example if all entries of *N* are set to 2, the level of measurement redundancy at each bus is 1.

5.3. REAL-TIME SIMULATION RESULTS

Tables 5.1 – 5.3 show results for optimal PMU placement considering islanding conditions. The 14 bus system (Figure 5.2) has been split into two islands and the optimal locations of PMUs for complete observability both during normal operating conditions and during islanding conditions has been obtained. Results show that for the same level of redundancy, the system utilizes more PMUs when islanding operating conditions are considered. A total of four PMUs is required in order to ensure full observability during both normal operating conditions and during islanding conditions, whereas only three PMUs are needed if islanding is not considered.

Three cases for VSLI estimation were considered for the IEEE 14 bus system. The first one being the normal operating condition, and the second and third cases were two N-1 contingencies involving the loss of lines 2-3 and line 2-4 respectively.

Performance of the ESN for the estimation of VSLI is shown in Tables 5.1 – 5.4. The ESN training is implemented in a one-step calculation and carried out on a desktop computer (Processor speed 3.33GHz). Table 5.4 shows that the training time was less than 0.1 second for an ESN.

Table 5.1. IEEE 14 Bus System Split into Two Islands

No.	Buses	Lines opened
1	1,5,6,11,12,13	1-2,2-5,4-5,11-10, 13-14
2	2,3,4,7,8,9,10,14	
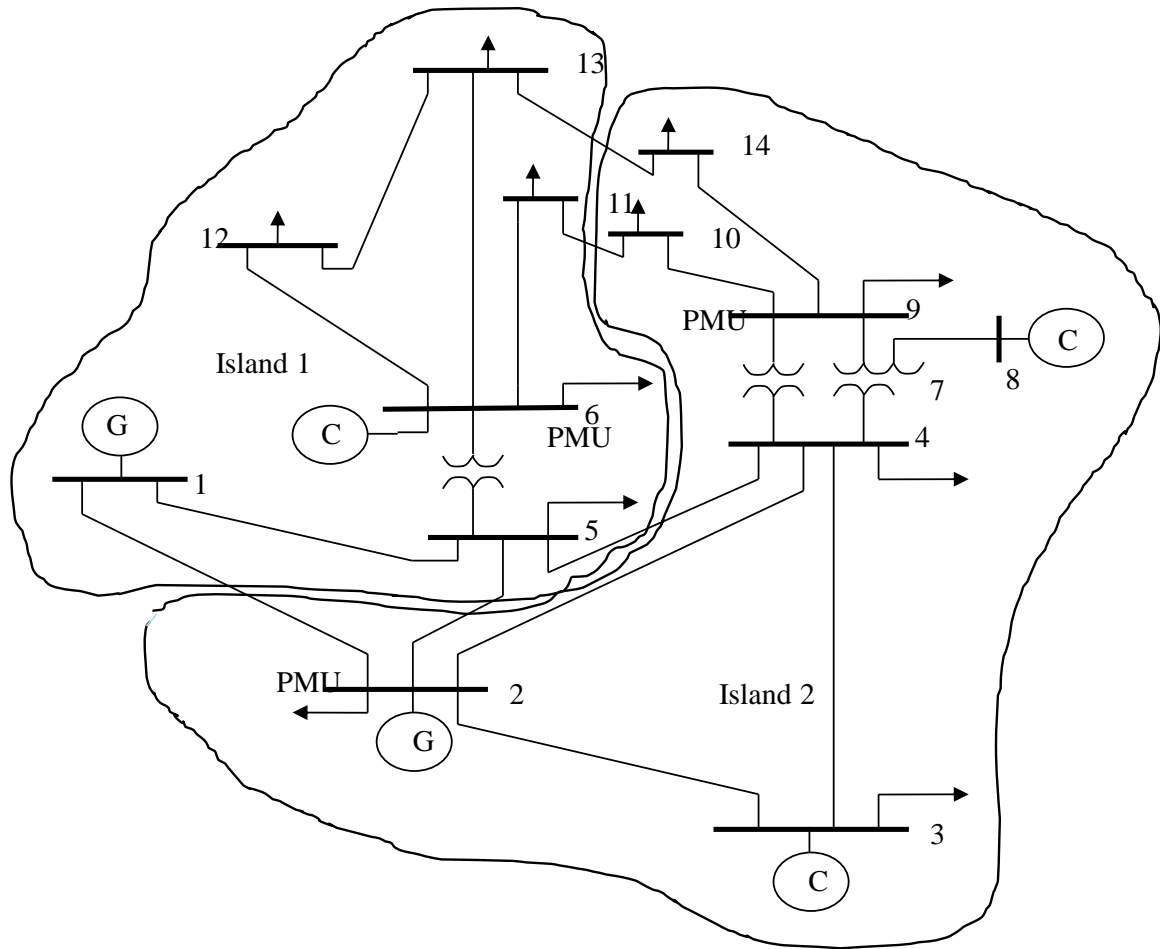
Figure 5.2. IEEE 14-bus test system split into 2 islands

Table 5.2. Optimal PMU Locations for IEEE 14 Bus Systems

System Configuration	Optimal PMU Locations
Normal operating conditions	2,6,9
Split into two islands	1,2,6,9

Table 5.3. VSLI Estimation for IEEE 14 Bus System

	ESN		
	Number of Weights	Training Time (sec)	Mean square Error (%)
IEEE 14 bus system	1100	0.067	4.31 x10^{-5}

The accuracy of the trained ESN in estimating the VSLI is shown in Table 5.4. The table shows that on average the mean square error on testing for the ESN was 4.31 x10-5. System voltage profiles shown in Figure 5.3 show that as load factor is increased, voltage at load buses declined. Bus 14 has the lowest voltage profile while bus 2 is the strongest bus with a higher voltage profile.

Graphs of VSLI compared with PV curve analysis for the IEEE 14 bus test system are shown in Figures 5.3 – 5.5. In Figures 5.3 and 5.4 a correlation between PV curve analysis and VSLI index is demonstrated. As shown with both the PV curves and the VSLI approach, bus 14 reaches the voltage stability limit before other buses, and bus 2 has the greatest voltage stability margin shows that bus 14 has the highest value of VSLI and the value approaches one as the load factor approaches 0.62. This result is in agreement with the result found using P-V curve analysis in [50].

Finally, estimated VSLI of the system for the two N-1 contingencies are shown in Figures 5.5 and 5.6. In Figure 5.5, the system approaches voltage instability at load factor of nearly 0.45 while in Figure 5.6 the system approaches voltage instability at the load factor of nearly 0.5. The results show that the system has a lower voltage stability margin following the loss of line 2-3 than when line 2-4 was lost.
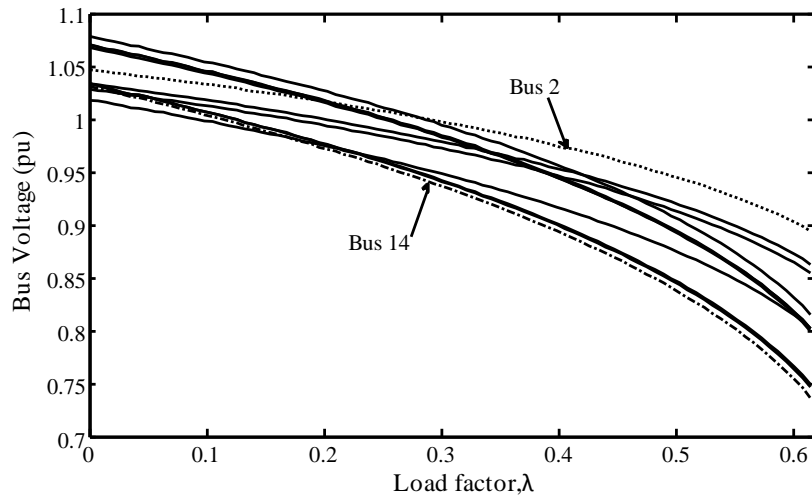
Fig. 5.3. Bus voltage profiles for the IEEE 14 bus system. The diagram shows P-V curves at the different load buses. Bus 14 has the lowest voltage profile while bus 2 has the higher voltage profile compared with other load buses.
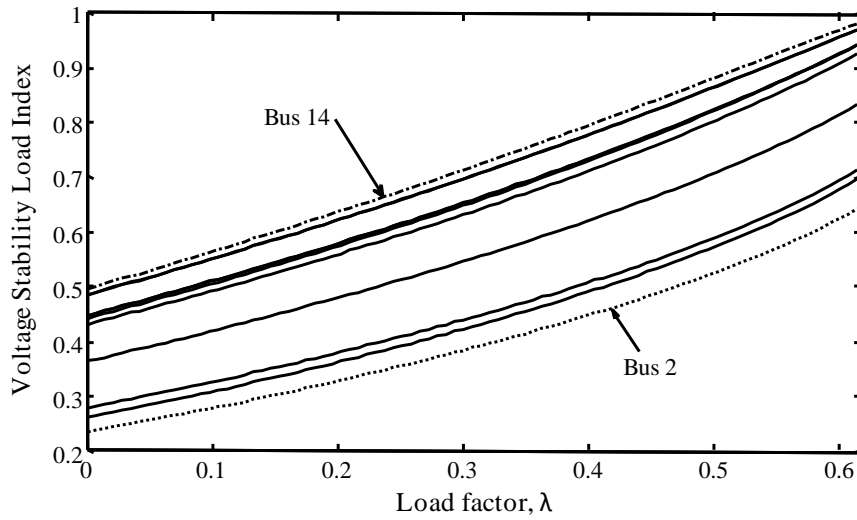
Fig. 5.4. VSLI for the IEEE 14 bus system. VSLI results show that the bus with the lowest voltage profile has a higher VSLI compared with other load buses. Bus 2 with the higher voltage profile has the least VSLI.
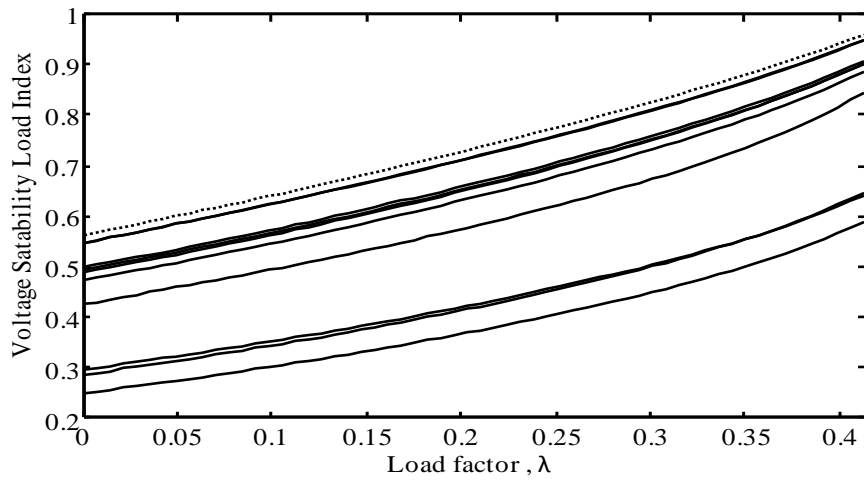
Fig. 5.5. Estimated VSLI for the IEEE 14 bus system with the loss of line 2-3. When one transmission line is lost, the system is more stressed resulting in higher values for VSLI than those for the system with all lines in service.
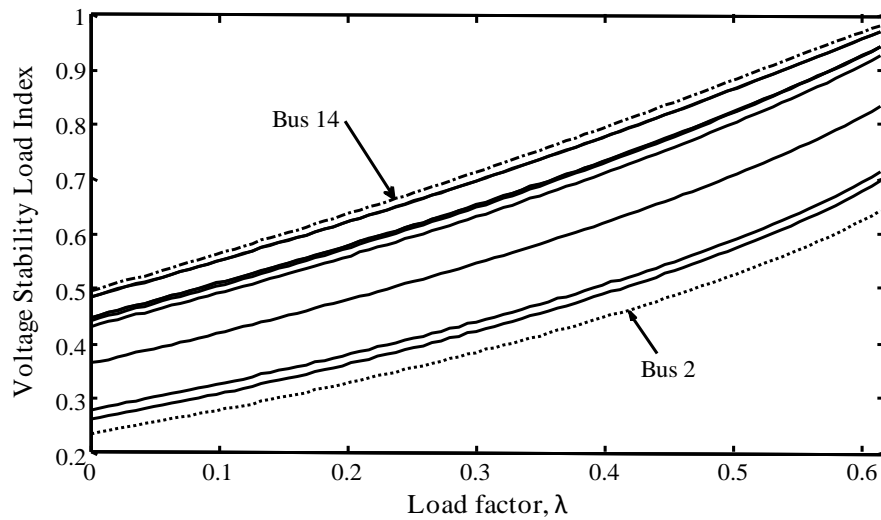
Fig. 5.6. Estimated VSLI for the IEEE 14 bus system with the loss of line 2-4. When one transmission line is lost, the system is more stressed resulting in higher values for VSLI than those for the system with all lines in service.

Table 5.4. ESN Performance at Each Load Bus

Bus No.	Mean Square Error
2	4.27×10^{-5}
3	5.36×10^{-6}
4	3.21×10^{-4}
5	1.11×10^{-5}
6	1.91×10^{-5}
9	1.18×10^{-6}
10	9.38×10^{-6}
11	1.2×10^{-5}
12	4.27×10^{-5}
13	4.44×10^{-5}
14	4.3×10^{-5}
Ave MSE	4.31×10^{-5}
Max MSE	3.21×10^{-4}
Min MSE	1.18×10^{-6}
Std dev	9.34×10^{-5}

The proposed method for optimal PMU placement considering islanding was then applied on the IEEE 14 bus (Figure 5.2), and the IEEE 39 bus, and IEEE 68 bus test systems (Figures 5.7 and 5.8 respectively) in order to evaluate its scalability as the size of the power system increases. Results of the algorithm for the three test systems are shown in Tables 5.5 and 5.6.

For each system the islanding configuration is given for which the algorithm is used to determine the optimal PMU locations to ensure system observability both during normal operation and during islanded conditions. Results for optimal location of PMUs in each of the three systems show that the number of PMUs required for complete observation for both islanded and un-islanded is comparable. Thus by applying this algorithm a minimum set of PMUs and their locations can be determined to assure voltage stability monitoring during defensive islanding.

Results of the performance of the ESN approach for estimating VSLI is presented in Figures 5.9 to 5.11. The plots show the accuracy of the ESN approach in estimating VSLI of the system buses. The ESN approach for the IEEE 14 bus test system is the most accurate while the accuracy of the ESN for the IEEE 39 bus is less that of the IEEE 14 bus and that for the IEEE68 bus system has the least accuracy.
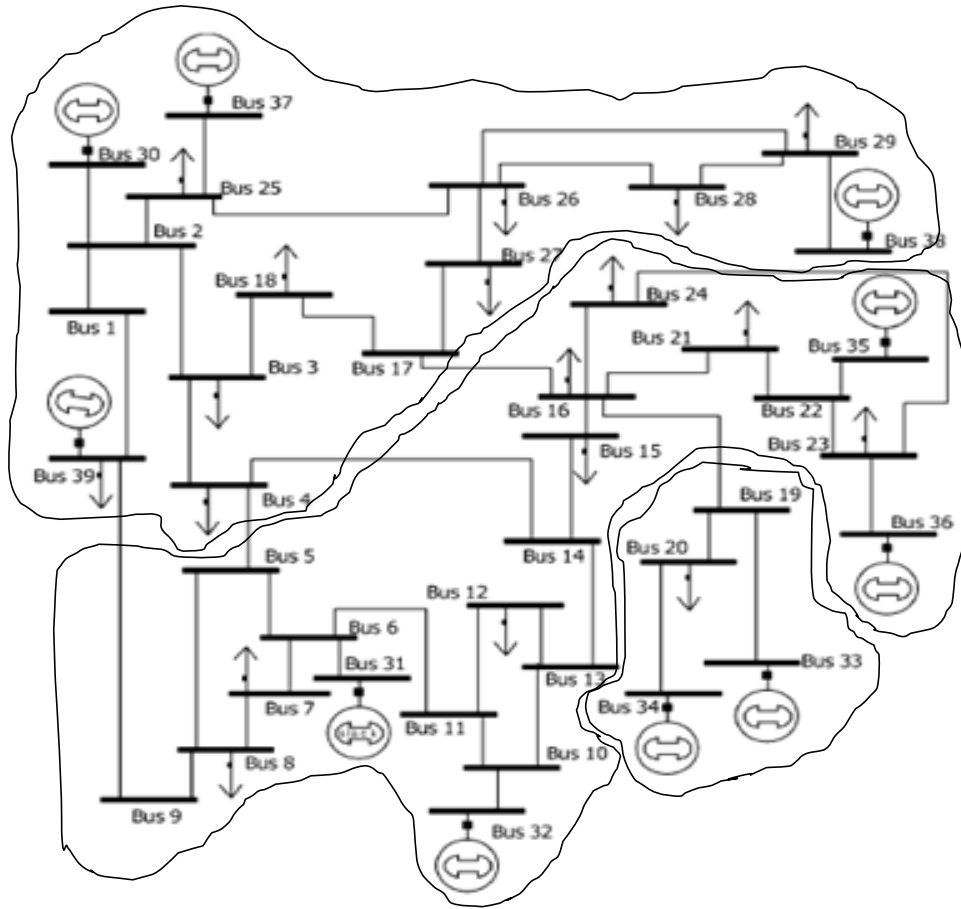
Figure 5.7. IEEE 39-bus test system split into 3 islands
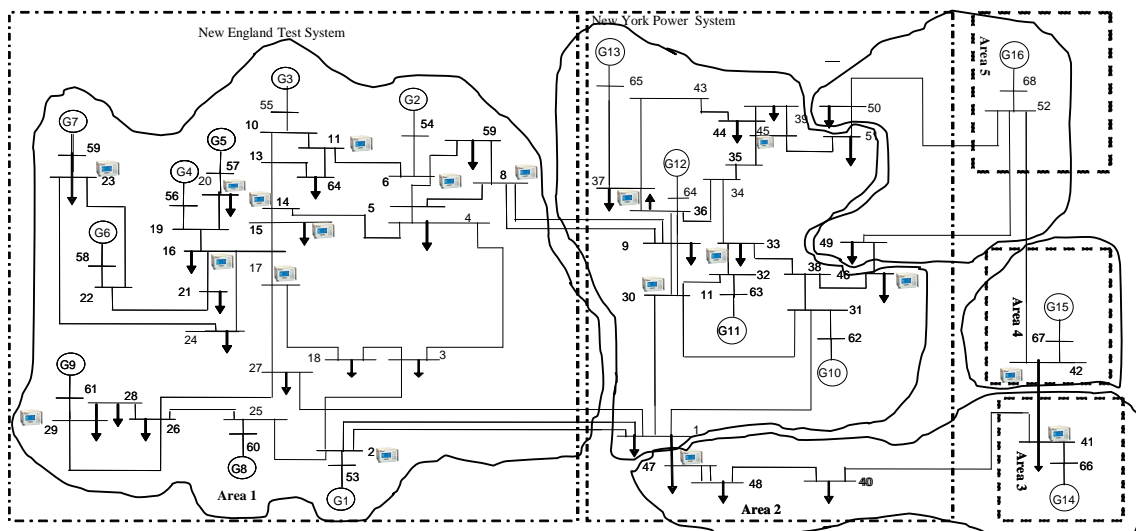
Figure 5.8. IEEE 68-bus test system split into 5 islands

Table 5.5. Test Systems Split into Islands

	No.	Buses	Lines opened
14 bus system	1	1,5,6,11,12,13	1-2,2-5,4-5,11-10,13-14
	2	2,3,4,7,8,9,10,14	
39 bus system	1	1,2,3,4,17,18,25,26,27 28,29,30,37,38,39	9-39,4-5,4-14 16-17,16-19
	2	5,6,7,8,9,10,11,12,13 14,15,16,21,22,23,24	
	3	19,20,33,34	
68 bus system	1	42,67	1-2,1-27 8-9,1-47 41-42,42-52 50-51,46-49
	2	40,41,47,48,66	
	3	49,50,52,68	
	4	2,3,4,5,6,7,8,10,11,12,13,14,15,16, 17,18,19,20,21,22,23,24,25,26,27,28, 29,53,54,55,56,57,58,59,60,61	
	5	9,30,31,32,33,34,35,36,37,38, 39,43,44,45,46,49,51,62,63,64,65	

Plots of target VSLI against ESN estimated VSLI are shown in Figures 5.9 -5.11. The Figures show very close agreement between estimated and calculated values of VSLI. The 14 bus system has a determination coefficient 0.9971 and the 39 bus system has determination coefficient of 0.9956, while the 68 bus system has 0.9937.

The performance of ESN approach is successful with a high level of accuracy in all the three tests systems with a slight decrease in determination coefficient as the test system size increases. The ESN used to estimate VSLI for the IEEE 14 bus has the highest accuracy of the three, followed by the 39 bus system and the 68 bus system respectively. This observation points to the fact that as the size of the system increases the accuracy of the method is reduced. In all three cases the ESN had a dynamic reservoir

with 100 neurons in the dynamic reservoir. Table 5.7 shows the Mean Square Error and training time.

Table 5.6. Optimal PMU Locations for Normal and Islanded System operation

	System Configuration	Optimal PMU Locations
14 bus system	Normal operating conditions	2,6,9
	Split into two islands	1,2,6,9
39 bus system	Normal operating conditions	2,6,9,10,13,14,17,19,20,22,23,25,29
	Split into three islands	2,3,5,6,9,10,13,15,17,19,20 21,22,23,25,29,39
68 bus system	Normal operating conditions	1,8,11,14,18,19,22,23,26,29,33,37,40, 45,46,52
	Split into five islands	2,8,11,14,17,20,22,23,29,30,34, 37,40,41,42,45,46,47,52
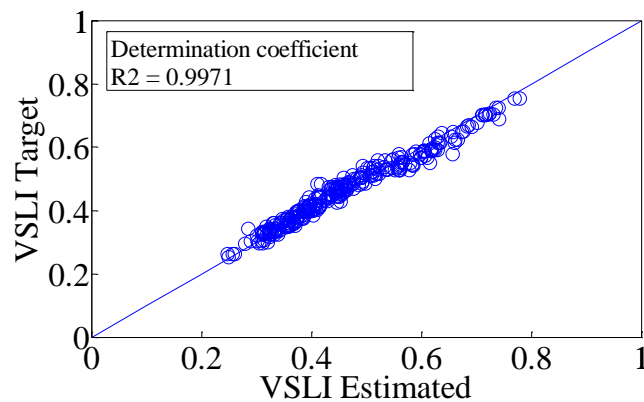
Fig. 5.9. Plot of calculated VSLI against the ESN estimated value for IEEE 14 bus test system
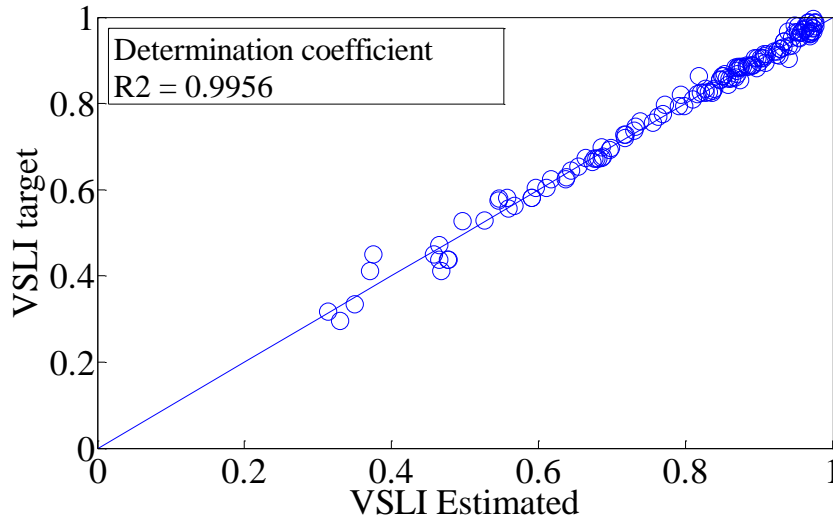
Fig. 5.10. Plot of calculated VSLI against the ESN estimated value for IEEE 39
bus test system
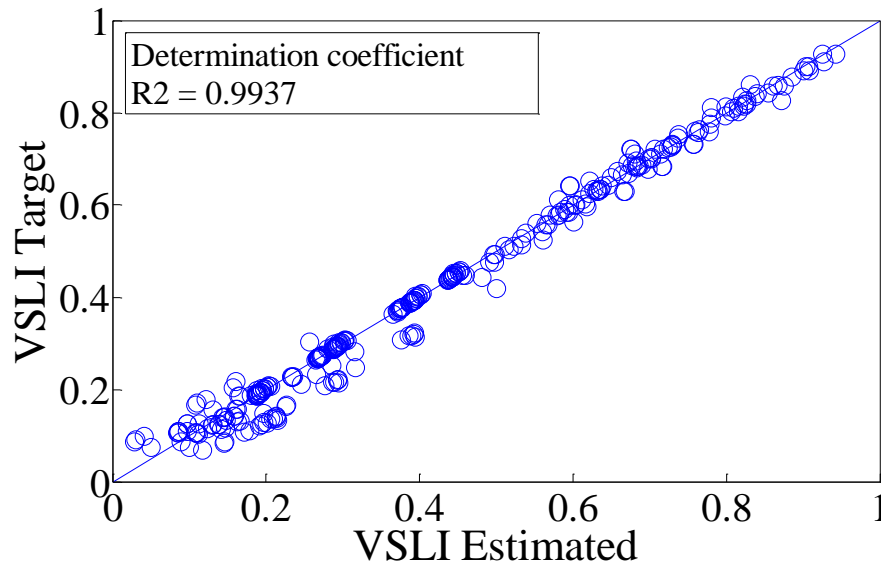
Fig. 5.11. Plot of calculated VSLI against the ESN estimated value for IEEE 68
bus test system

The ESN approach for monitoring VSLI was applied to the IEEE 68 bus system
with a Wind Farm (WF) and Plug-in Electric Vehicle (PEV) shown in Figure 5.12. The
system is the modified IEEE 68 bus system to include a wind farm and plug-in electric
vehicles at bus 39 and bus 35 respectively.
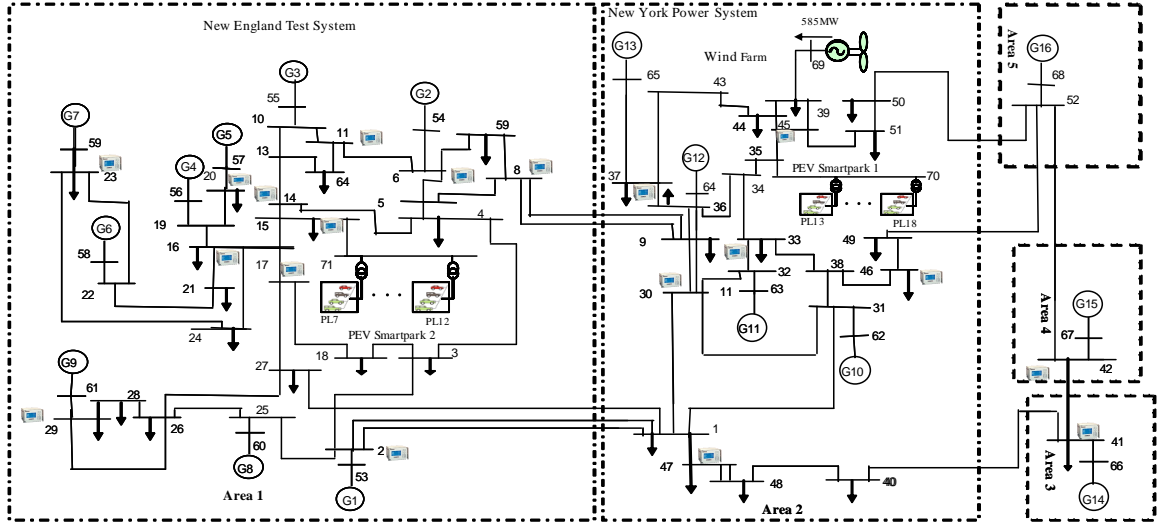
Fig. 5.12 Test system with wind farm and PEVs included.

The load area considered has a net load capacity of 742MW. The wind farm is rated 585MW. The aggregated PEV load at bus 35 is 180MW.The performance of the ESN approach for estimating VSLI in the smart grid with a wind farm and plug-in electric vehicles is shown the in Figures 5.12 and 5.13. A three phase, 5 cycles ground fault is simulated at bus 45 in the load area with WF and PEVs. The output of the ESN is compared with calculated values of VSLI at three load buses in the area.

The structure of the ESN used for monitoring VSLI in this test system is shown in Figure 5.13. The system consists of 5 PMU's placed at the optimal buses for the system to remain observable during normal and islanded operating conditions. Six ESN NNs are needed to evaluate the VSLI in this system (Figure 5.13).

For each island the average of the MSE's at load buses was obtained. The results presented in Table 5.7 show the performance of the approach for each island to have better performance based on MSE when compared to that of the un-islanded system. Figure 5.12 shows the dynamic response of voltage, VSLI and active and reactive power at load buses 35, 39 and 44. Figure 5.13 shows very close agreement between the ESN output and the calculated VSLI at the three load buses.
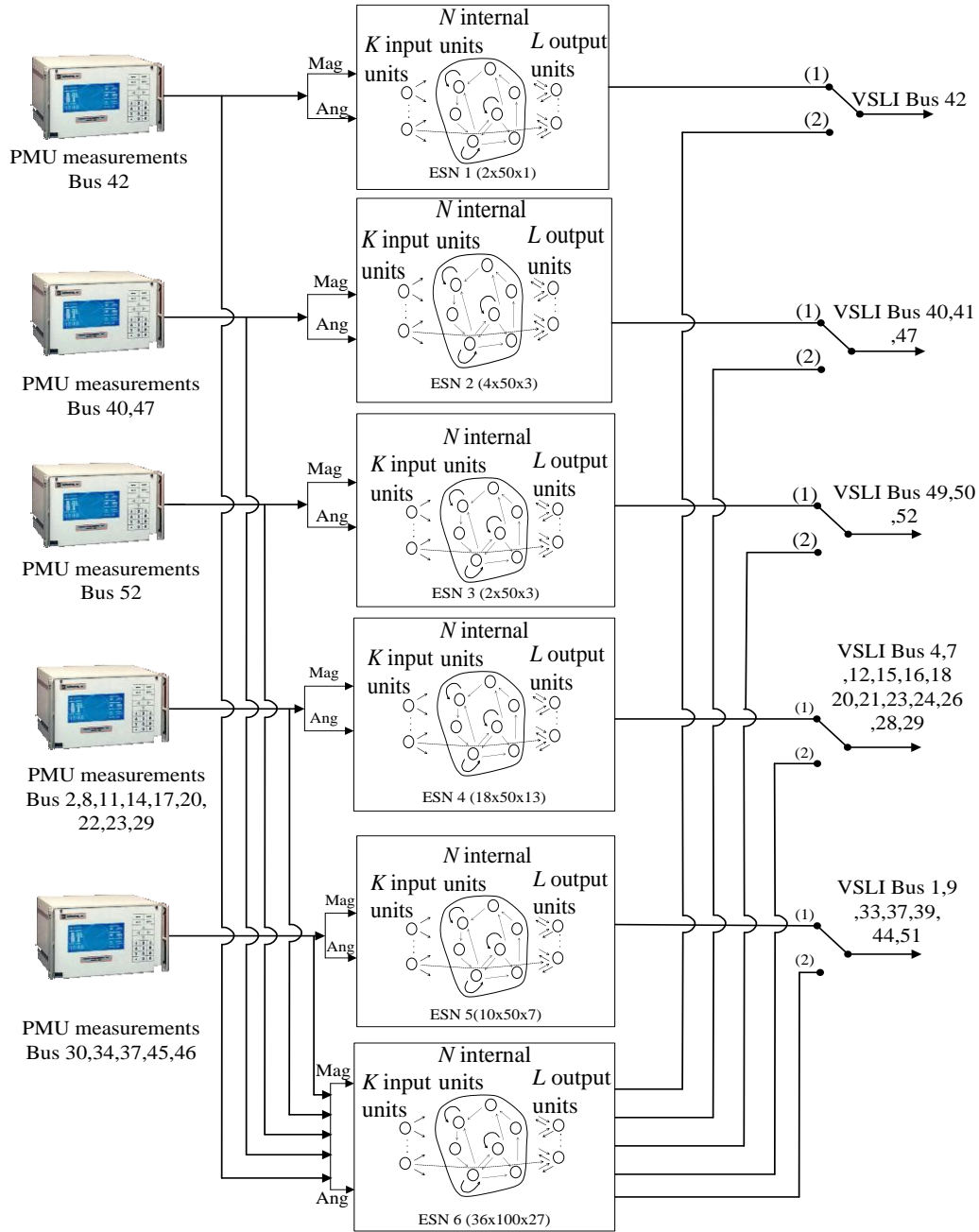
Fig. 5.13. Structure of ESN for VSLI estimation under normal and islanded operating conditions for IEEE68 bus system.

The results shown in Figure 5.12 and 5.13 demonstrate the dynamics of the WF and PEV during the three phase fault and their impact on system voltages. During the fault, the WF draws a high amount of reactive power, while its output real power is reduced.

Table 5.7. VSLI with Islanded Power System

IEEE 68	Using separate ESNs for each Island			Using Single ESN for all Islands		
bus	AVE MSE	Max MSE	St. Dev.	AVE MSE	Max MSE	St. Dev.
Island 1	8×10^{-5}	1.09×10^{-2}	7.5×10^{-4}	2.0×10^{-3}	6.1×10^{-2}	4.6×10^{-3}
Island 2	2.96×10^{-4}	3.5×10^{-2}	2.41×10^{-3}	5.9×10^{-3}	1.0×10^{-2}	4.0×10^{-3}
Island 3	2.26×10^{-4}	2.8×10^{-2}	1.86×10^{-3}	5.9×10^{-2}	8.8×10^{-1}	1.3×10^{-1}
Island 4	2.1×10^{-4}	1.2×10^{-2}	1.4×10^{-3}	2.2×10^{-3}	3.2×10^{-2}	1.1×10^{-3}
Island 5	1.3×10^{-3}	7.5×10^{-2}	7.5×10^{-3}	2.3×10^{-3}	4.2×10^{-1}	2.6×10^{-2}

The PEV on the other hand has a steady reduction in real power as well as real power out. The impact of the event is reduced system voltages and oscillations in VSLI (Figure 5.14). Figure 5.15 shows the corresponding VSLI at the three load buses following the fault. The three phase fault results in increase in VSLI at the load buses as voltages decrease owing to the increase of reactive power drawn by the WF during the fault.
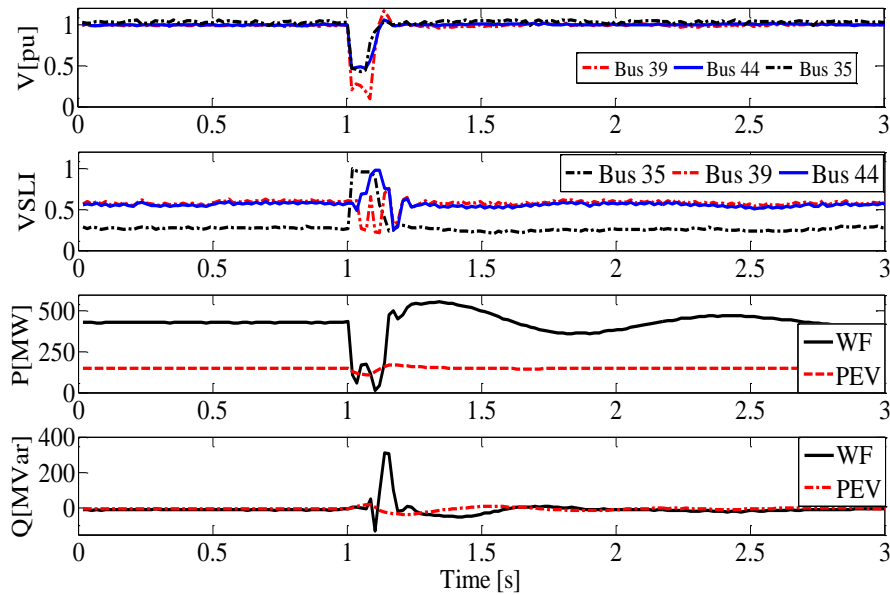
Fig. 5.14. Real power, reactive power and system voltages after a three phase fault.
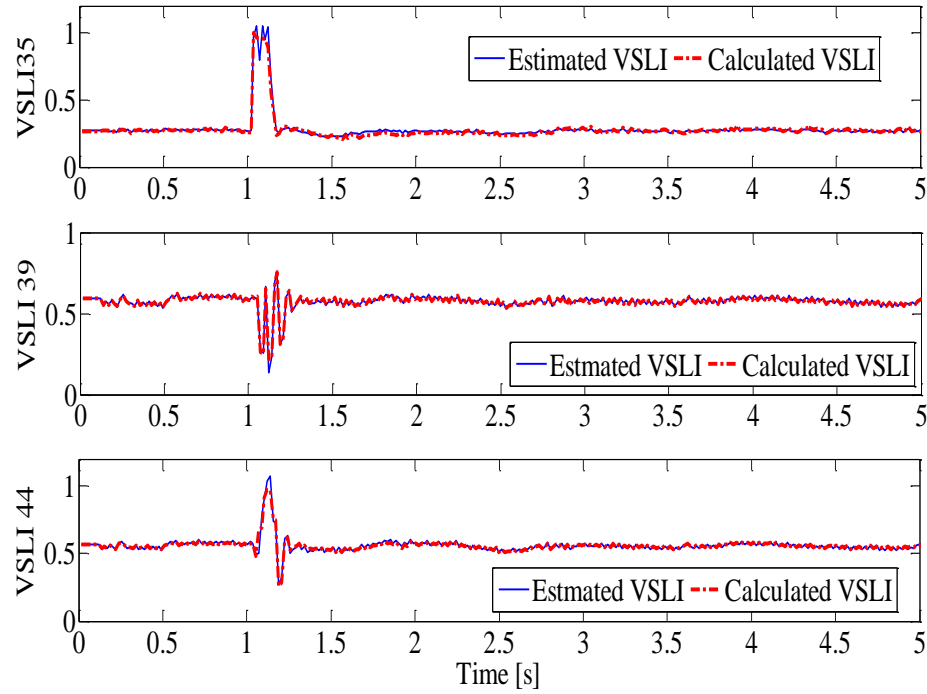
Fig. 5.15. ESN estimation of VSLI index during fault.

5.4. SUMMARY

An intelligent method for monitoring voltage stability in a smart grid using PMU information is presented in this dissertation. The method uses an Echo State Network to estimate Voltage Stability Load Index. The development of an optimal algorithm for placement of PMUs to ensure full system observability of the system both during normal and islanded operating conditions has been presented.

The optimal location of PMUs assure the smallest number of PMUs needed in order to implement voltage stability monitoring of the complete system during normal operating conditions and during defensive islanding conditions. Scalability of the approached has been studied using three test systems. Results for the three test system show a very close fit between estimated VSLI and target VSLI. The method of islanded ESN shows that the performance of the ESN in individual islands is better than that of a single ESN for the entire network. Finally the performance of the ESN approach for

monitoring VSLI in a smart grid with WF and PEV is illustrated. Results show a very close fit between the output of the ESN and calculated values of VSLI. The most accurate is the case of the smallest system with accuracy getting less with increased system size.

6. ADAPTIVE DYNAMIC PROGRAMMING FOR SECONDARY VOLTAGE CONTROL IN A POWER SYSTEM

6.1. INTRODUCTION

Voltage stability control in a power system with variable loads and sources, such as wind farms (WFs), that are intermittent in nature, require coordinated control of reactive power in order to assure optimal use of existing reactive power sources for maximizing voltage stability. The increased penetration of WFs and the use smart grid technologies such as plug-in electric vehicles have resulted in new challenges for power system stability control and opportunity for providing additional reactive power [55, 56]. Wind farms based on Doubly Fed Induction Generator (DFIG) can draw large amounts of reactive power during faults as the rotor side convertor terminals are short-circuited. During the fault duration, the wind turbine generator behaves like a squirrel cage induction generator and draws an increased amount of reactive power. The Static Synchronous Compensator (STACOM) is a power electronics based shunt FACTs device that can provide variable reactive power compensation needed to support system voltage and ensure adequate voltage stability margin both at the local and surrounding buses. However such FACTs devices are expensive and cannot be extensively used in increasingly complex smart grids. In order to optimize the reactive power support and voltage control provided by FACTs devices, a nonlinear optimal controller that dynamically adjusts the set reference voltage values for the STATCOM is developed in this dissertation.

Traditional linear PI controllers for STATCOM control are designed to operate optimally around specified operating points. As operating conditions change, the performance of these traditional controllers degrades, and is no longer optimal. To overcome this problem, an Adaptive Dynamic Programming (ADP) based controller is proposed. The proposed ADP controller is a non-linear optimal controller that is capable of optimal control for voltage stability through a wide range of system operating conditions.

To formulate the utility used in Adaptive Dynamic Programming, the Voltage Stability Load Index (VSLI) at load buses is estimated using the method of Echo State Network as described in section 5. The VSLI estimation approach is a Neural Network approach for determining the distance of the power system to instability. Reference [57] introduces a method of using an artificial neural network to predict the voltage stability margin of a power system obtained by continuation power flow based on synchrophasor measurements of voltage magnitudes and phase angles. In this dissertation, the VSLI approach developed uses voltage phasor information provided by PMUs in order to compute the voltage stability limit margin. The voltage stability margin gives the distance of the power system to the voltage stability limit. The technique uses local information at every load bus to obtain the Voltage Stability Load Index (VSLI) as a measure of the distance to instability in real-time.

The modified IEEE 68-bus test power system including two STATCOMs and a WF is modeled in the PSAT/MATLAB simulation. A closed loop model of the controller is used to provide auxiliary voltage (reactive) power control signals for coordinated optimal control of reactive power reference settings of the STATCOMs.

The rest of this dissertation is organized as follows: section II describes the smart grid model used for the development and testing of the ADP controller, while sections III and IV present the development of the training process. Simulation results showing the effectiveness of the proposed controller are presented in section V. Section VI is the conclusion.

6.2. POWER SYSTEM MODEL

Smart grids must be able to accommodate increasing penetrations of wind energy sources, and be able to support increased demand as the complexity of the electric grid continues to increase due to advances in use of smart grid technologies. Increased penetration of renewable energy sources such as wind farms have been driven by the need for more environmentally friendly energy sources and economic reasons [58]. Wind farms are intermittent in nature; and the power output of a wind farm is dependent on the wind speed and the control strategy for the wind generators such as that for DFIGs [59].

During fault conditions the amount of reactive power demand of wind farms is increased. An intelligent control method based on voltage stability load index of the system and adaptive dynamic control of reactive power resources in the smart grid is proposed to dynamically vary the reference voltage set point of two STATCOMs in order to improve system voltage control is implemented in this dissertation.

Figure 6.1 shows the Smart Grid model of modified IEEE 68 bus system with wind farm, and two STATCOMs included at buses 69, bus 70, and bus 50 respectively. The STATCOMs are used to perform secondary voltage control at buses 35, 39 and bus 50. Both the STATCOMs are first controlled using conventional PI controllers to perform voltage control for the load area and supply reactive power for voltage control.
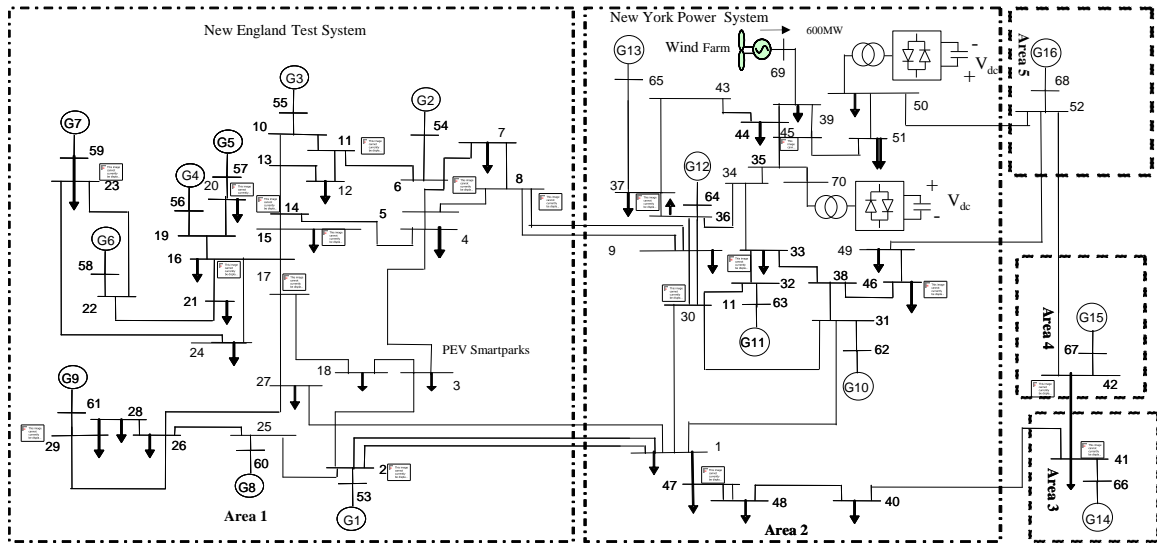
Fig. 6.1 Modified IEEE 68 bus system with WF, and STATCOMs included in addition to the normal PI controller used in the STATCOMs, the ADP controller provides auxiliary voltage signals that ensure optimal control of system voltages.

6.3. PROPOSED CONTROLLER

The advent of phasor measurement units has made it possible for voltage magnitude and phase angle information for the system to be readily measured and utilized for monitoring voltage stability of the system in real-time. The proposed Adaptive Dynamic Programming controller utilizes voltage stability monitoring

information in order to provide auxiliary inputs for two STATCOMs aimed at improving system voltage control.

The ADP controller proposed is based on the Action Dependent Heuristic Dynamic Programming (AD-HDP) model of the Adaptive Critic Designs (ACD) family proposed by Werbos. The ADHDP is a model independent approach to the Heuristic Dynamic Programming (HDP) [33]. However, in the current application, the model is included to provide the estimated voltage stability load index of the system that is needed to provide the utility function used with the critic network of the controller. Figure 6.2 shows a schematic of the proposed controller interfacing with the plant where, Vref$_{\_STATCOM\_1}$ and Vref$_{\_STATCOM\_2}$ are auxiliary reference voltage signals for the two STATCOMs, and A(k) = [ΔVref$_{\_STATCOM\_1}$, ΔVref$_{\_STATCOM\_2}$] is a vector of the controller outputs. Since the approach does not require a model to predict plant variables, but uses actual measurements of plant variables, its operation is inherently faster and more suitable for on-line learning control applications.
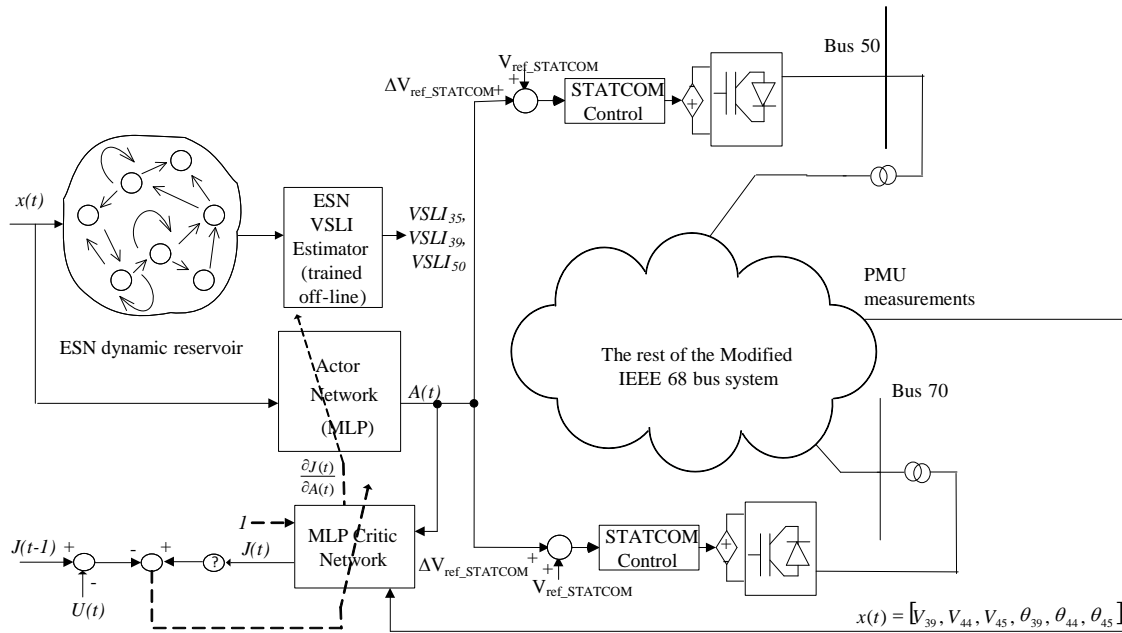
Fig. 6.2 Proposed AD-HDP based Secondary Controller. The ADP controller provides auxiliary voltage reference signals for two STATCOMs.

Adaptive Critic Design systems utilize concepts of reinforcement learning and dynamic programming in implementing the design of optimal control systems. ACDs have explored the possibility of designing systems in the continuous state space and addressing generalization and design robustness [33, 34]. There are three main components that and ACD consists of: the actor which is trained to dispense optimal control actions to the plant that maximizes/minimizes the cost to go function over time. The critic network approximates the cost to function of dynamic programming at each time step thus providing an evaluation of each control action. The model network is used to provide future states of the plant and is needed to estimate cost-to-go function over future time intervals.

In the present application, the on-line plant information used in the approach consists of measurements of bus voltage magnitude and phase angles at three load buses. This information is also used as input for an ESN based estimator for Voltage Stability Load Index of the bus voltages used in the utility formulation. Thus input information to the controller consists of voltage magnitude and phase angles at the control buses and the utility.

The critic network consists of a multilayer perceptron with three layers: the hidden layer neurons have sigmoidal activation functions while the input and output layers are linear function neurons. The Critic network learns to approximate the cost-to-go function, $J(t)$ using the measured plant outputs and the actor outputs and the utility $U(t)$. The cost-to-go function J is given by:

$$J(t) = \sum_{k=0}^{\infty} \gamma^k U(t+k) \tag{1}$$

Where $U(t)$ is the utility function which can be described by a linear combination of plant measurements of VSLI at the three load buses that are being controlled and γ is a discount factor for infinite horizon problems ($0 < \gamma < 1$). The value of γ used in this dissertation starts with a small value of 0 during training and increased gradually is small steps to 0.75. The small value of γ at the start assures that a smaller component of the utility future terms are used initially until the controller achieves stability, then the value

of γ is increased gradually to take into account future values of the utility. The utility function used in this dissertation is given in (2) and selection of the coefficients was done by testing different values experimentally.

$$U(t) = A_1(VSLI_{35SS} - VSLI_{35}(t))^2 + A_2(VSLI_{39SS} - VSLI_{39}(t))^2$$
$$+ A_3(VSLI_{50SS} - VSLI_{50}(t))^2 \tag{2}$$

The actor network minimizes the cost-to-go function *J(t)* by providing inputs *A(t)* to the plant and the critic network, with utility function based on VSLI. The actor provides optimal control laws to the plant. The three neural networks together form the adaptive dynamic programming controller for voltage stability control.

6.3.1. Model Network. The model network developed in this dissertation uses an ESN NN to estimate VSLI at three load buses. As given in equation (2) values of VSLI are used for computing the utility function measure. The ESN structure has six input neurons with linear functions, 100 internal neurons based on sigmoidal function and three linear neurons at the output. Where the ESN inputs are measured values of voltage magnitude and phase angle at bus 35, bus 39, and bus 50. The ESN consisting of a dynamic reservoir with input, internal and feedback weight matrices (W^{in}, W, and W^{out}) respectively with the echo state property was developed following the steps described in [32].

The input and output layer neurons have linear functions; while dynamic reservoir neurons have sigmoid functions. The ESN outputs are the estimated values of VSLI at the three load buses for adaptive dynamic control (Figure 6.3).

$$y(n+1) = f(u(n+1)W^{out}, x(n+1), y(n)) \tag{3}$$
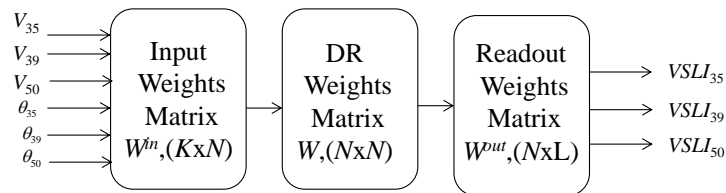
Fig. 6.3 ESN Model Structure

The ESN is trained offline using data collected for a wide range of operating conditions. Training and testing data is collected for the system with: (i) uniformly increasing load from 0 to 5 load factor in the New-York Area (Buses 33, 35, 36, 39, 44, 50, and 51), and (ii) with each of the three buses participating in VSLI monitoring (Bus 35, 39, 50) stressed individually over a load factor of 0 to 5. A total of 1256 training and testing data sets are used to train the ESN for estimating VSLI. The large set of training data used assures that the ESN is trained for a wide range of operation conditions, in order to ensure that the ESN is successful when implemented for online estimation of VSLI. The inputs to the ESN are measurements of voltage magnitudes and angles at buses 35, 39, and 50 that are normalized in the range of -1 to 1 for better performance. The outputs are values of VSLI estimated at the three buses, 35, 39, and 50. Different sizes of the dynamic reservoir are used: 20 units, 50 units, and 100 units. The performance of each size ESN for estimating VSLI is shown in Table 6.1.

Table 6.1 Esn Performance

DR units	Av. MSE	Min. MSE	Max. MSE	Std. dev.
20	3.2×10^{-4}	4.8×10^{-5}	9.4×10^{-4}	2.8×10^{-4}
50	2.8×10^{-4}	3.1×10^{-5}	7.8×10^{-4}	2.0×10^{-4}
100	1.5×10^{-4}	1.4×10^{-5}	4.5×10^{-4}	1.3×10^{-4}

The performance of the ESN with 100 units in the DR is comparatively better than that of the ESNs with 50 and 20 units since it has the lowest MSE; it is thus used for the model network used in the rest of the work in this section.

6.3.2. Utility Function Design. The objective of the adaptive dynamic programming controller developed in this dissertation is to minimize Voltage Stability Load Index (VSLI) deviations at buses 35, 39, and 50. Therefore the utility function utilizing VSLI deviations at the three load buses has been defined as given in equation (6) below.

$$U(t) = A_1(VSLI_{35SS} - VSLI_{35}(t))^2 + A_2(VSLI_{39SS} - VSLI_{39}(t))^2$$
$$+ A_3(VSLI_{50SS} - VSLI_{50}(t))^2$$

(6)

The subscripts '*ss*' represent steady state values of VSLI. The coefficients A1, A2, and A3 are weighting factors with a total sum of 1 such that VSLI deviations at each bus contribute to the utility function proportionally to the voltage stability sensitivity of each bus (Table 6.2). QV sensitivity analysis of the system is performed to determine bus participation at each of three buses. Appendix C gives the QV sensitivity data for the system used to determine the utility function.

Table 6.2 VSLI Coefficients

Eigenvalue #	Eigenvalue	Bus #	Participation Factor	VSLI coefficient
31	152.77	35	0.13237	0.36
36	126.34	50	0.17925	0.4
49	100.49	39	0.13543	0.24

Bus 39 has the highest Q-V sensitivity since its participation is higher in the smallest of the three eigenvalues. The second most sensitive is bus 50 then followed by bus 35. The coefficients of the utility function A1, A2, and A3 are chosen to give weighting factors of VSLI values at the three buses to take into account the eigenvalues and participation factors. The eigenvalue is multiplied by the participation factor and each coefficient is a fraction of the total of the three products.

6.3.3. Critic Network. The critic network is implemented using a three layer multilayer perceptrom (MLP). The inputs to the critic are the measured plant states consisting of voltage magnitudes and angles at the three buses, 35, 39, and 50 and outputs of the action network along with their two time-delayed values. The output of the critic is the estimated cost-to-go function J(k) in (1).

The critic network learns the following error over time:

$$\|E_C\| = \frac{1}{2} \sum_k E_C^T(k) E_C(k) \tag{4}$$

where,

$$E_C(k) = J(k) - \gamma J(k+1) - U(k) \tag{5}$$

and *U(k)* is a utility measure that serves as the performance measure for the ADP controller, and γ is a discount factor between 0 and 1. Firstly, the critic network is pre-trained using PRBS signals to provide auxiliary voltage reference signals for the STATCOM 1 and STATCOM 2 as well as input signals to the critic network together with measurements of voltage magnitude and angles at buses 35, 39, and 50. Two time delayed values for critic inputs are used during training as shown in Figure 6.4.
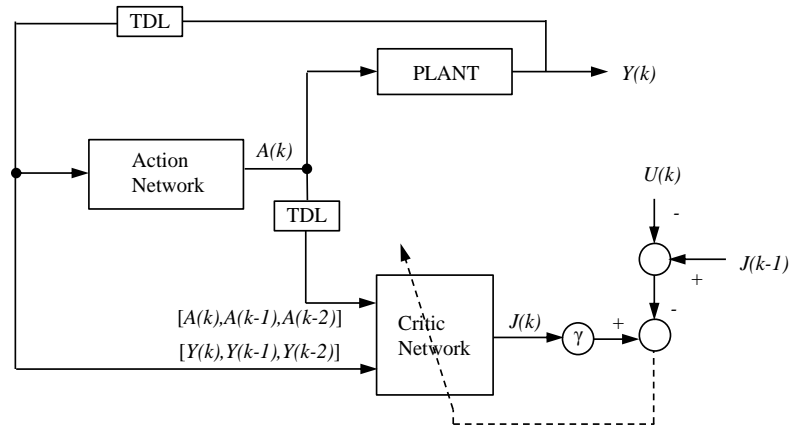
Fig. 6.4 Critic Network Adaptation. The utility function is derived using equation (2). Critic network adaptation is done using backpropagation by minimizing the critic error in (5).

The critic is trained to approximate the cost-to-go function *J(t)* of the Hamilton-Jacobi-Bellman equation (1). The critic network training cycle is shown in the flow chart in Figure 6.5. During training, the discount factor is varied from 0 and increased gradually as the controller stabilizes to about 0.75.
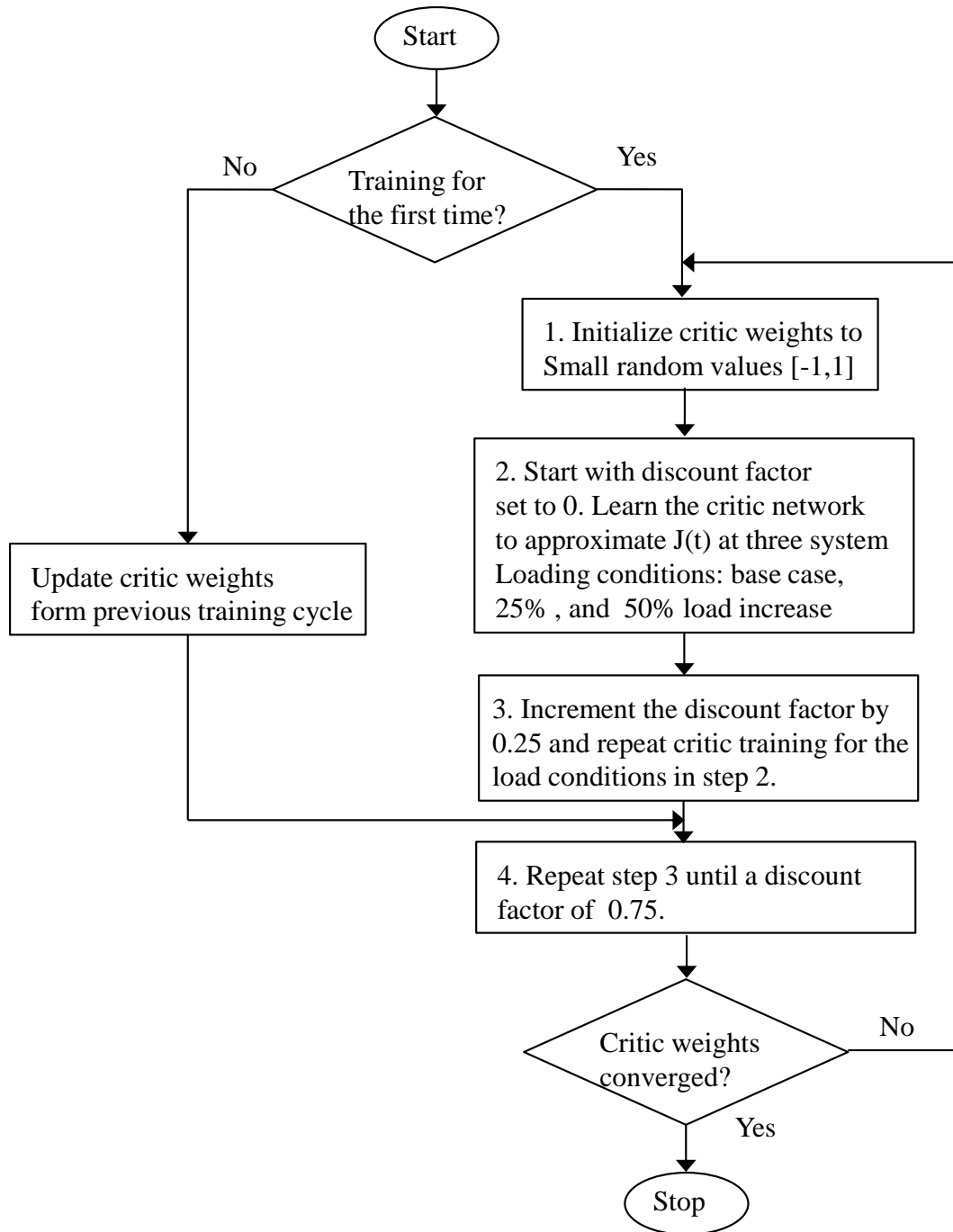
Fig 6.5. Flowchart for the critic network training.

6.3.4. Action Network. The objective of the action network is to optimize the system control trajectory so that the cost-to-go function *J(t)* is minimized over time. To achieve this objective the action network is adapted $E_A(k) = \partial J(k)/\partial A(k)$, using the

error signal, obtained by backpropagating a constant, $\partial J(k)/\partial J(k)=1$ through the critic network (Figure 6.6).

After critic pre-training, the actor is pre-trained using the PRBS as input for the plant and the critic network. The actor error signal is obtained by backpropagating 1 through the critic network. After the actor pre-training, the output of the actor is fed to the plant (STATCOM 1 and STATCOM 2 auxiliary voltage reference) and the critic network. The critic and the actor are then further trained alternately. During the critic and actor alternate training, critic weights are adapted while actor weights are kept constant and then critic weights are kept constant while actor weights are adapted. The alternate training cycles are repeated until there is no more change in both actor and critic weights (Figure 6.7).
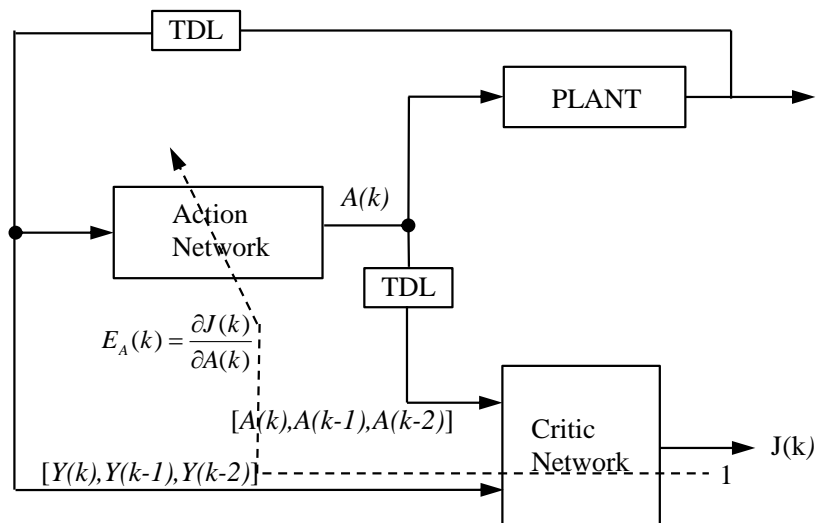
Fig. 6.6 Action Network Adaptation. The action network error is obtained by backpropagating a constant 1, through the critic network.

```
              ┌─────────┐
              │  Start  │
              └─────────┘
                   │
                   ▼
        ┌──────────────────────────┐
        │ 1. Initialize actor      │
        │ weights to               │
        │ Small random values      │
        │ [-1,1]                   │
        └──────────────────────────┘
                   │
                   ▼
        ┌──────────────────────────┐
        │ 2. Pre-train actor       │
        │ network with PRBS        │
        │ auxiliary voltage        │
        │ reference signals for    │
        │ STATCOMS 1 and 2.        │
        └──────────────────────────┘
                   │
                   ▼
        ┌──────────────────────────┐
        │ 3.Train the actor        │
        │ network for NA           │
        │ using the trained        │
        │ critic network           │
        └──────────────────────────┘
                   │
                   ▼
        ┌──────────────────────────┐
        │ 4.Alternately train      │
        │ critic and actor         │
        │ networks for NC and NA   │
        │ cycles repeatedly.       │
        └──────────────────────────┘
                   │
                   ▼
              ◇ Actor and critic
                Weights converged? ◇──── No
                   │
                   ▼
              ┌─────────┐  Yes
              │  Stop   │
              └─────────┘
```
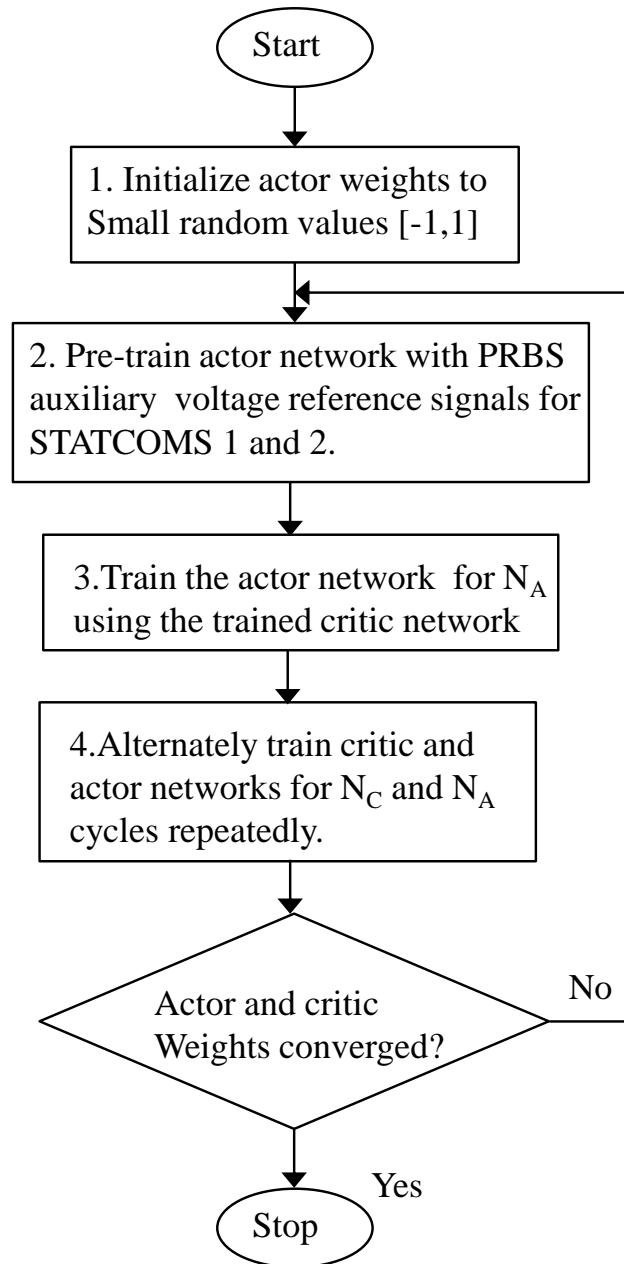
Fig 6.7. Flowchart for the actor and critic alternate training.

6.3.5. Closed Loop Training for Actor and Critic Networks. The training stage of the critic and action networks has two separate training cycles: one for the critic and the other for the action network. The critic is pre-trained to approximate the cost-to-go function $J(t)$. During critic pre-training, pseudorandom binary signals (PRBS) are used as auxiliary inputs to the plant. Measured states of the plant consisting of voltage

magnitudes and angles at buses 35, 39, and 50 are used as input signals for the critic network. After the critic pre-training is complete, critic weights are fixed, the action network is pre-trained using the PRBS signal as the inputs to the plant and resulting plant states as action network inputs. The action network learns to track the PRBS signal. The pre-trained critic and action networks are then trained one after the other using the output of the action network as input for the plant as described in the diagrams shown in Figure 6.7 for a number critic network training cycles, N_C and action network training cycles, N_A respectively. The procedure of training the critic and action networks one after the other is repeated until accepted performance in achieved [64-66].

The signal flow diagram for the Adaptive Dynamic Controller developed in this dissertation is shown in Figure 6.8 and the description is provided below:
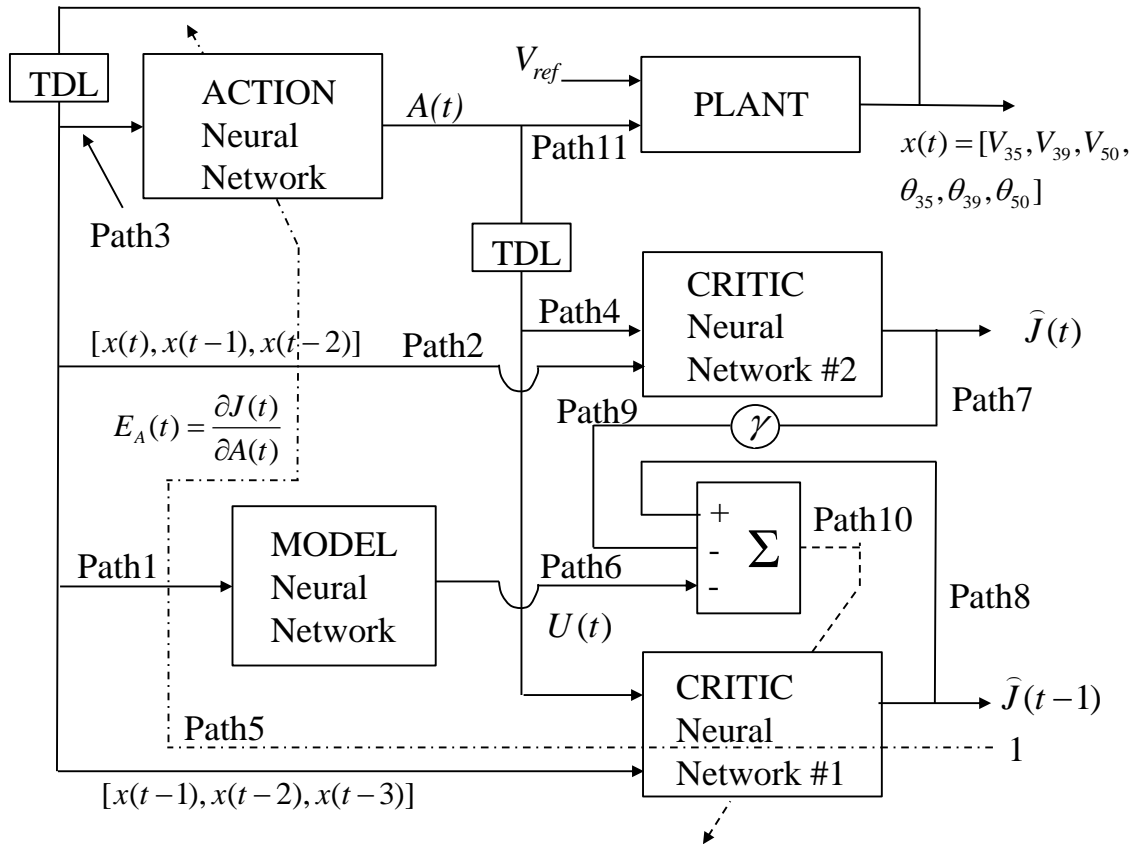
Fig. 6.8 Adaptive Dynamic Programming controller signal flow diagram.

(i)   Path 1 represents the outputs of the plant fed into the model network, to provide the utility function. The outputs of the plant are: *x(t), x(t-1), and x(t-2).*

(ii)   Path 2 represents the outputs of the plant fed into the Critic network #2. These outputs are: *x(t), x(t-1), and x(t-2).*

(iii)   Path 3 represents the outputs of the plant fed into the Action network. These outputs are: *x(t), x(t-1), and x(t-2).*

(iv)   Path 4 represents the outputs of the Action network fed into the Critic network. These outputs are: *A(t), A(t-1), and A(t-2).*

(v)   Path 5 represents the backpropagated signal of the output of the Critic network fed into the Action network, $\partial J / \partial A$. These outputs are the backpropagated signal on path 5 is obtained from:

$$\frac{\partial J(t)}{\partial X_C(t)} = W_C^{out}(t).diag\left[d_{Ci}(t)(1-d_{Ci}(t))\right]W_C^{in}(t)$$

Where d_{Ci} are the decision vector elements, and W_C^{out} and W_C^{in} are the output and input weights of the critic network respectively.

(vi)   Path 6 represents the utility function:

$$U(t) = 36*(0.2313 - VSLI_{35}(t))^2 + 24*(0.1930 - VSLI_{39}(t))^2$$
$$+ 40*(0.3505 - VSLI_{50}(t))^2$$

(vii)   Path 7 represents the output of Critic network#2,*J(t)*

(viii)   Path 8 represents the output of Critic network#1,*J(t-1)*

(ix)   Path 9 is the product of the discount factor γ and the path 7 signal, resulting in the term $\gamma \widehat{J}(t)$.

(x)   Path 10 represents the Critic network error $E_{C2j} = Path8 - Path9 - Path6$

$$E_{C2j} = \widehat{J}(t-1) - U(t) - \gamma J(t)$$

(xi)   Path 11 represents the output of the Action network which is fed to the plant:

$$A(t) = [\Delta V_{ref\_STATCOM1}, \Delta V_{ref\_STATCOM2}]$$

6.4. SIMULATION RESULTS

The development of an adaptive dynamic programming controller for secondary voltage control in a smart grid is implemented for the modified IEEE 68 bus system. In order to evaluate the performance of the ADP controller, the modified IEEE68 bus system is simulated with the variation of load in the load area and evaluating the system response with and without the controller. Test results for each stage of the controller development are presented in this section.

6.4.1. Model Network. Simulation results in Figures 6.9 - 6.15 show the on-line performance of the model network for estimation of VSLI estimation. The impact of the WF on system voltages and estimated VSLI index are also. With no WF included, the system voltages have a flat profile at steady state (Figure 6.9) and the steady VSLI values (Figure 6.10).
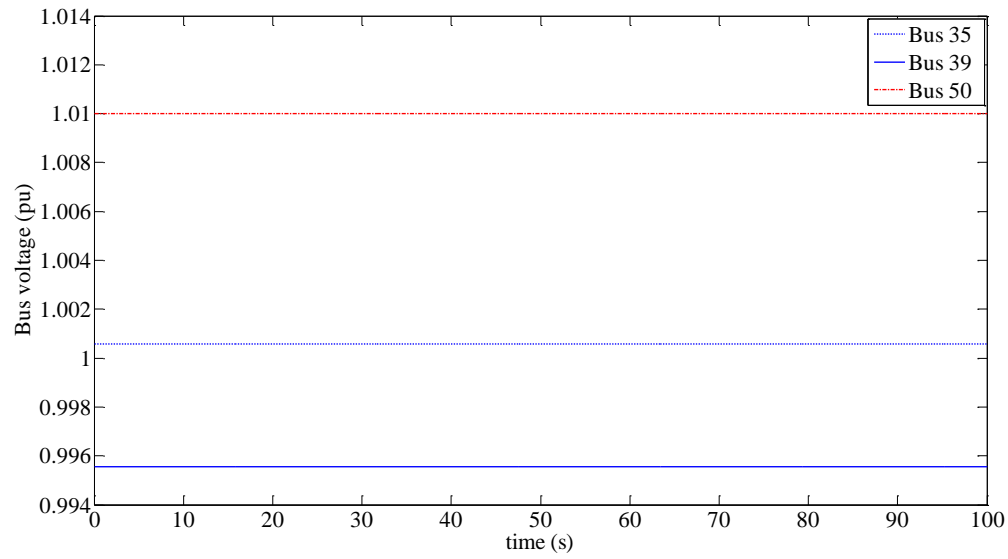
Fig. 6.9 Bus voltage at steady state with no wind farm included.
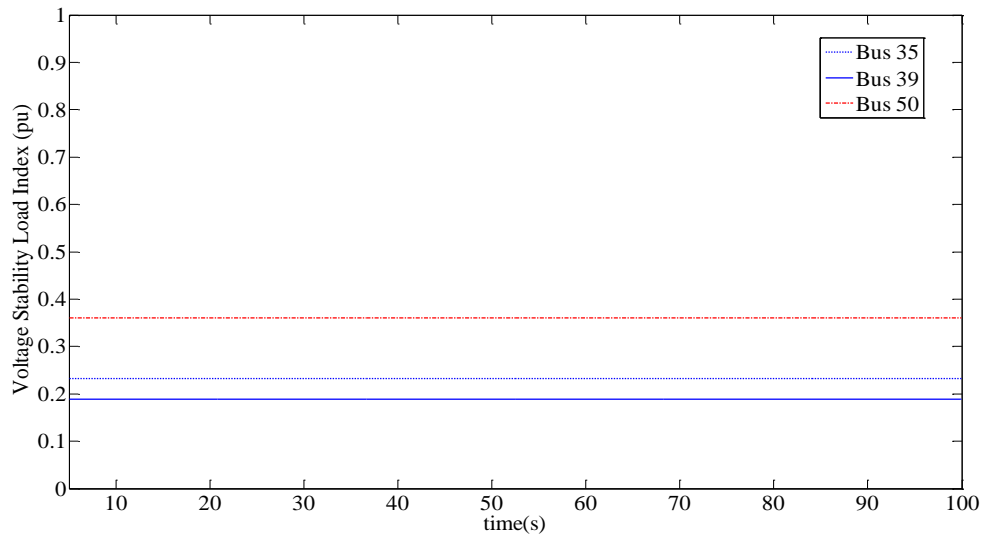
Fig. 6.10 VSLI at steady state with no wind farm included.

The effect of WF speed variation on system voltage and VSLI are shown in Figure 6.11 to 6.14. The plot of wind speed variation used in the simulation is generated randomly to model wind speed change in DFIG wind farms. As shown in Figures 6.11 and 6.12, variations in wind speed result in the real power output of the DFIG fluctuating. The effect of the fluctuations on system voltages and VSLI are captured in the plots in Figures 6.13 and 6.14 respectively. The results show that the ESN approach successfully estimates VSLI in the system with the WF model included.
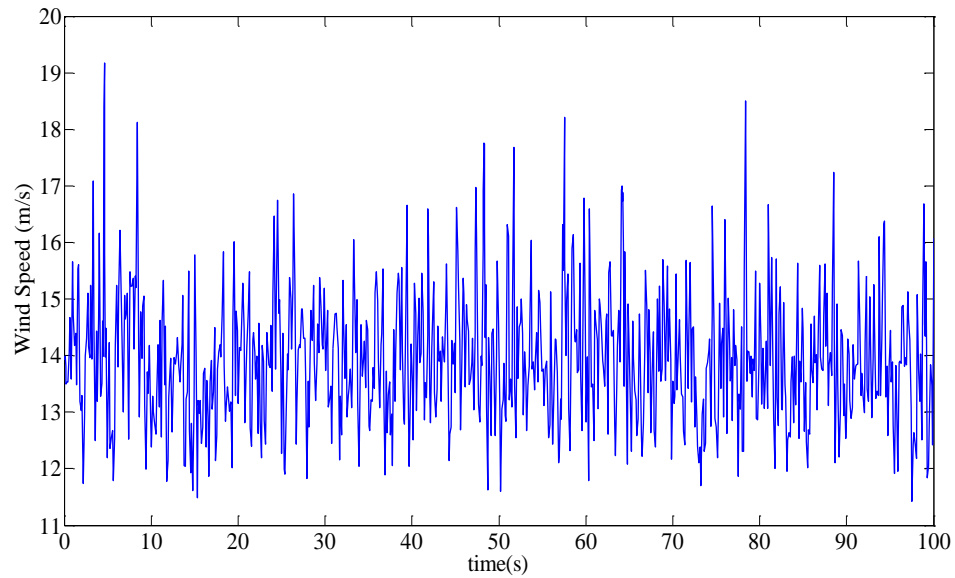
Fig. 6.11 Wind Speed
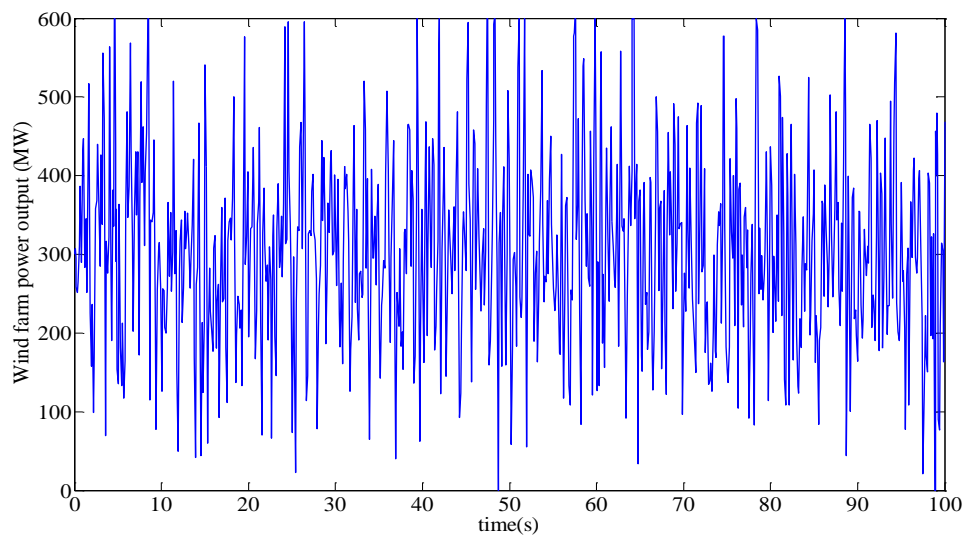
Fig. 6.12 Wind Farm Power Output
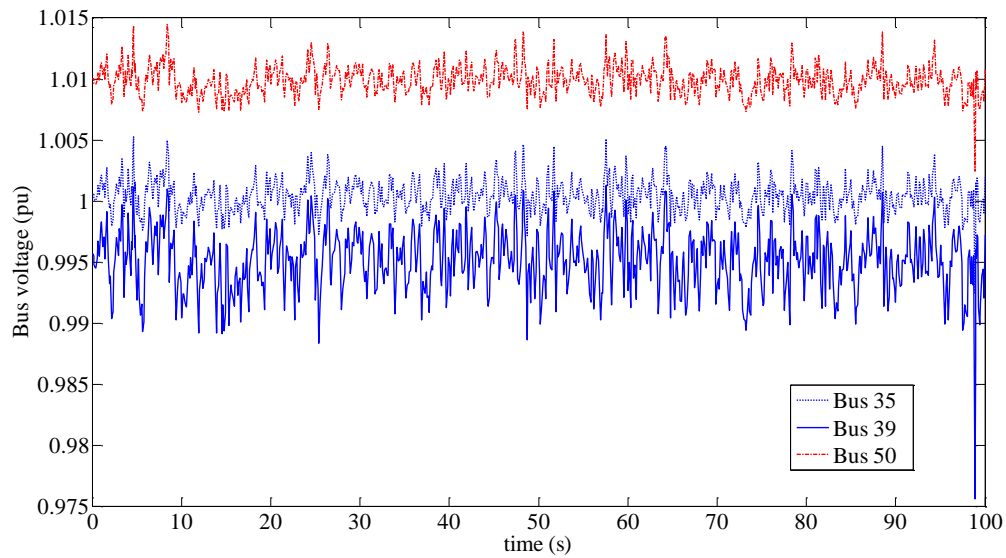
Fig. 6.13 System voltages with wind farm included.
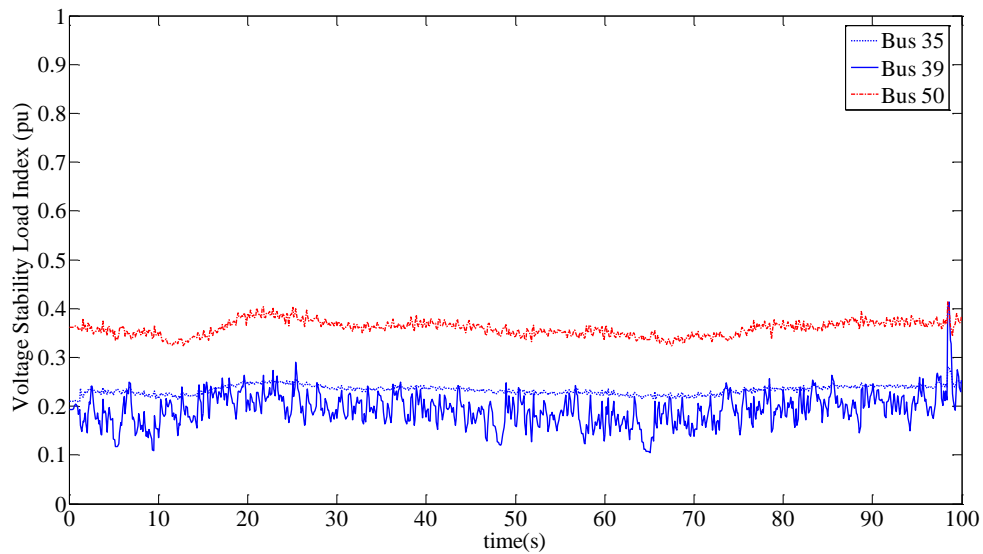
Fig. 6.14 VSLI at steady state with wind farm included.

Further, the performance of the ESN approach for estimating VSLI during faults is considered. A three phase to ground fault is applied at bus 1 for 80 ms. The graph in Figure 6.15 shows the plot of VSLI at the three load buses considered both with the WF and no WF included. The results show that the ESN approach successfully captures the system dynamics during the fault.
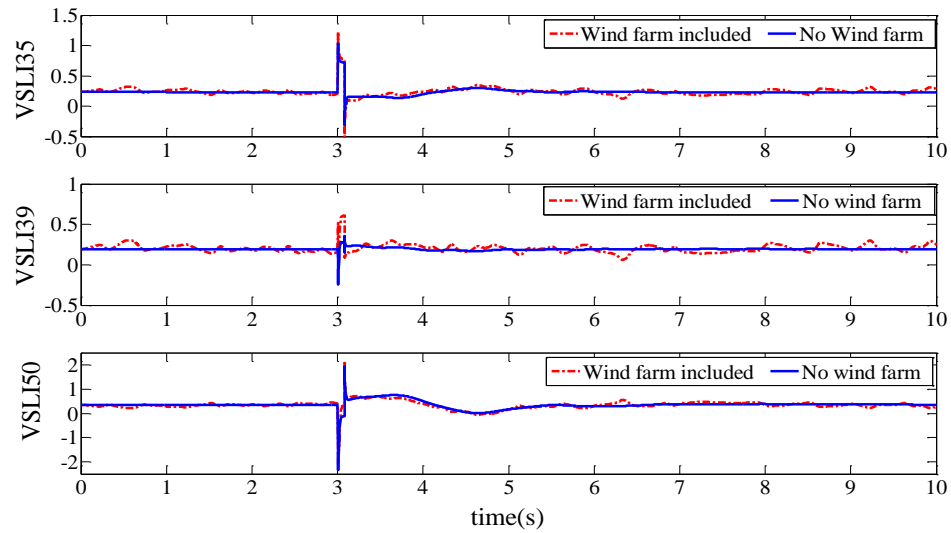
Fig. 6.15 Comparison of ESN VSLI estimation with and without the wind farm

6.4.2. Utility Function. The utility function is derived from the Model network output of VSLI at three load buses using (2). Figure 6.16 shows the calculated utility for the base case system with a fault at bus 1 and the STATCOM auxiliary voltage reference using a PRBS respectively. The auxiliary reference PRBS for the STATCOM is shown in Figure 6.17. These results validate the performance of the utility function to accurately capture the system dynamics
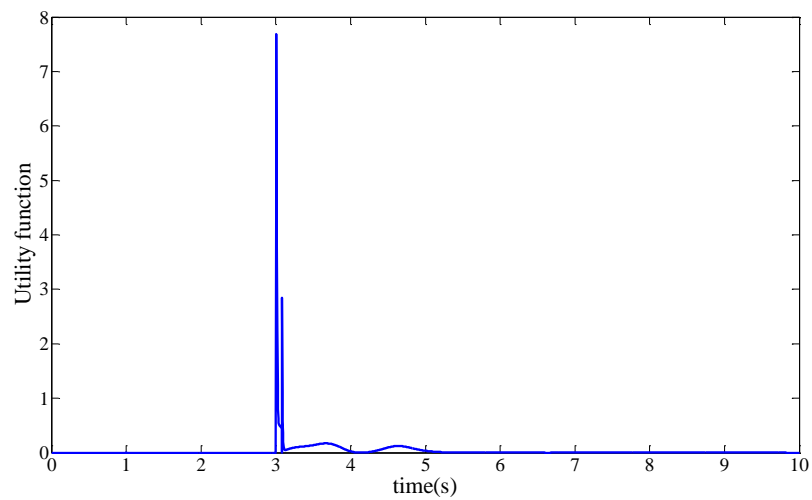
Fig. 6.16 Utility function during an 80ms three phase ground fault at bus 1
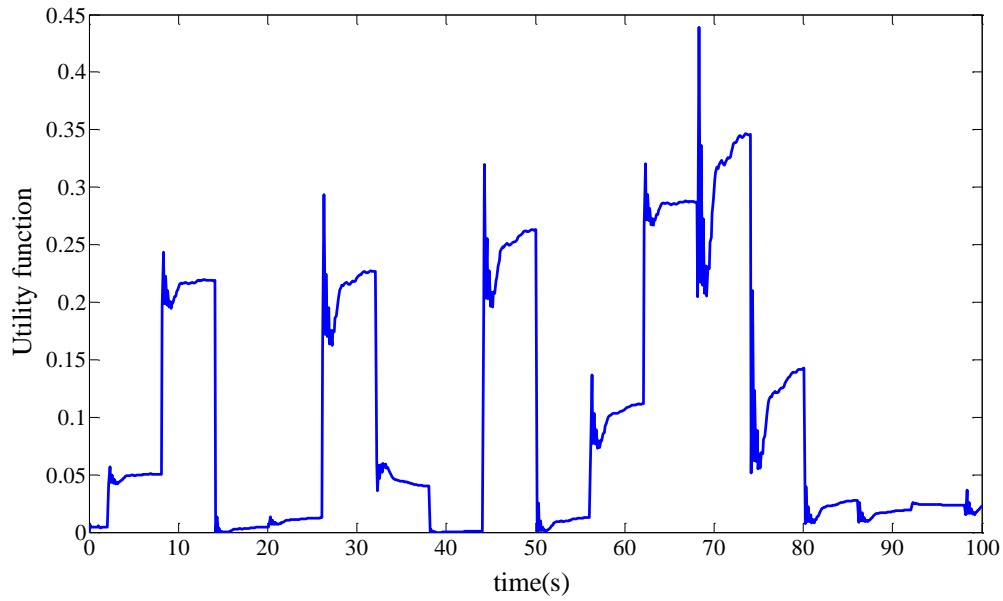
Fig. 6.17 Utility function Performance with PRBS Signal

6.4.3. Critic Network. The critic network is trained using the procedure described in section 6.3.2 for different operating conditions of the plant. Simulation results for critic training under three different operating conditions: base case and 50% load increase. The training procedure starts with the discount factor, γ is first set to 0, and the critic learns for three loading conditions of the system then the load factor is increased by 0.25, again the critic is trained for three loading conditions above. The process of incrementing the discount factor and training for each of the different loading conditions is carried out until critic network is trained. Simulation results at each step of the actor training procedure above are presented in Figures 6.18 to 6.41 below.

6.4.4. Actor Network. Simulation results for the Actor pre-training are presented in this section. PRBS signals are used to perturb the plant and the trained critic network is used to train the actor network by providing feedback signals used for actor training. The Actor network pre-training results using the trained critic with PRBS signal inputs are shown in Figures 6.42 to 6.48 below. Figures 6.42 to 6.48 show the system voltages, actor error signals, pseudo-random binary signals, and critic outputs during actor pre-training.
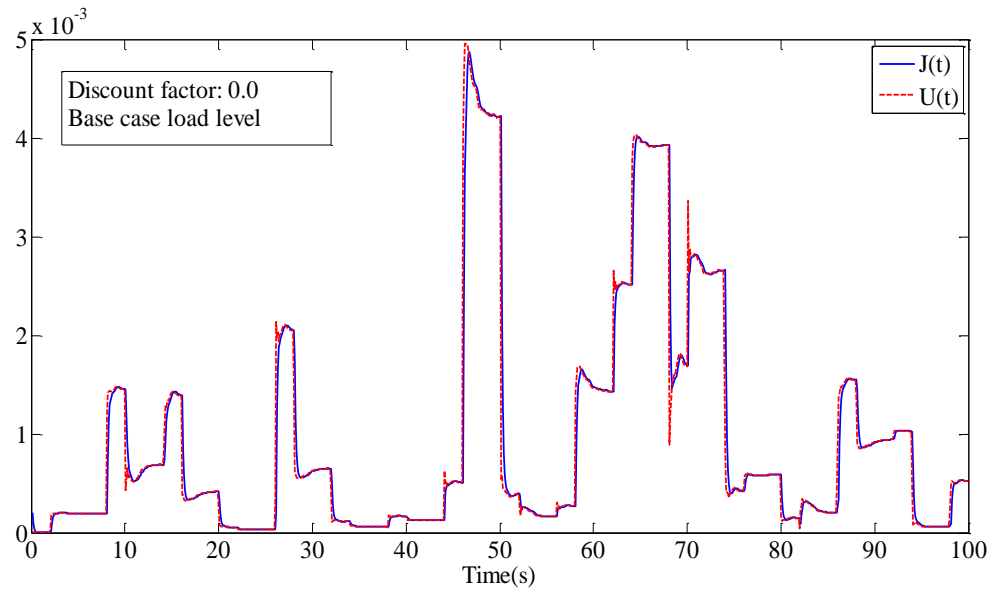
Fig. 6.18. Base case with discount factor set to 0. Plot of utility function U(t), cost-to-go function, J(t).
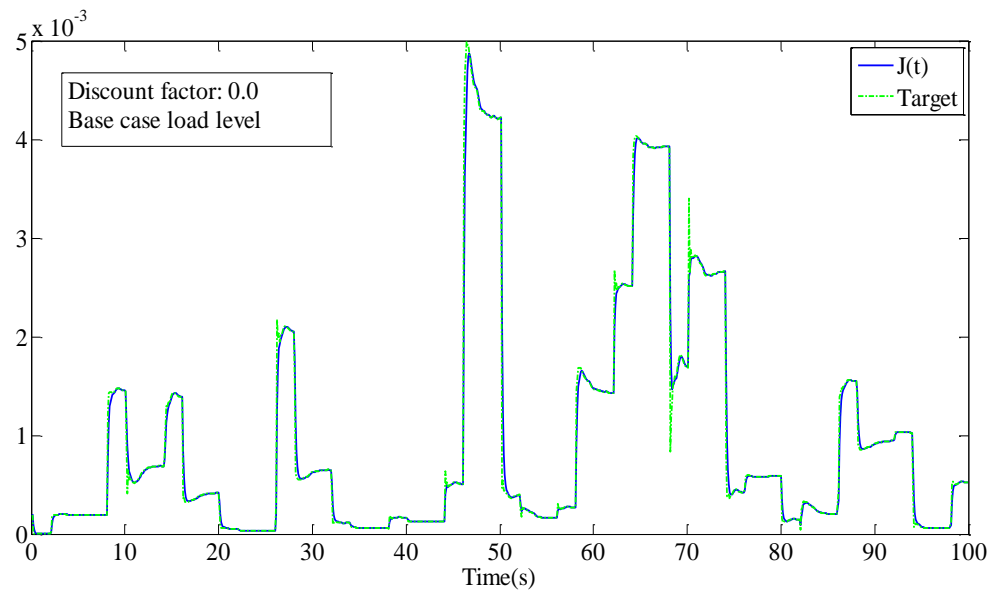
Fig. 6.19 Base case with discount factor set to 0. Plot of cost-to-go function, J(t) and its target.
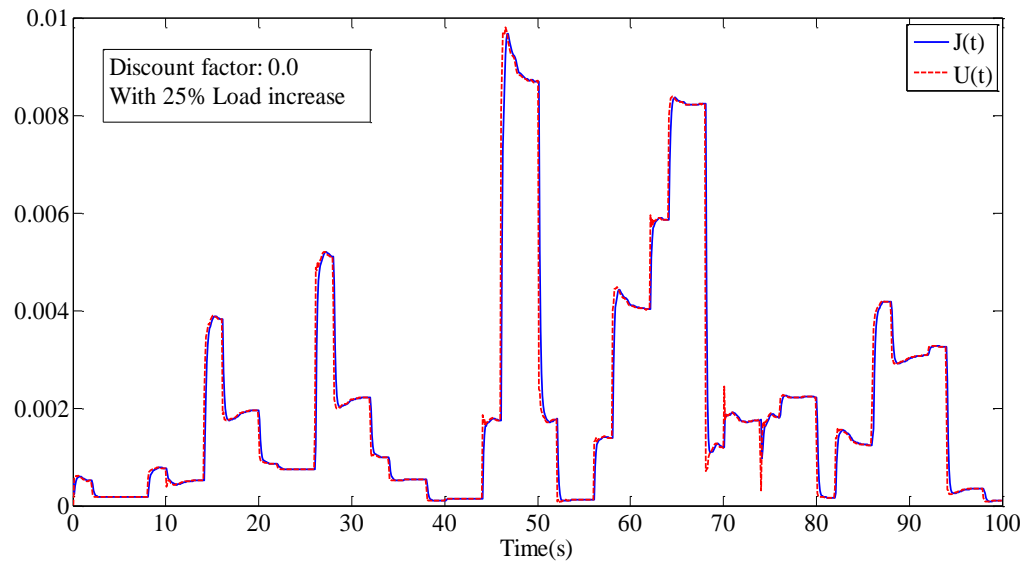
Fig. 6.20 25% load increase with discount factor set to 0. Plot of utility function, U(t), cost-to-go function, J(t).
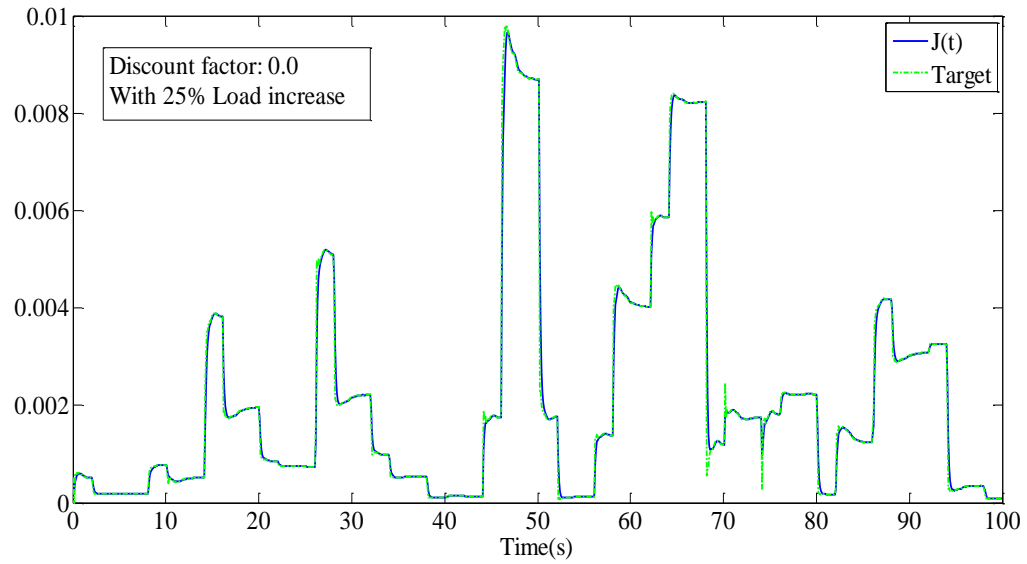
Fig. 6.21 25% load increase with discount factor set to 0. Plot of cost-to-go function, J(t) and its target.
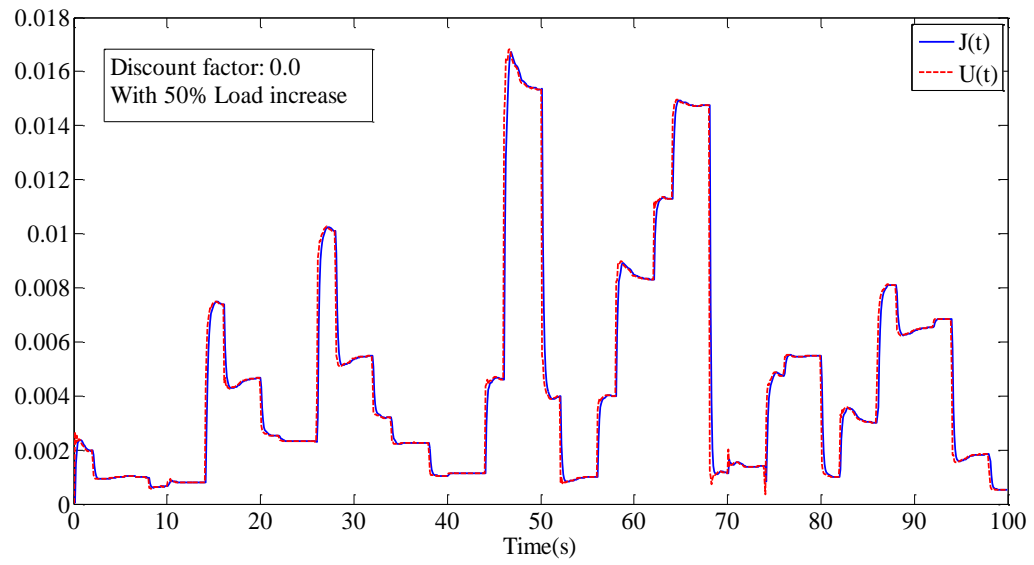
Fig. 6.22 50% load increase with discount factor set to 0. Plot of utility function, U(t), cost-to-go function,J(t).
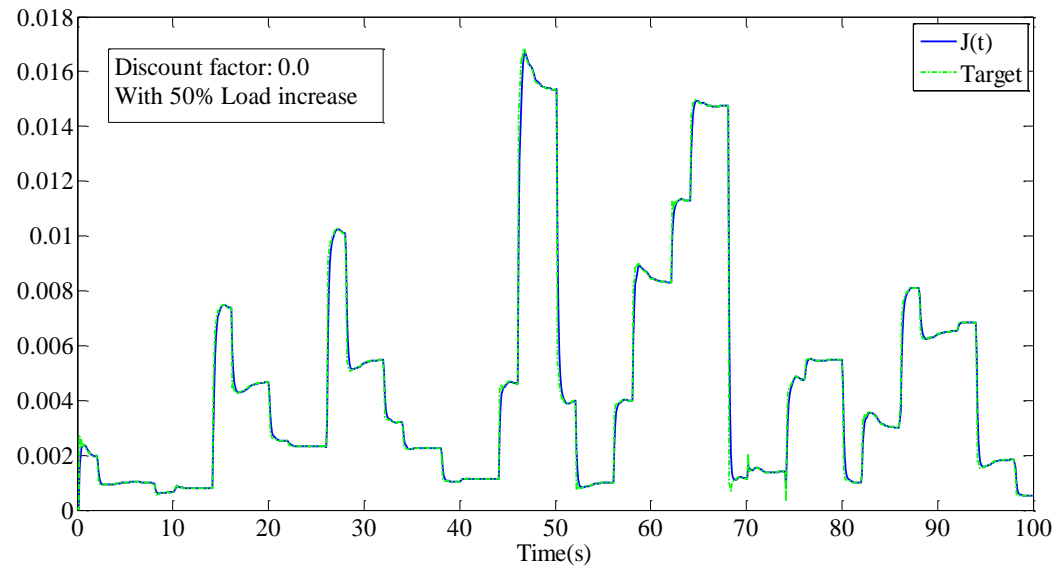
Fig. 6.23 50% load increase with discount factor set to 0. Plot of cost-to-go function, J(t) and its target.
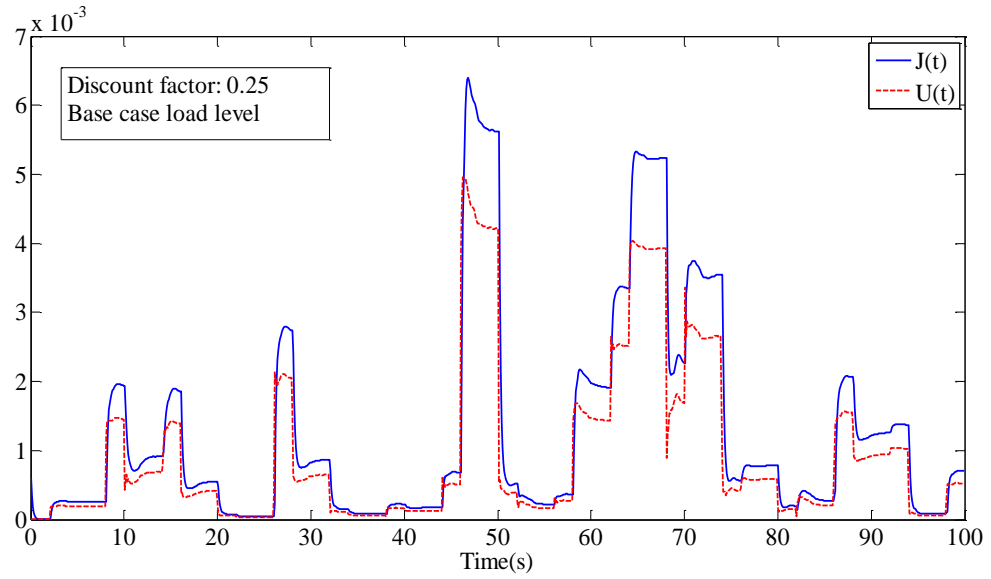
Fig. 6.24 Base case with discount factor set to 0.25 Plot of utility function, U(t), cost-to-go function, J(t).
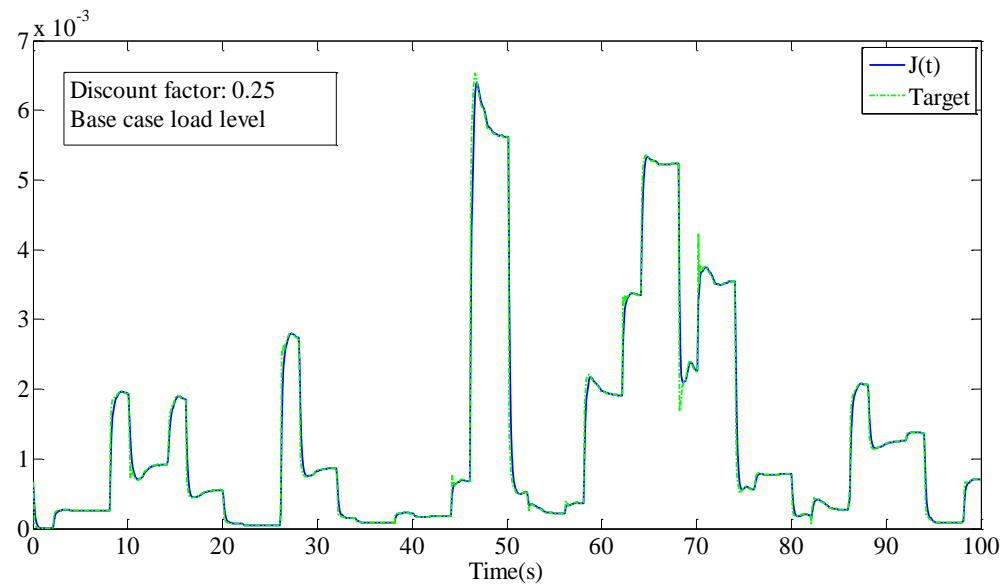
Fig. 6.25 Base case with discount factor set to 0.25 Plot of cost-to-go function, J(t) and its target.
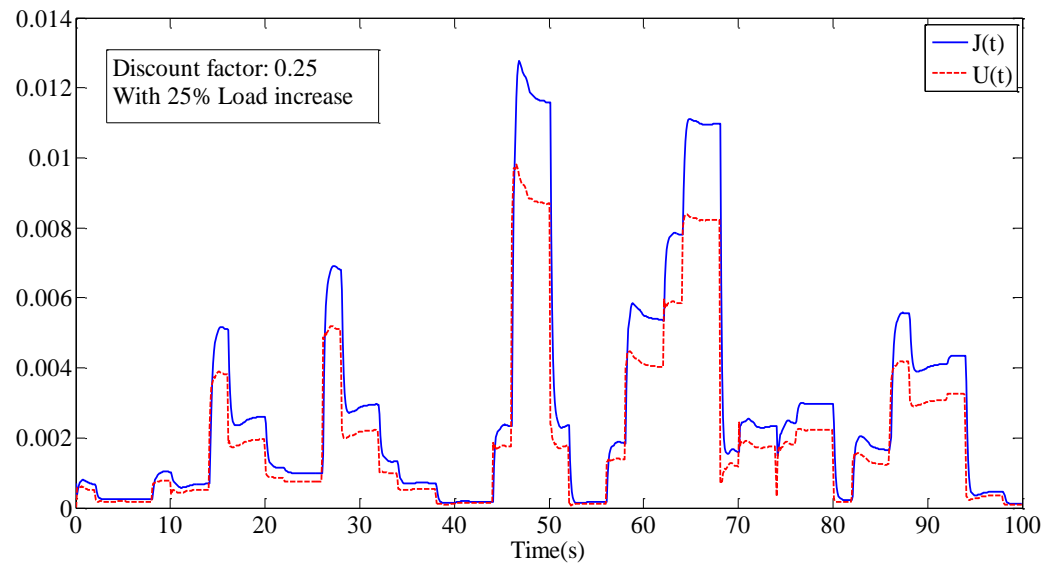
Fig. 6.26 25% load increase with discount factor set to 0.25 Plot of utility function, U(t), cost-to-go function, J(t).
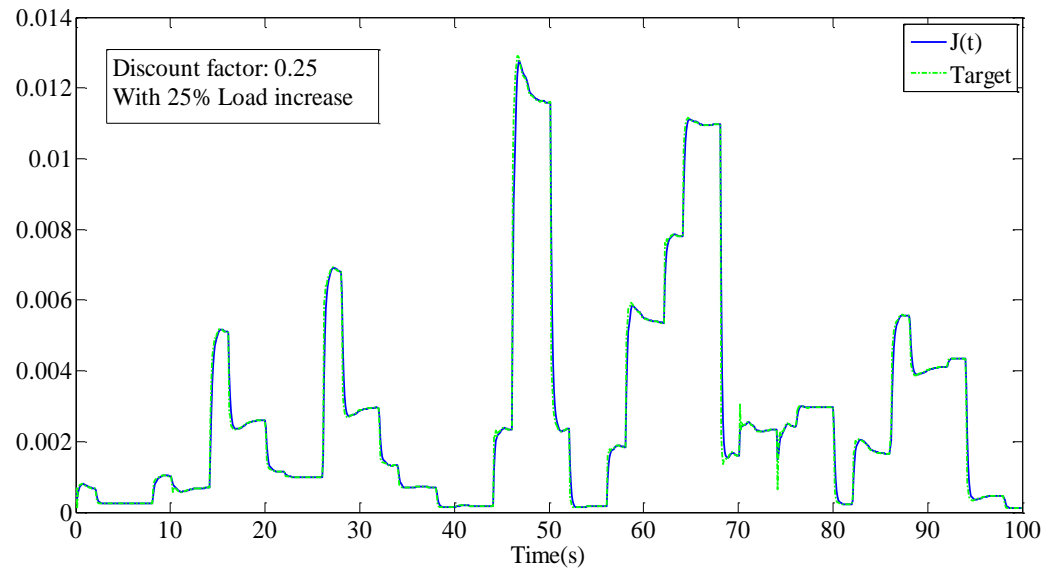
Fig. 6.27 25% load increase with discount factor set to 0.25 Plot of cost-to-go function, J(t) and its target.
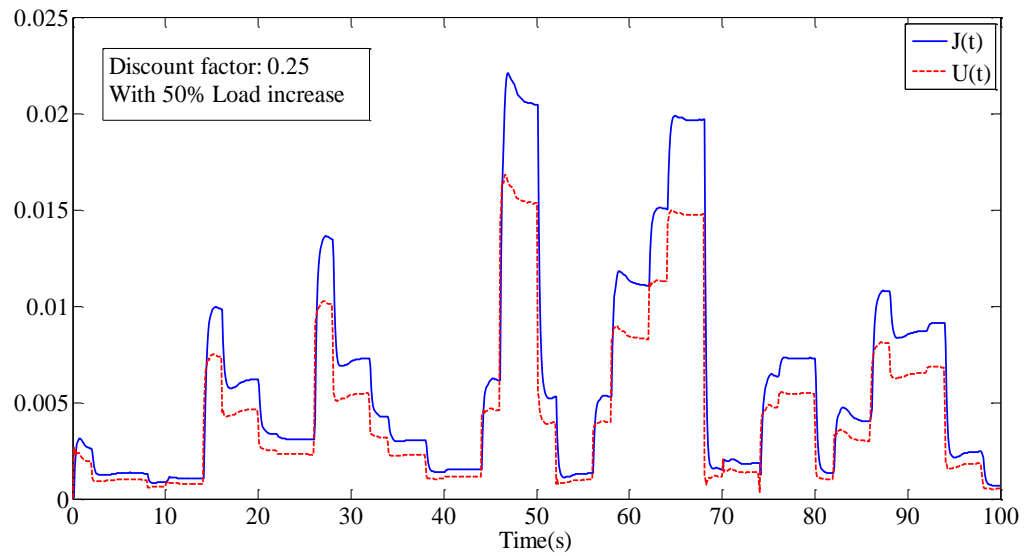
Fig. 6.28 50% load increase with discount factor set to 0.25 Plot of utility function, U(t), cost-to-go function, J(t).
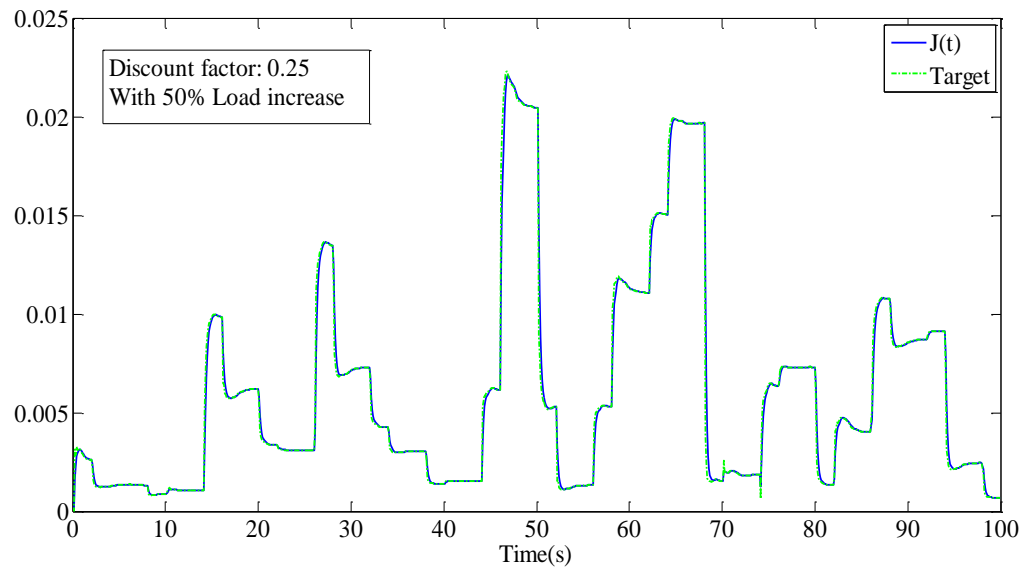
Fig. 6.29 50% load increase with discount factor set to 0.25, Plot of cost-to-go function, J(t) and its target.
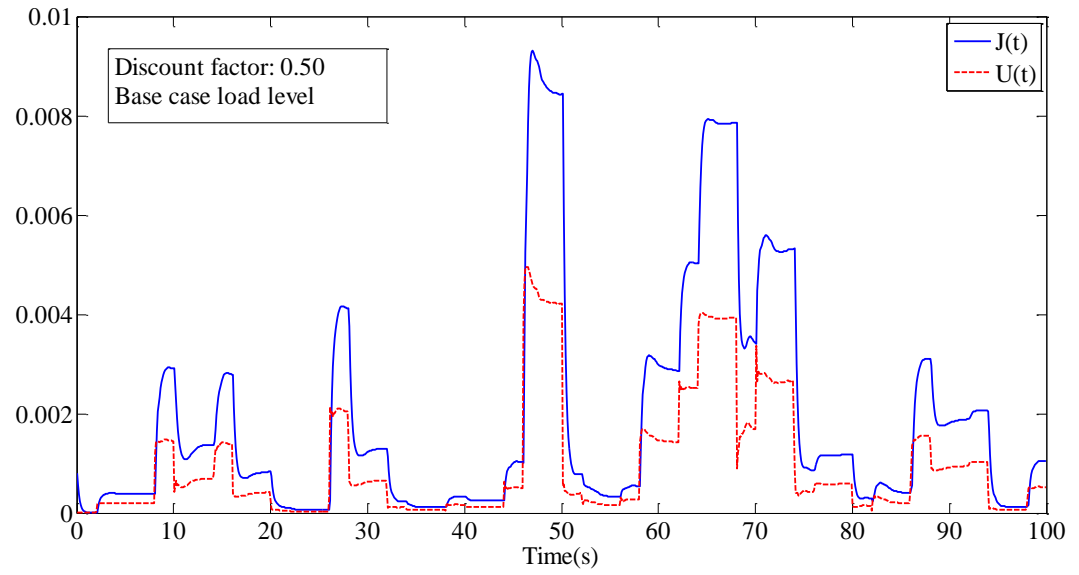
Fig. 6.30 Base case with discount factor set to 0.5, Plot of utility function, U(t), cost-to-go function, J(t).
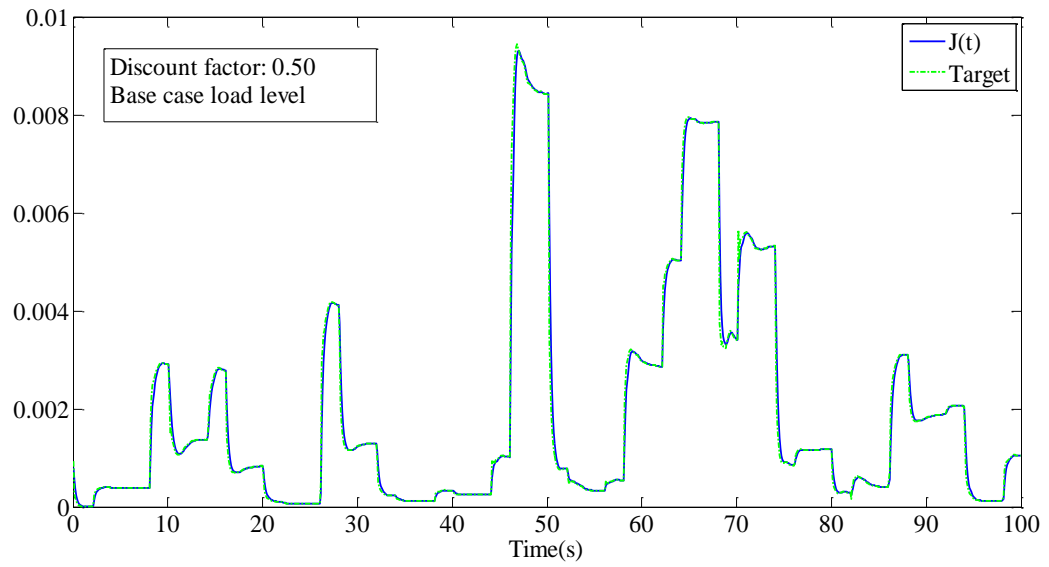
Fig. 6.31 Base case load level with discount factor set to 0.5, Plot of cost-to-go function, J(t) and its target.
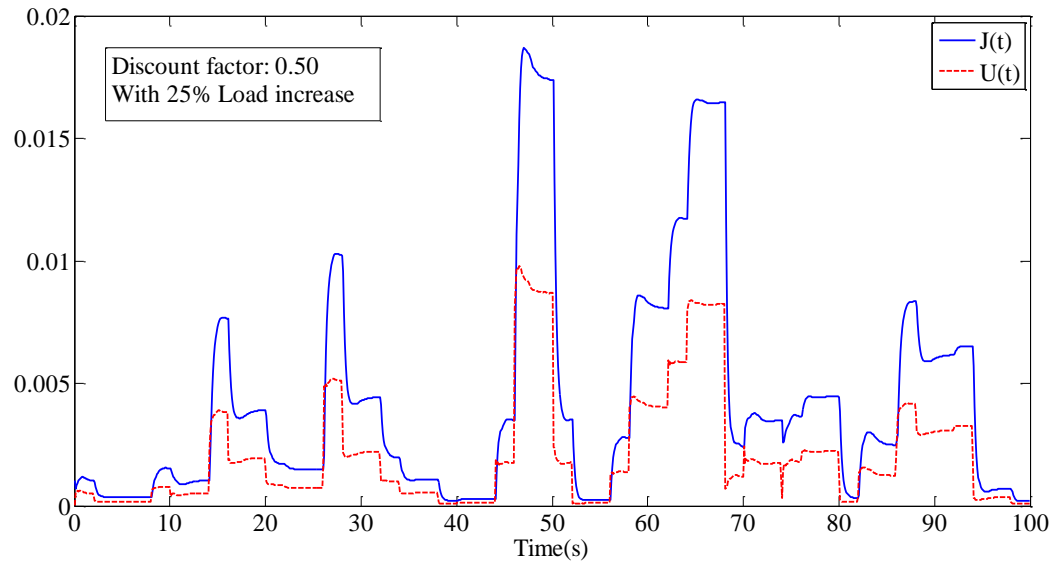
Fig. 6.32 25% load increase with discount factor set to 0.5 Plot of utility function, U(t), cost-to-go function, J(t).
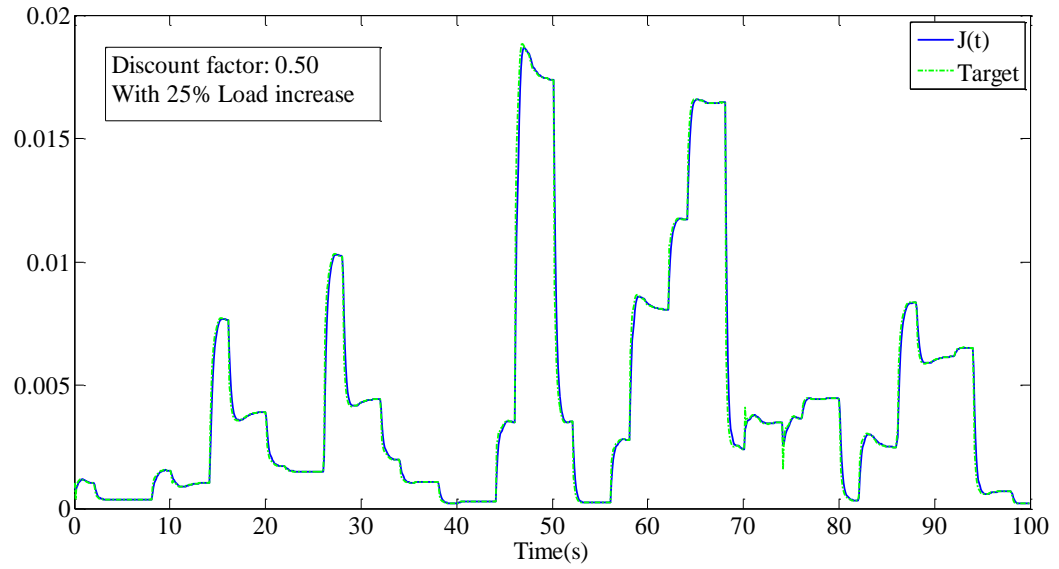
Fig. 6.33 25% load increase with discount factor set to 0.5, Plot of cost-to-go function, J(t) and its target.
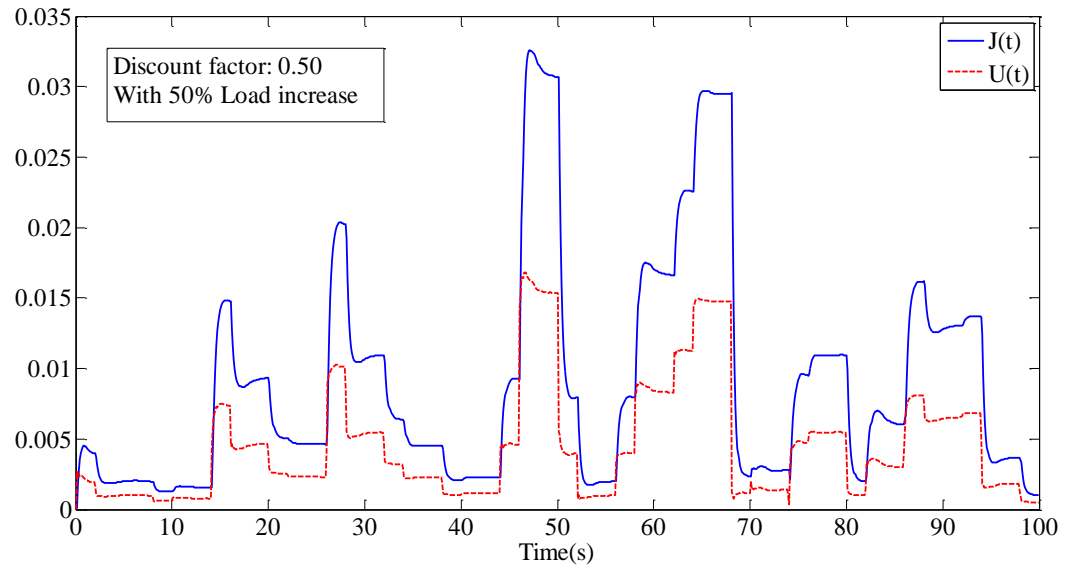
Fig. 6.34 50% load increase with discount factor set to 0.5 Plot of utility function, U(t), cost-to-go function, J(t).
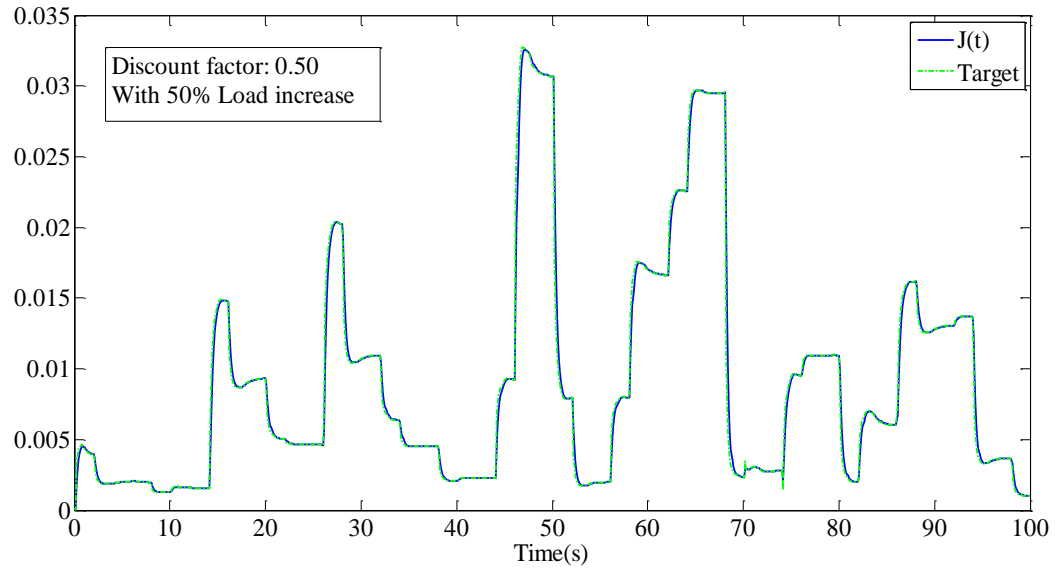
Fig. 6.35 50% load increase with discount factor set to 0.5, Plot of cost-to-go function, J(t) and its target.
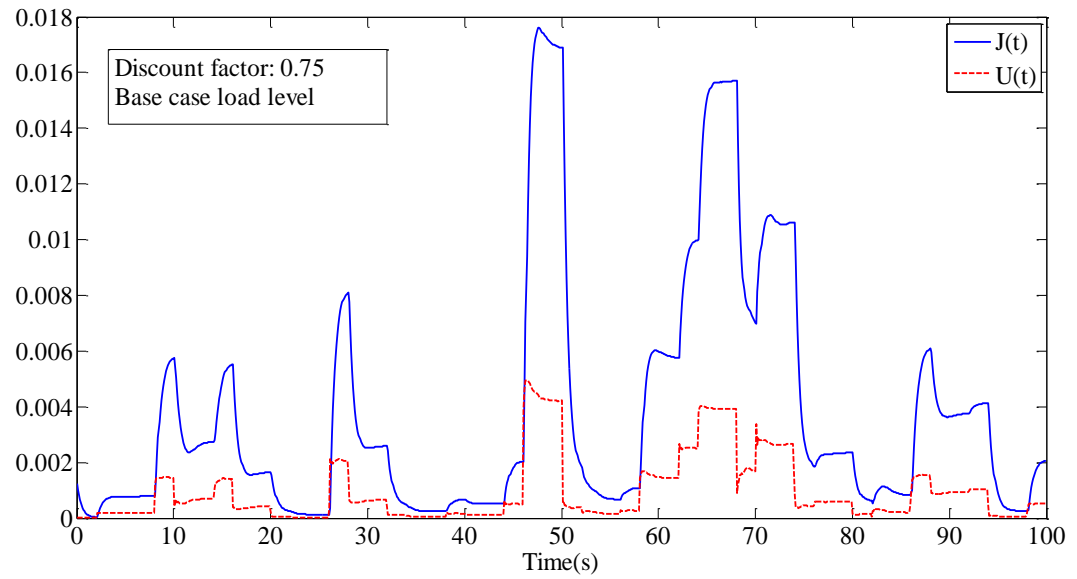
Fig. 6.36 Base case with discount factor set to 0.75, Plot of utility function, U(t), cost-to-go function, J(t).
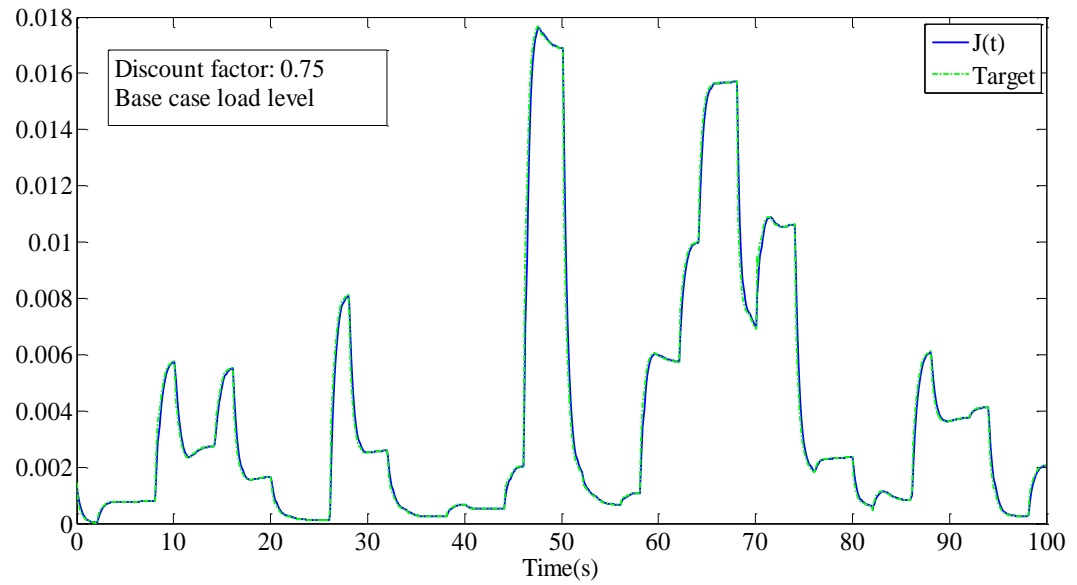
Fig. 6.37 Base case load level with discount factor set to 0.75, Plot of cost-to-go function, J(t) and its target.
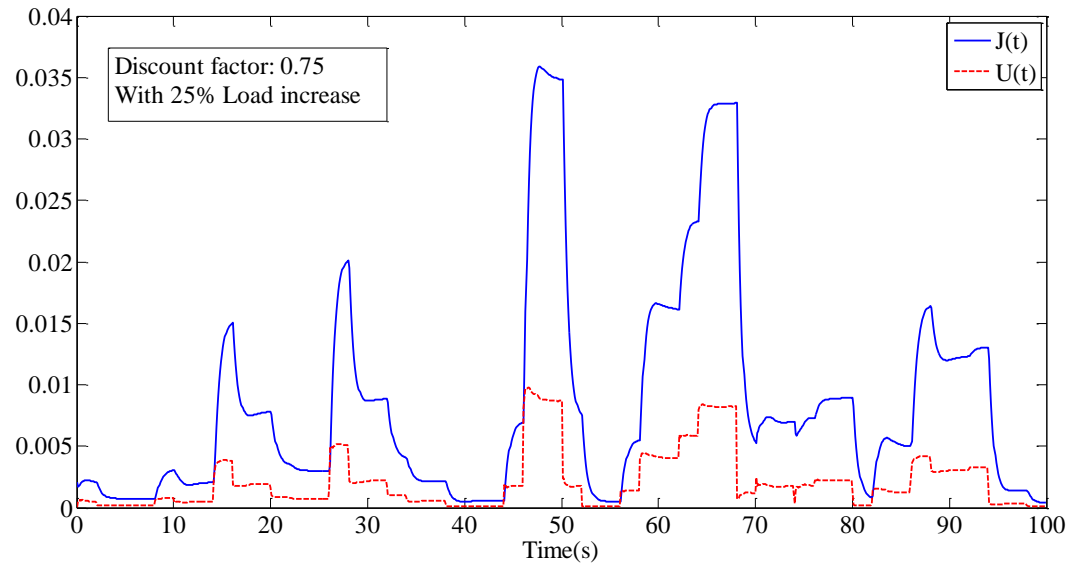
Fig. 6.38 25% load increase with discount factor set to 0.75 Plot of utility function, U(t), cost-to-go function, J(t).
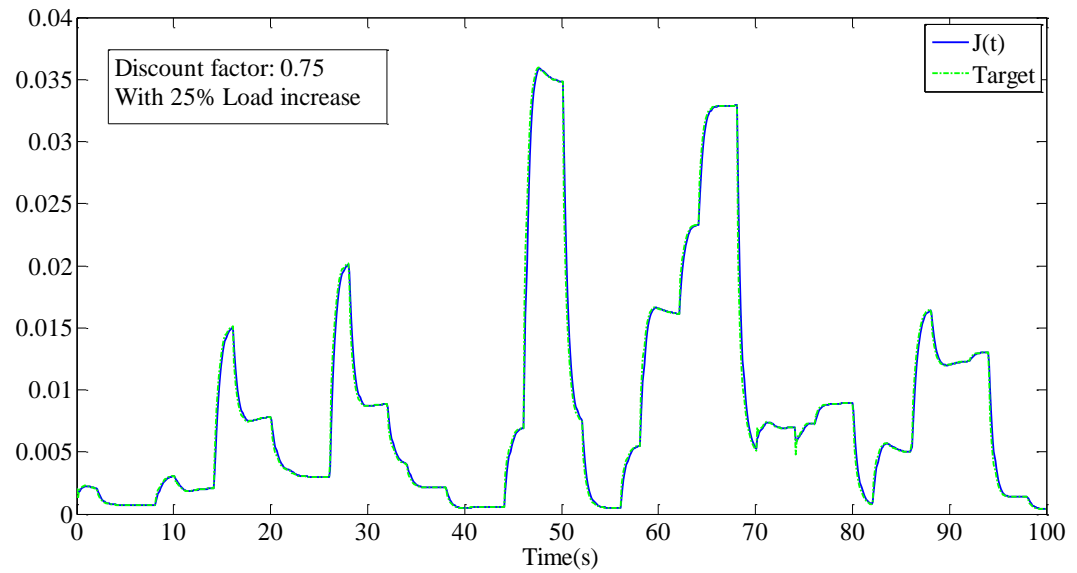
Fig. 6.39 25% load increase with discount factor set to 0.75, Plot of cost-to-go function, J(t) and its target.
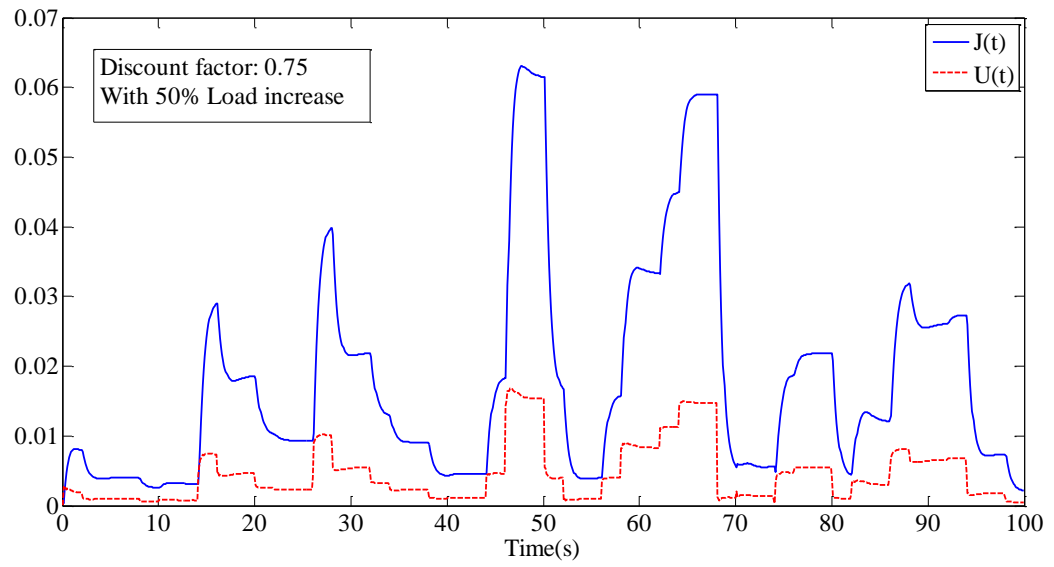
Fig. 6.40 50% load increase with discount factor set to 0.75 Plot of utility function, U(t), cost-to-go function, J(t).
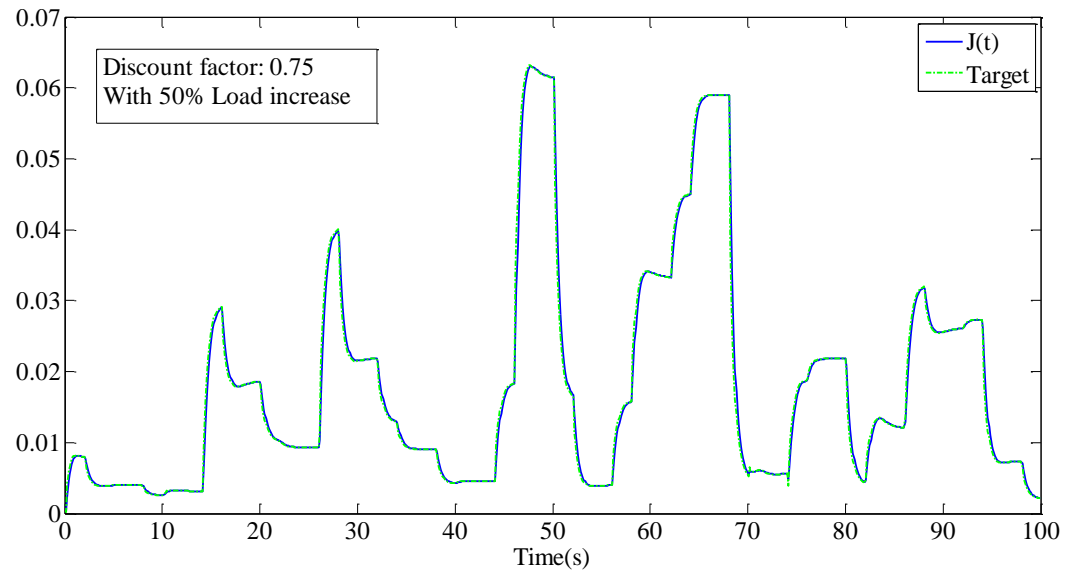
Fig. 6.41 50% load increase with discount factor set to 0.75, Plot of cost-to-go function, J(t) and its target.
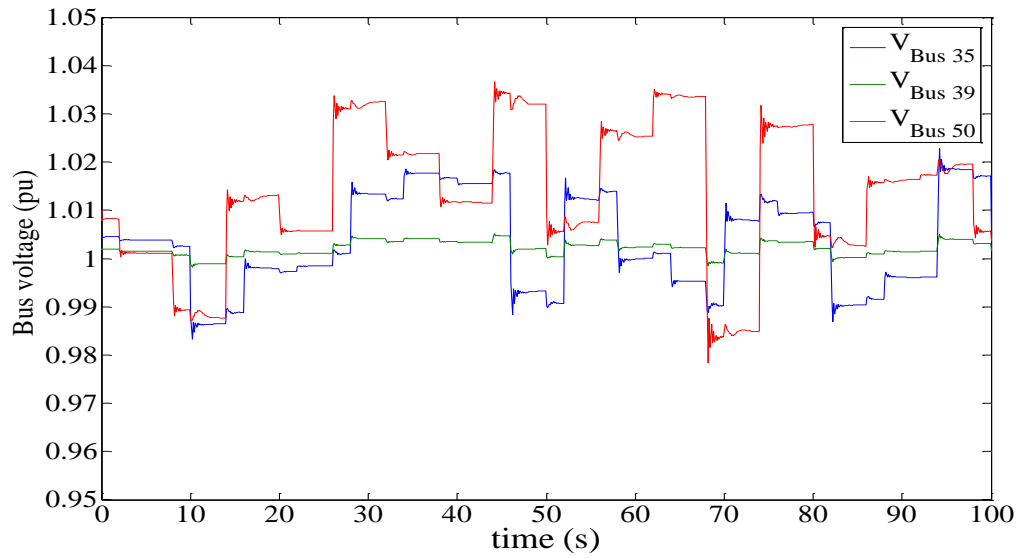
Fig. 6.42 System voltages at bus 35, 39, and 50 during actor pre-training with PRBS signals injected to the STATCOMs at bus 35 and bus 50.
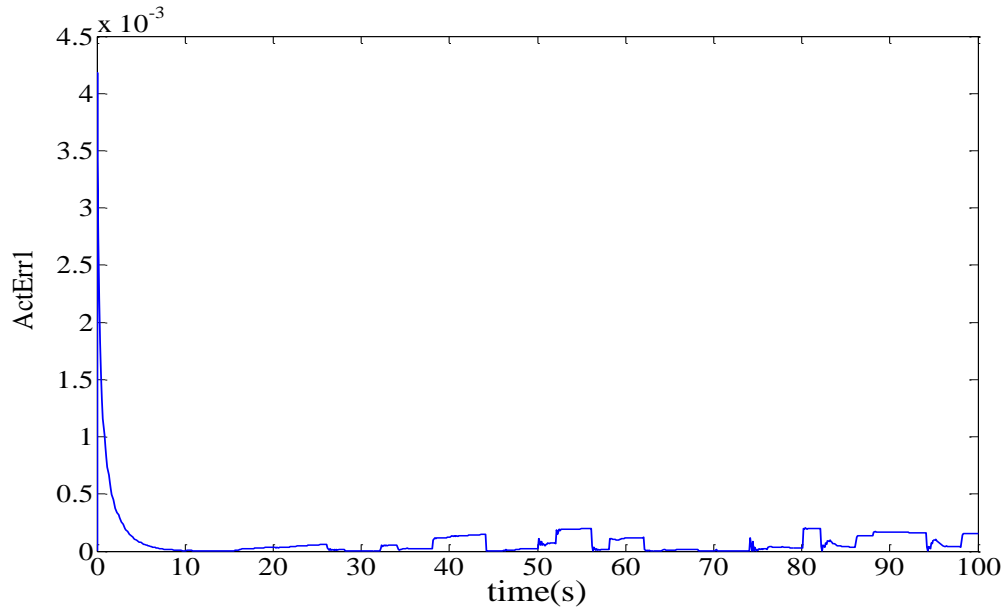
Fig. 6.43 shows Actor error signal for STATCOM 1 during the actor pre-training. Feedback from critic network is used to provide the actor error signals by backpropagating a constant 1 through the critic network.
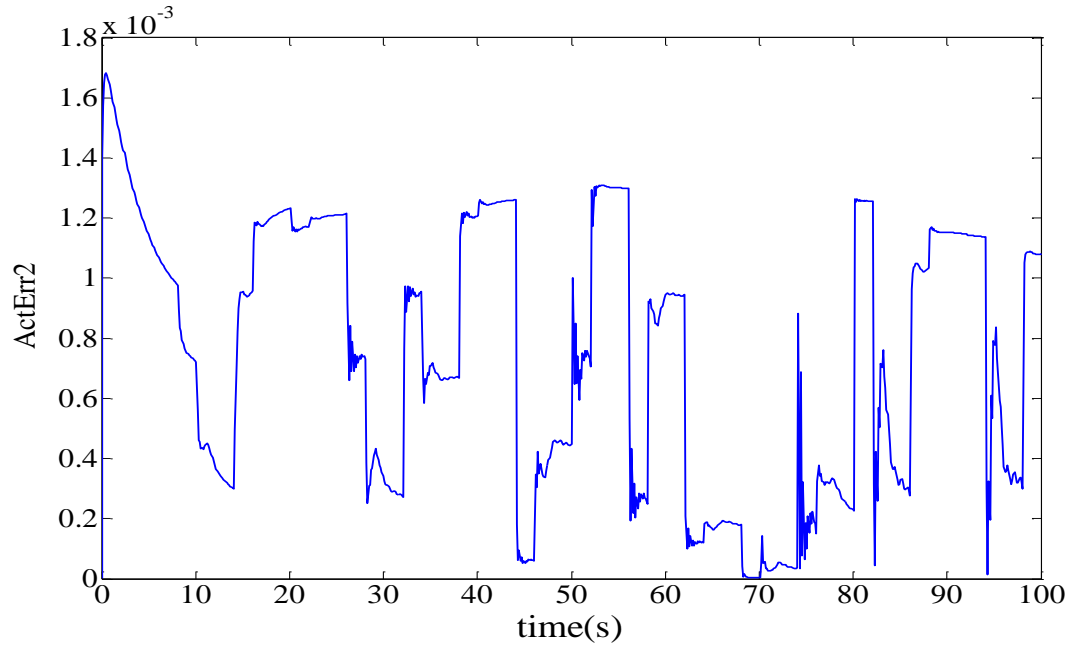
Fig. 6.44 Actor error signal for STATCOM 2 during the actor pre-training. Feedback from critic network is used to provide the actor error signals by backpropagating a constant 1 through the critic network.
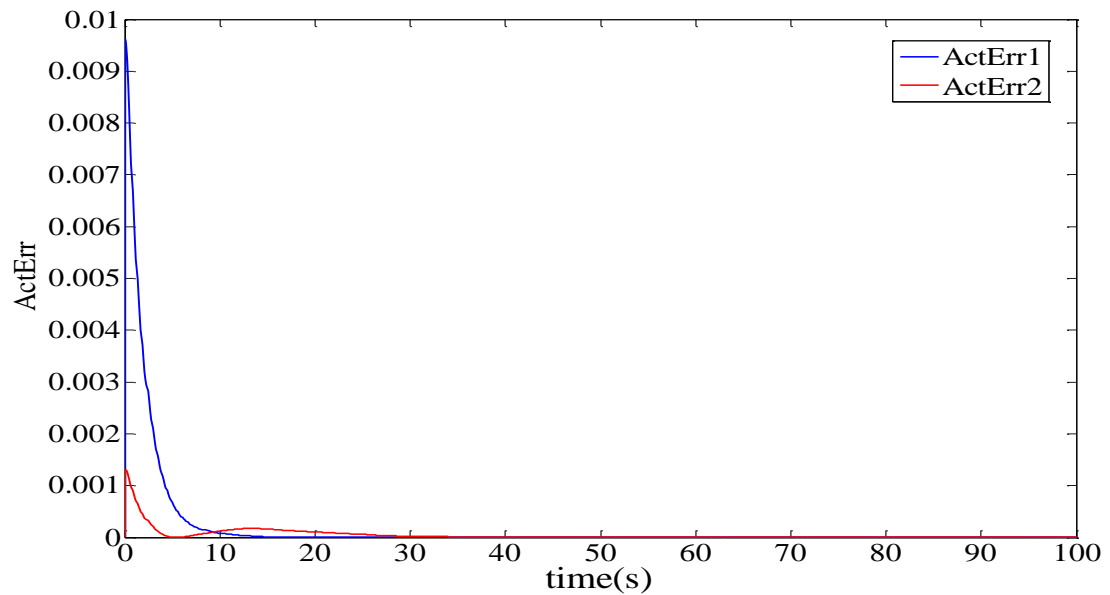
Fig. 6.45 Actor error signals during the actor pre-training. Feedback from critic network is used to provide the actor error signals by backpropagating a constant 1 through the critic network.

The weights of the critic network are kept constant during the actor training period, and PRBS signals are used to perturb the power system by providing auxiliary voltage reference input signals for the two STATCOMS.
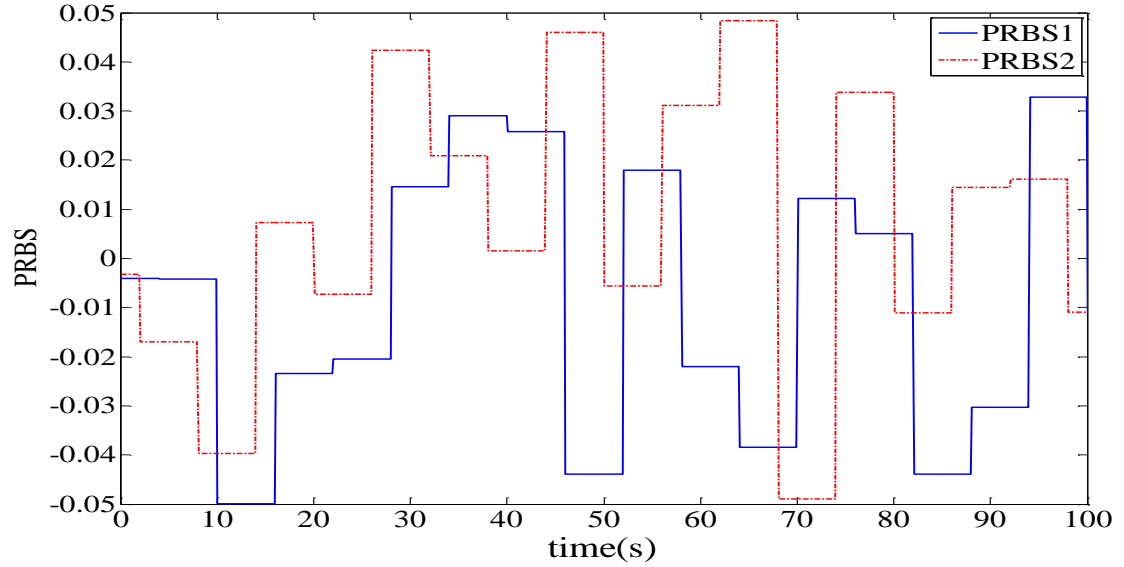
Fig. 6.46 PRBS signal used to perturb the power system during the actor pre-training phase.
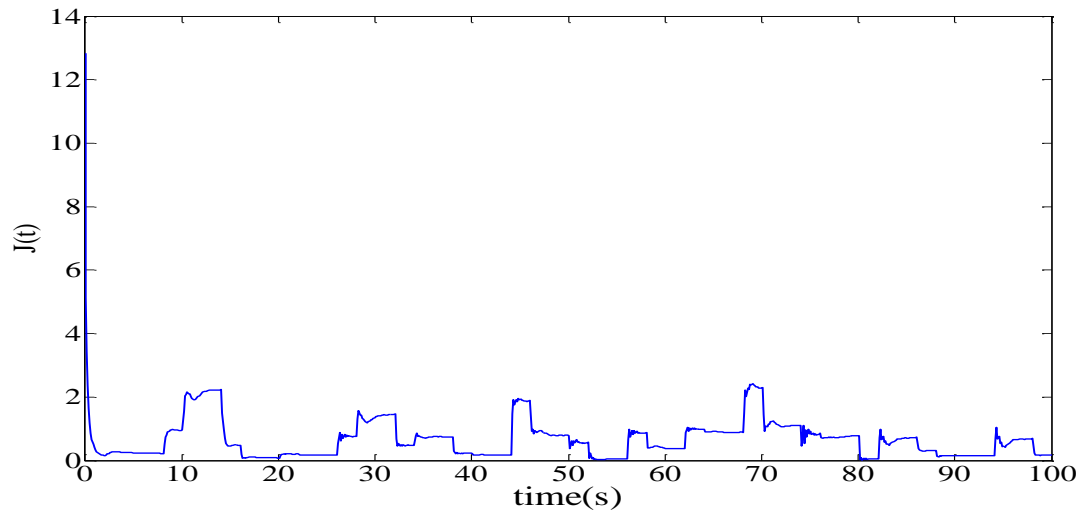
Fig. 6.47 Output of the critic network, J(t) during actor pre-training with critic weights not fixed.
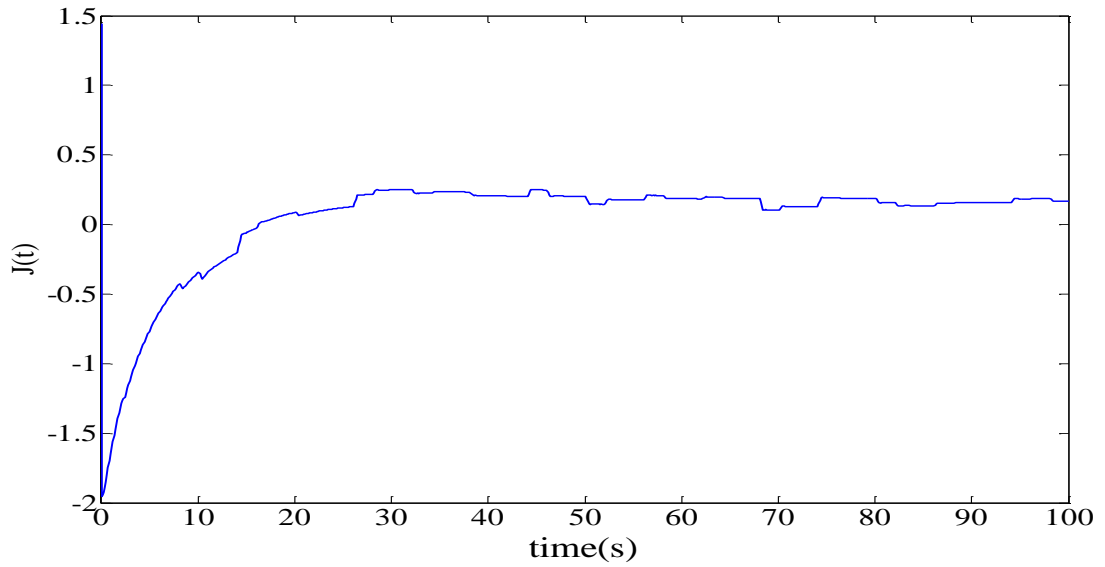
Fig. 6.48 Output of the critic network, J(t) during actor pre-training with critic weights fixed.

6.4.5. Closed Loop Training of Actor and Critic Networks. The pre-trained actor and critic neural networks are trained in closed loop with the plant to achieve desired optimal control (i.e. the performance that minimizes the cost to go function J(t).). References [36], [38], [79], and [80] have discussed the general guidelines that are applicable for training Adaptive Critic Designs (ACDs). Chapter 4 of reference [38] discusses guidelines for selecting appropriate parameters that include learning rate, values of starting weights for actor and critic network and choosing the discount factor for the ADP controller. It is noted that the selection the appropriate utility function as well as the parameters of the controller are eminently useful for designing the ADP controller. A comparison of different approaches for performing closed loop training of the ADP controller is also discussed. In this dissertation, training of the ADP was performed initially by alternately training the critic and actor networks in epochs as described in section 6.3.2 were performed. Subsequently, the simultaneous training of the actor and critic network in closed loop was performed to obtain successful controller training. Additional steps taken in the training approach enable controller convergence include scaling of inputs to the controller by using deviations of bus voltages and angles scaled between -1 and 1 instead of actual p.u values. The actor network output is also scaled appropriately by initially operating the controller in open loop, with the plant at

steady state to obtain the actor output at steady state. The control signal feed to the plant accounts for the steady state output of the actor by using the deviation of the actor output from its steady state value to provide auxiliary controls for the two STATCOMs.

The trained controller was tested using two cases for system load increase and decrease from the base case: Case I the load at the test buses is varied through a load factor of 1 p.u. from the base case load, and Case 2: the load at the test buses is varied in the range of 2 p.u from the base case value. Figures 6.49 through 6.60 show the response of system voltages at the controlled buses with and without the controller. The results show that the system voltage profile at the test buses is improved during the system load variations. With the controller in place, voltage deviations remain with 2% of the nominal voltage compared with 3.5% without the controller with a load variation at 1.0 p.u. For the load variation of 2.0 p.u, the deviations are 5% with the controller and 7% without the controller, which is significant in maintaining system voltage stability.
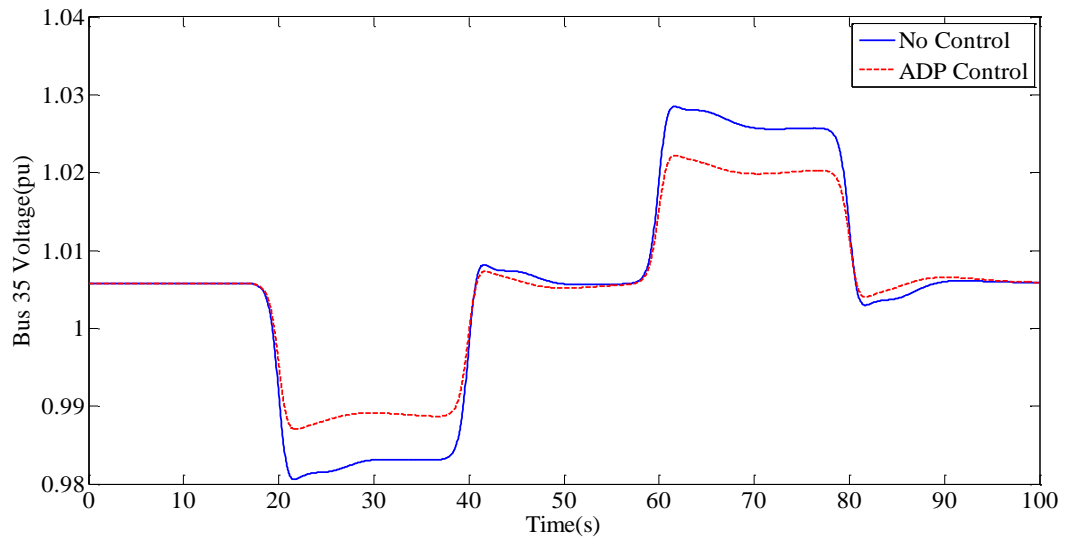
Fig. 6.49. Plot of the voltage at bus 35 with load variation for the case of no controller compared with the case with the ADP controller. The graph shows plots of voltage profile at bust 35 with load varied by 1 p.u. First the load is reduced from the base case at time t=17 seconds followed by an increase of the same magnitude he load in increased by 1.p.u followed by a reduction of the load at 60 seconds.

Similar voltage profiles at other system buses for case 1 are shown below:
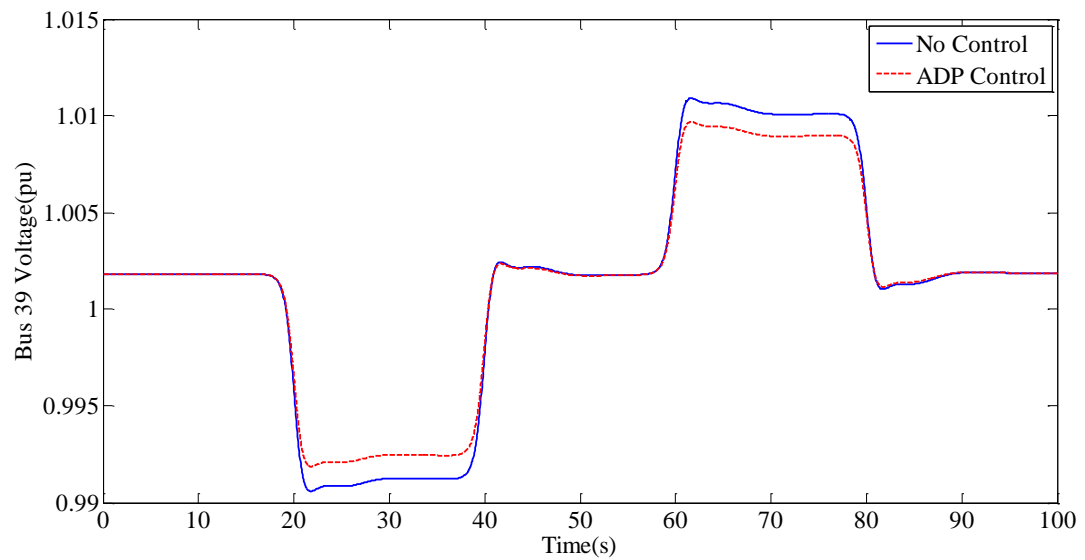
Fig. 6.50. Plot of the voltage at bus 39 with load variation for the case of no controller compared with the case with the ADP controller for 1.0 p.u load variation.
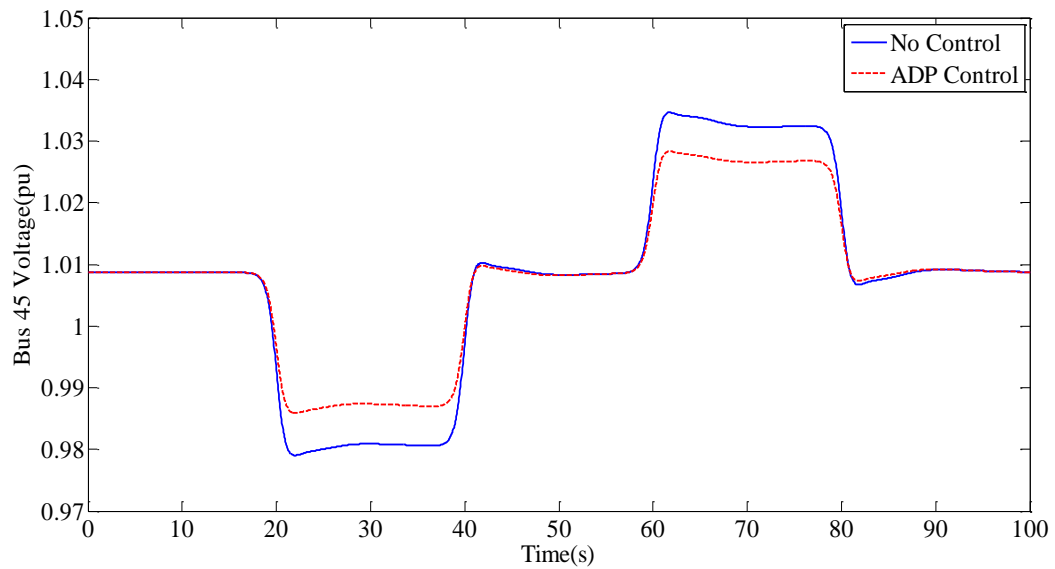
Fig. 6.51. Plot of the voltage at bus 45 with load variation for the case of no controller compared with the case with the ADP controller for 1.0 p.u load variation.
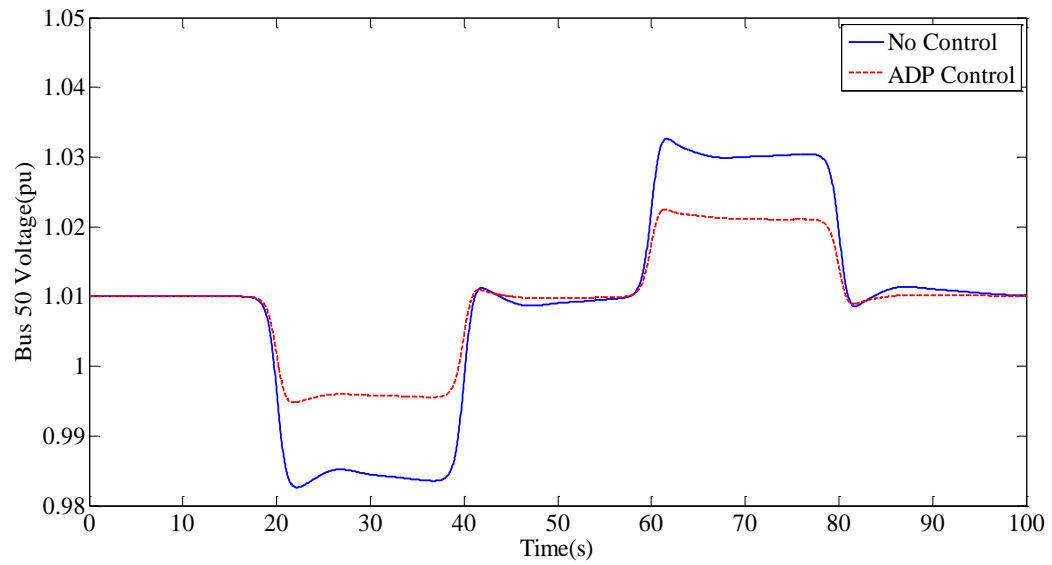
Fig. 6.52. Plot of the voltage at bus 50 with load variation for the case of no controller compared with the case with the ADP controller for 1.0 p.u load variation.
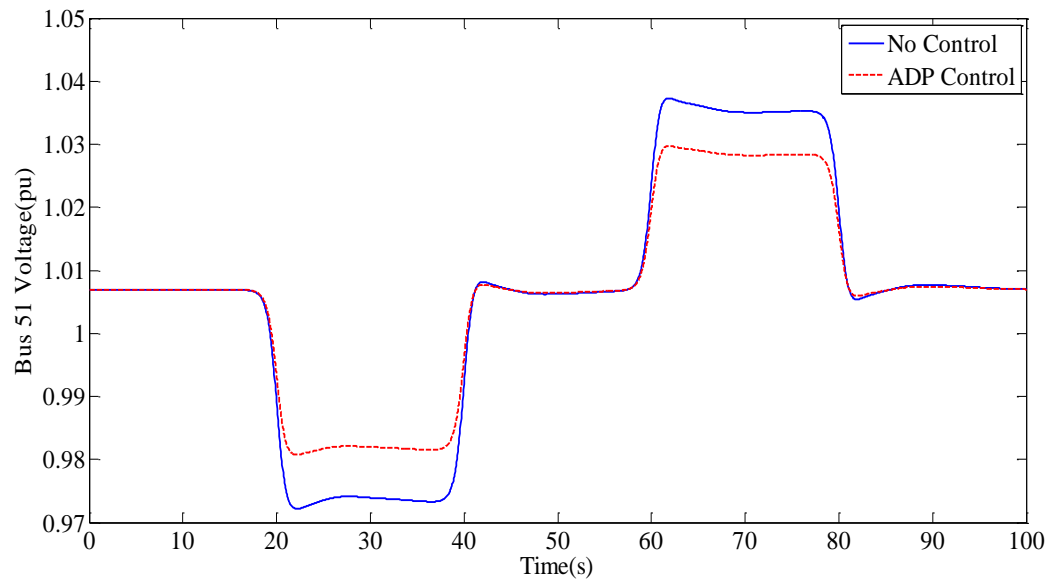
Fig. 6.53. Plot of the voltage at bus 51 with load variation for the case of no controller compared with the case with the ADP controller for 1.0 p.u load variation.
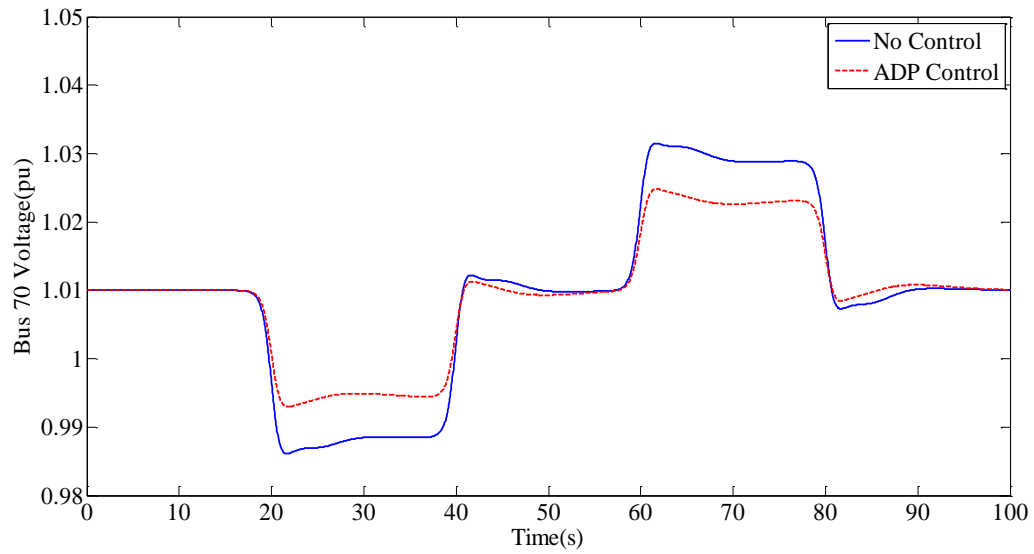
Fig. 6.54. Plot of the voltage at bus 70 with load variation for the case of no controller compared with the case with the ADP controller for 1.0 p.u load variation.
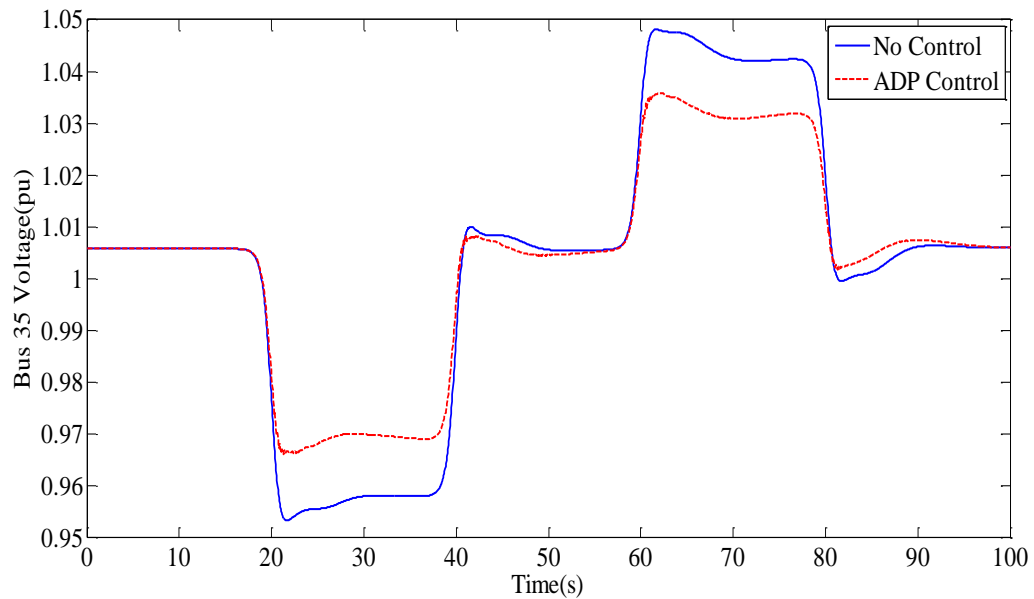
Fig. 6.55. Plot of the voltage at bus 35 with load variation for the case of no controller compared with the case with the ADP controller. The graph shows plots of voltage profile at bust 35 with load varied by 2 p.u. First the load is reduced from the base case at time t=17 seconds followed by an increase of the same magnitude he load in increased by 2.p.u followed by a reduction of the load at 60 seconds.

Similar voltage profiles at other system buses for case 2 (2.0 p.u load variation) are shown below:
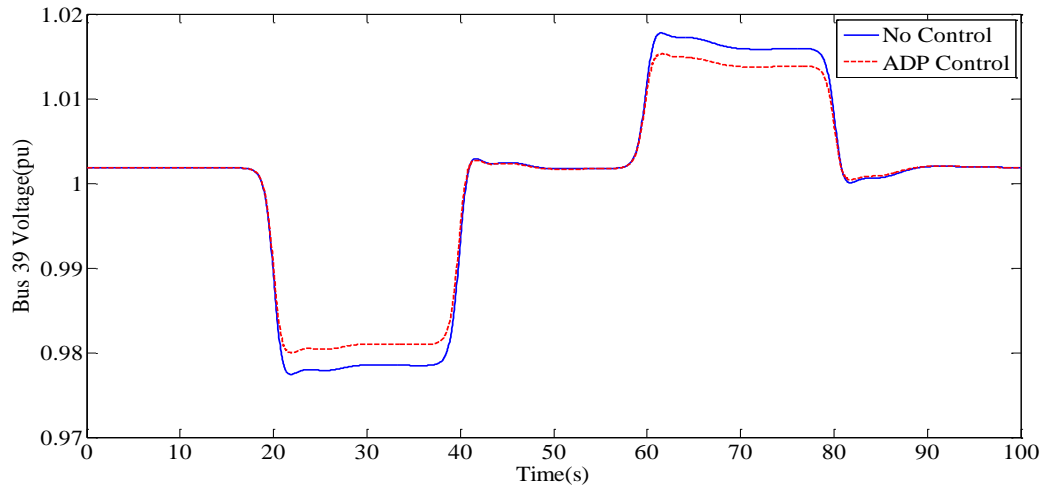
Fig. 6.56. Plot of the voltage at bus 39 with load variation for the case of no controller compared with the case with the ADP controller for 2.0 p.u load variation.
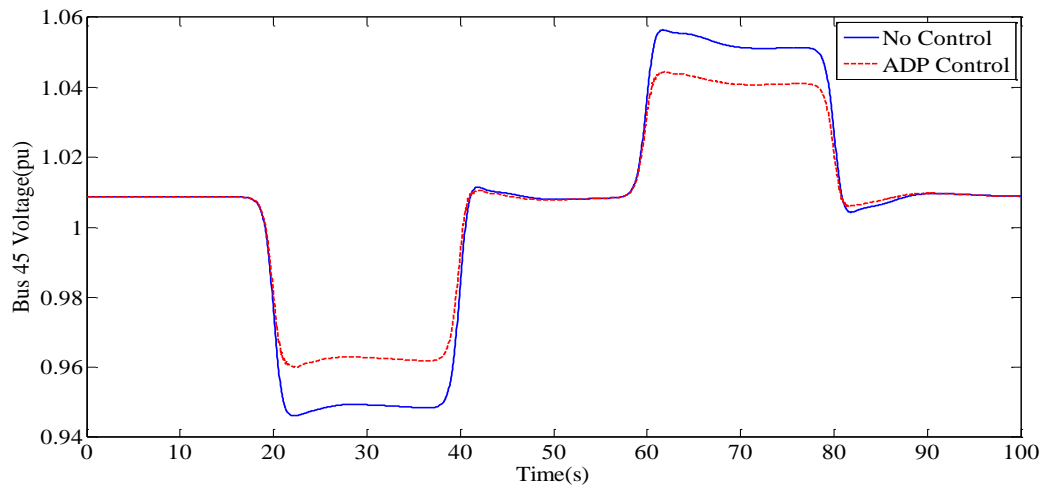
Fig. 6.57. Plot of the voltage at bus 45 with load variation for the case of no controller compared with the case with the ADP controller for 2.0 p.u load variation.
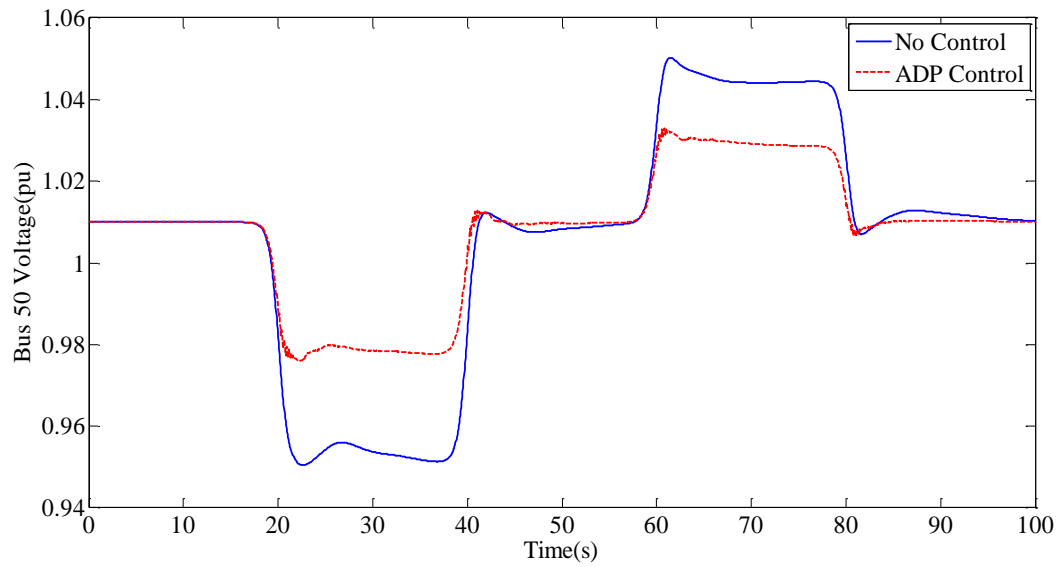
Fig. 6.58. Plot of the voltage at bus 50 with load variation for the case of no controller compared with the case with the ADP controller for 2.0 p.u load variation.
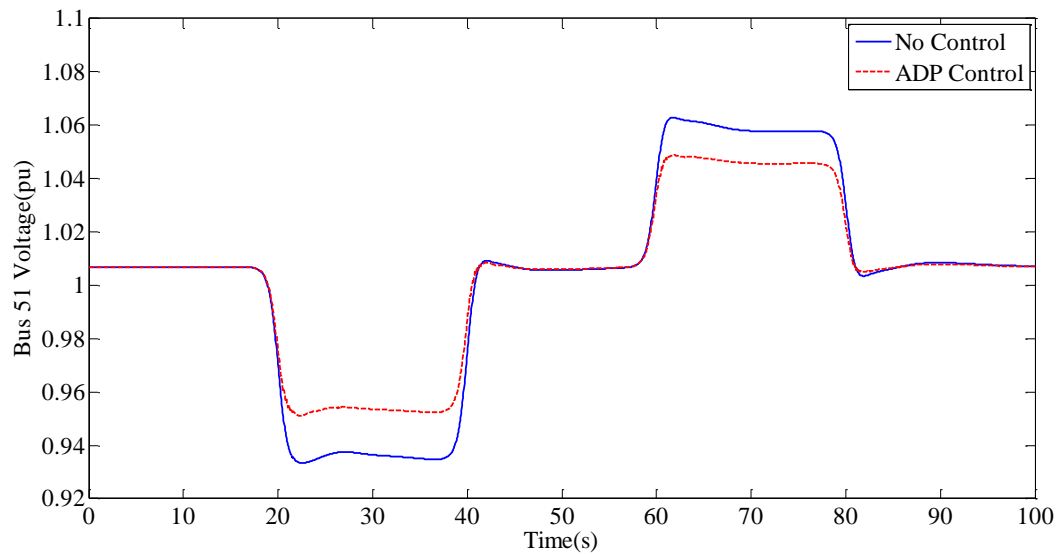
Fig. 6.59. Plot of the voltage at bus 51 with load variation for the case of no controller compared with the case with the ADP controller for 2.0 p.u load variation.
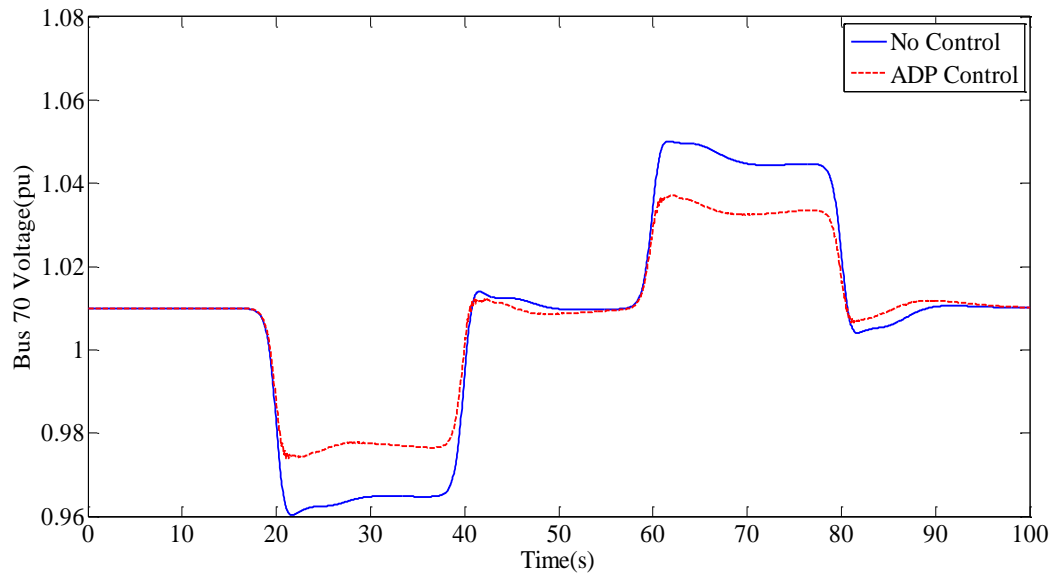
Fig. 6.60. Plot of the voltage at bus 70 with load variation for the case of no controller compared with the case with the ADP controller for 2.0 p.u load variation.

The impact of the ADP controller on the system voltages in the load area is seen in Figures 32(a)-(f) and 33(a)-(f) above. During the duration of increased load (app 17 seconds to about 40 seconds), system voltages decrease below nominal values, while system voltages increase with reduced loading (at 60 to 80 seconds). The graphs show the voltage profiles with the ADP controller (blue curve) and with the ADP controller (red dashed curve). It is seen from the plots that at each load bus, using the ADP controllers reduces the deviation of the voltage from nominal, pre-disturbance values, where as if no ADP controller is used the changes in voltage are much larger from their nominal values. Thus the results show that the ADP controller is successful in improving the system voltage profile during load variations.

6.4.6. ADP Control with DFIG Wind Farm. The impact of the ADP controller on system voltage and reactive power control is evaluated with a 200 MVA DFIG wind farm machine at bus 70 injecting real power into the system. As before the system is perturbed by increasing load at seven buses in the load area by 0.25 load factor.

The ADP controller is further trained with the WF injecting real and reactive power into the system. The ADP training process followed is described in section 6.3. Test results for the ADP controller with the WF injecting real power turned on are shown in the graphs in Figure 6.61 to Figure 6.67. When load is increased, the STACOM provides reactive power support in order to maintain bus voltages close to the pre-disturbance values. However, when the ADP is not used, the reactive power output of the STATCOM is lower than when the ADP controller is used (Figure 6.61 and 6.62). The real power draw by the DFIG WF shows little variation in the cases of using the ADP controller and with no ADP controller as shown in Figure 6.63.
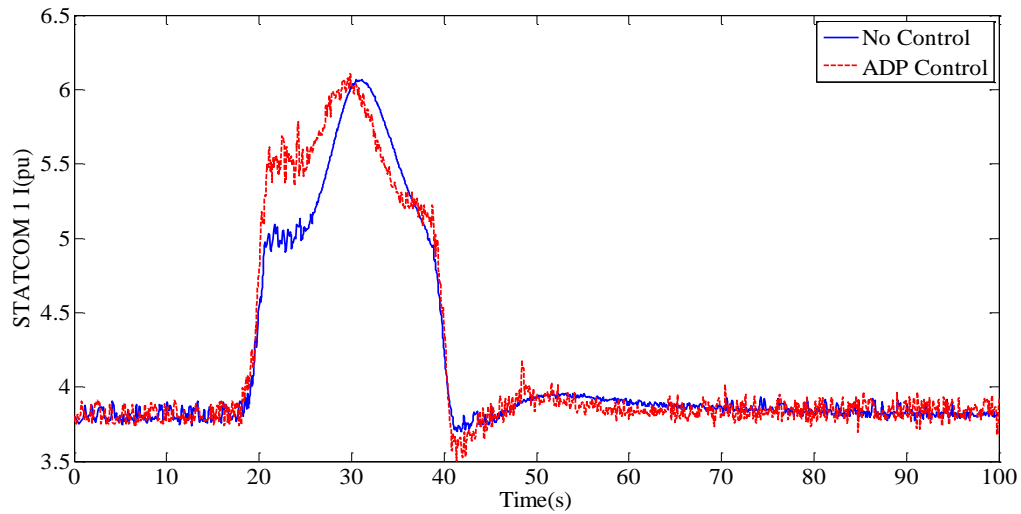
Fig. 6.61. Plot of STATCOM 1 current that is proportional to reactive power output following load variation. The solid line shows the response of the STATCOM with no ADP controller while the red dotted line shows the response of the STATCOM with ADP controller.
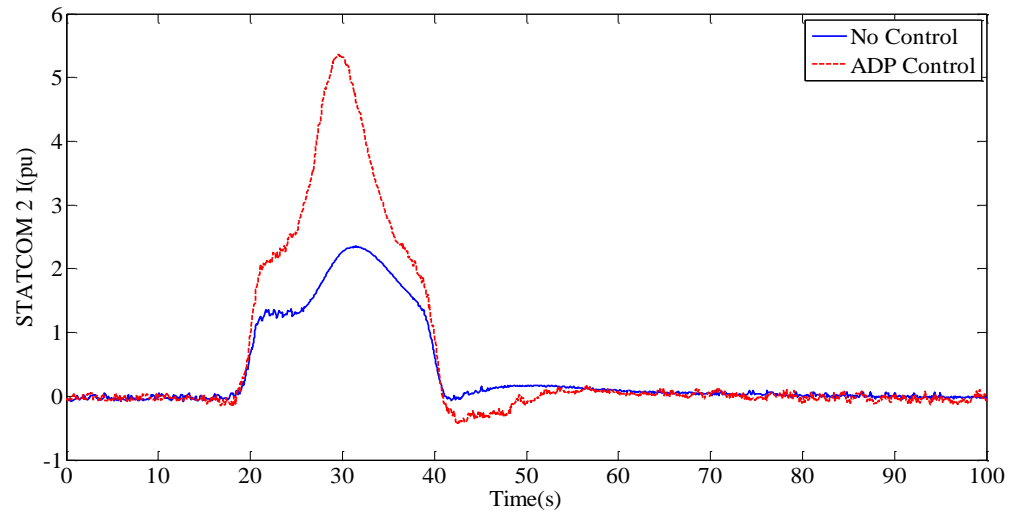
Fig. 6.62. Plot of STATCOM 2 current that is proportional to reactive power output following load variation. The solid line shows the response of the STATCOM with no ADP controller while the red dotted line shows the response of the STATCOM with ADP controller.
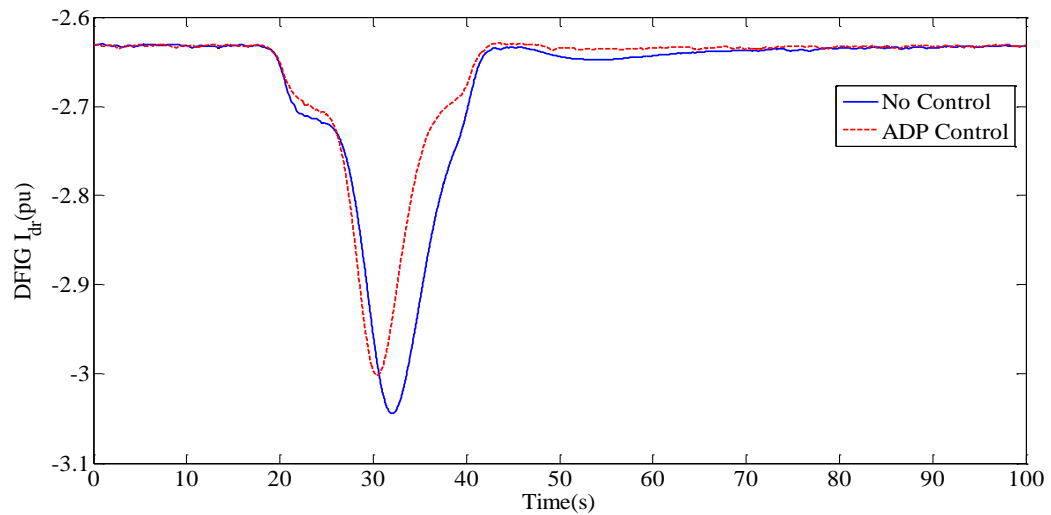
Fig. 6.63. Plot of DFIG current that is proportional to real power output (with opposite polarity) following load increase. The solid line shows the response for the DFIG WF with no ADP controller while the red dotted line shows the response of the STATCOM with ADP controller.
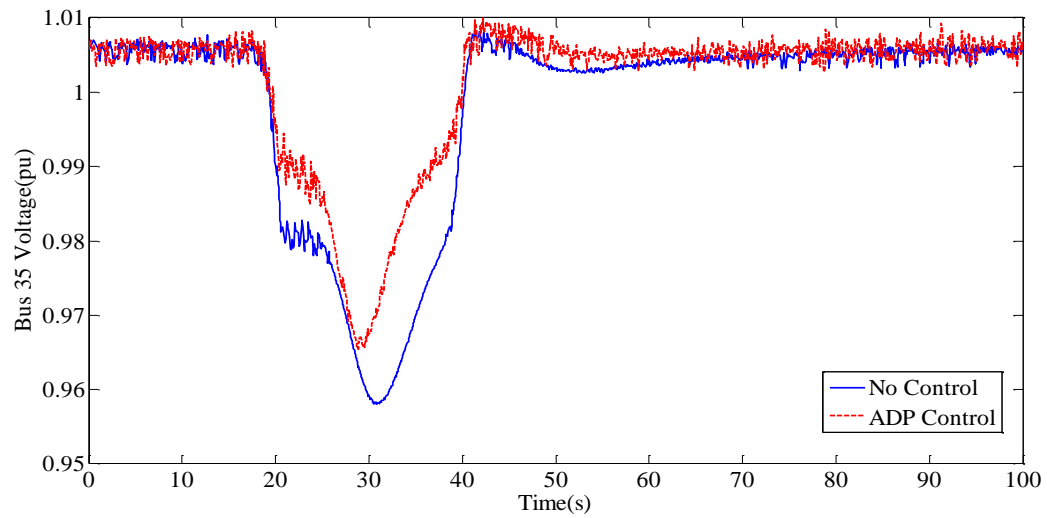
Fig. 6.64. Plot of bus 35 voltage following load variation. The solid line shows the bus voltage with no ADP controller while the red dotted line shows the bus voltage with ADP controller.
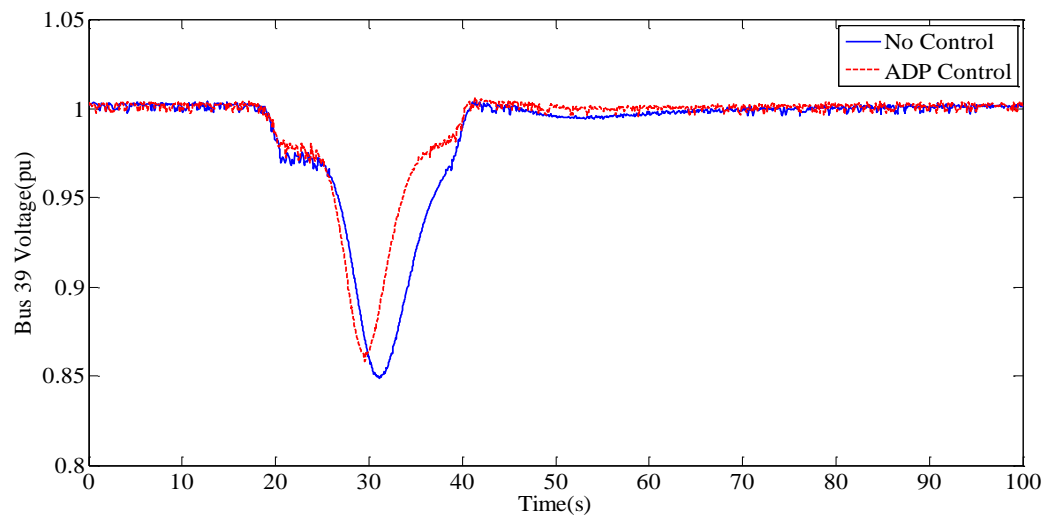
Fig. 6.65. Plot of bus 39 voltage following load variation. The solid line shows the bus voltage with no ADP controller while the red dotted line shows the bus voltage with ADP controller.
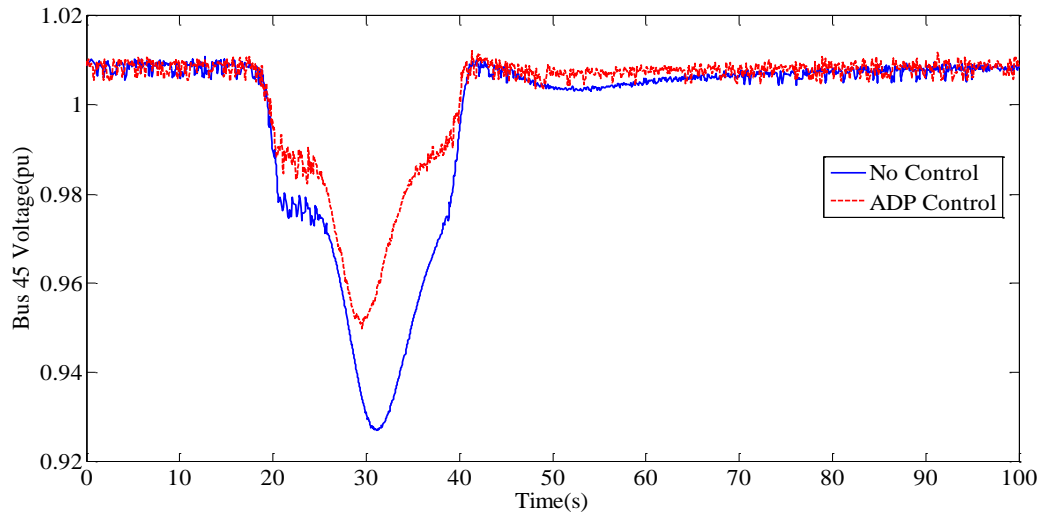
Fig. 6.66. Plot of bus 45 voltage following load variation. The solid line shows the bus voltage with no ADP controller while the red dotted line shows the bus voltage with ADP controller.
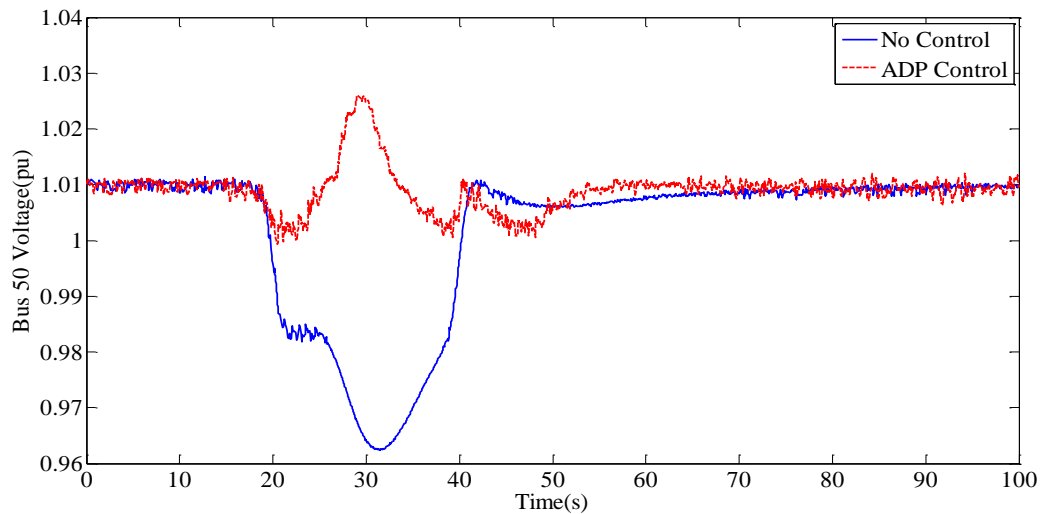
Fig. 6.67. Plot of bus 50 voltage following load variation. The solid line shows the bus voltage with no ADP controller while the red dotted line shows the bus voltage with ADP controller.

The above simulation results show that the ADP controller improves the reactive power support in the system, and therefore system voltage profile is better with the ADP controller compared with the case of no ADP controller (Figures 6.64 to 6.67). Further as the reactive power drawn by the DFIG changes, the reactive power output of the

STATCOM is dynamically varied so as to compensate for reactive power flow thereby maintaining system voltage closer to their nominal values.

6.5. SUMMARY

Development of an Adaptive Dynamic Programming (ADP) based controller for secondary voltage control has been presented. The controller is based on the Action-Dependent Heuristic Dynamic Programming (AD-HDP) model of the family of Adaptive Critic Designs (ACDs). A model network for the system based on the Echo State Network (ESN) is used for estimation of Voltage Stability Load Index (VSLI) at load buses that are used in the utility function formulation. The actor and critic networks are based on MLP neural networks that minimized the cost-go-function. The ADP provides auxiliary voltage reference values for two STATCOMs for voltage stability control. Simulation results have shown that by using the proposed ADP controller, the system voltage profiles in the load area and reactive power control of the STATCOM can be improved, thereby improving system voltage stability.

7. CONCLUSION

7.1. INTRODUCTION

Development of computational approaches for online monitoring and control of voltage stability in smart grids have been presented. The work presented in this dissertation focus on the development of a computational intelligence method for estimation of voltage stability load index that measures the distance of a power system to its voltage stability using phasor measurement unit information. Furthermore, the dissertation presents an online control approach for voltage stability based on adaptive dynamic programming. The development of the reactive power coordinating controller and its implementation in a smart grid has been presented.

7.2. RESEARCH SUMMARY

The outputs of the research work presented as dissertations in the Sections of this document can be summarized as follows:

Section 3: A computational method using active and reactive power for estimation of voltage stability load index is developed. Voltage stability load index of at a bus can be obtained analytically provided that parameters of the Thevenin equivalent network can be obtained. In practice the no-load values of the Thevenin equivalent cannot be easily measured without disruption of load. A multi-layer perception is trained to estimate VSLI at load buses in a 14 bus power system using active and reactive power measurements of voltage magnitudes and phase angles. The approached is tested in power system that includes plug-in electric vehicles to test its performance during variation of charging and discharging cycles of PEV loads.

Section 4: Estimation of VSLI in power system using two different types of neural networks with the aim of comparing their performance is presented. VSLI estimation using the procedure discussed in dissertation 1 is done using an MLP and as ESN. The performance of the two approaches form monitoring VSLI in smart grid is compared. Simulation results showing performance of both MLP and ESN by mean

square error show that the ESN outperforms the MLP in estimating VSLI in that the smart grid.

Section 5: Phasor measurements units are costly equipment and their deployment is done in a manner that ensures the minimum units needed for complete observability for voltage stability monitoring are used. A method using a genetic algorithm for optimal location of PMUs to ensure complete observability of the power system is developed. PMUs have been more available with the advent of smart grid technologies. A computational approach for estimating VSLI using PMU voltage magnitude and angle measured is developed. The approach uses echo state networks for estimating VSLI using PMU measurements. Performance of the ESN approach for estimating VSLI is evaluated for a 14 bus system under two different operating contingencies.

An intelligent algorithm for optimal PMU placement in power system to ensure complete observability during normal operating conditions and when the system is islanded developed is implemented on three test systems. Assessment of the scalability of the ESN based approach method using PMU information for monitoring voltage stability. The dissertation shows the performance of the technique as the system size is increased. Demonstrates that the ESN based approach for VSLI estimation can be used during power system islanding. Application of the new method for online voltage stability in a smart grid consisting including wind generation and SmartParks is done.

Section 6: Section 6 presents the development of a proposed voltage stability controller based on Adaptive Dynamic Programming. The controller is a non-linear controller capable of dynamically adjusting the reference values of two STATCOMs in order to optimally control the system voltage profile. The ADP controller uses the voltage stability load index obtained on-line via the Echo State Network approach. Simulation results have showed that the ADP controller improves the voltage response of the system compared to the case where only a traditional PI controller is used. The advantages of using the ADP controller is that the reactive power output of the STATCOM is adjusted dynamically as the system operation conditions change, thereby ensuring that the controller performs optimally during system excursions.

7.3. MAIN CONCLUSIONS

The study presented in this dissertation focuses on the development of computational approaches for monitoring and control power system voltage stability in smart grids using phasor measurement unit information. The need for intelligent methods for monitoring and control of power system voltage stability has become of significant importance as the power system evolves to incorporate smart grid technologies. The complexity of the system has increased not only due to renewable energy sources and bi-directional flow of electric power between customers and the grid but also from the interactions of the cyber systems that play major roles of communication, computing and control. Traditional methods of voltage stability monitoring and control need to be supplement with fast intelligent methods in order to meet the challenges of implementing a true smart grid and meeting the challenges of electric energy supply of the 21st century. In this research computational intelligence based methods for online monitoring of voltage stability have been developed. The approaches developed use high speed communication infrastructure (PMUs) in order to estimate voltage stability load index. Performance of the techniques development is tested on different test system to evaluate their performance. Finally the study focuses on use of estimated VSLI as a feedback control signal. The development of an ADP controller for Secondary Voltage Control using STATCOMs in a power system with wind farms modeled is presented.

7.4. SUGGESTIONS FOR FUTURE WORK

This dissertation has focused on the development of computational approaches monitoring and control of voltage stability in a smart grids. Studies conducted have led to the development of an echo state network approach for estimation of voltage stability load index using phasor measurement information. Given below are some suggested areas for future research for this work:

Performance of the ESN approach was tested on three different test systems, however actual applications in real-life sized power systems; it is important re-evaluate the scalability of the approach and optimizes the ESN structure.

In this dissertation, a method for optimal PMU placement to ensure observability for voltage stability monitoring and control during normal operating conditions and during islanding conditions has been developed. The limitation of these techniques is that it is applicable only for the case of defensive islanding of the power system. It is suggested that such a system looking at islanding in a general case be researched.

Echo state networks are one kind in the family of recurrent neural networks, similar studies with other types of advanced neural network structures such as cellular neural networks is suggested.

Voltage stability seldom happens in its pure form; in many events of catastrophic system failures leading to black-outs, the other two known types of power system stability: frequency stability and angle stability manifest in the same events. It is there desirable that the monitoring tool developed can be capable of providing frequency stability and angle stability information.

Lastly, this dissertation has focused on the stability of the physical system (power system) of the smart grid, but as was discussed in the introduction, then two main aspects of the smart grid consists of the cyber system and the physical system. Thus in order to monitor and control the stability of the smart grid, the stability of both the cyber system and physical system need to be addressed. It is suggested that further research focused on the cyber system stability be considered.

An alternative non-linear controller optimization method for training the ADHDP controller using – simulated annealing was explored while working this dissertation. The approach showed promising early results that are comparable to the actor – critic approach presented in this dissertation. The advantages of simulated annealing approach include the ability to finding the global optimum quickly, while avoiding getting trapped in local optimum points when compared with other methods of optimization. It is suggested that comparative studies to evaluate the performance of the simulated annealing algorithm and the approach of training the actor using the critic method can be made.

7.5. SUMMARY

Summary of the chapters included in this dissertation is presented, their main conclusions have been summarized and suggestions for future research have been presented.

APPENDIX A.

VOLTAGE STABILITY LOAD INDEX CALCULATION

The mathematical formulation of the Voltage Stability *L*-index (VSLI) technique used in this dissertation is derived from voltage equations of a two bus network as shown in Figure 10. Consider a line connecting two buses bus 1 and bus 2 where P_1 and Q_1 are real and reactive power injected into the line at bus 1 and P_2 and Q_2 are the real and reactive power at bus 2 as shown below. V_1 and V_2 are voltage magnitudes at bus 1 and bus 2 respectively and θ_1 and θ_2 and the corresponding voltage phase angles. The following equations can be derived:

$$P_1, Q_1, V_1 \angle \theta_1 \qquad\qquad P_2, Q_2, V_2 \angle \theta_2$$

$$r+jx$$

$$P_1, Q_1 \qquad\qquad\qquad P_2, Q_2$$
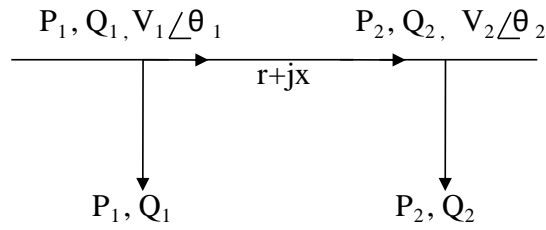
Figure 1. Two bus network

$$\left| I_1 \right|^2 = \frac{P_2^{\,2} + Q_2^{\,2}}{V_2^{\,2}} = \frac{P_1^{\,2} + Q_1^{\,2}}{V_1^{\,2}} \tag{2}$$

$$P_2 = P_1 - P_{loss} \tag{3}$$

$$Q_2 = Q_1 - Q_{loss} \tag{4}$$

$$P_{loss} = \left(\frac{P_2^{\,2} + Q_2^{\,2}}{V_2^{\,2}} \right) * r \tag{5}$$

$$Q_{loss} = \left(\frac{Q_2^{\,2} + Q_2^{\,2}}{V_2^{\,2}} \right) * x \tag{6}$$

$$|I_1|^2 = \frac{\left[P_2^2 + \left(\frac{P_2^2 + Q_2^2}{V_2}\right)r\right]^2 + \left[Q_2^2 + \left(\frac{P_2^2 + Q_2^2}{V_2}\right)x\right]^2}{V_1^2} \tag{7}$$

$$V_1^2 = V_2^2 + 2(P_2r + Q_2x) + \left(\frac{P_2^2 + Q_2^2}{V_2}\right)(r^2 + x^2) \tag{8}$$

The voltage equation can be written as:

$$V_2^4 + V_2^2[2(P_2r + Q_2x) + (P_2^2 + Q_2^2)(r^2 + x^2) = 0 \tag{9}$$

The expression is a quadratic equation in V_2^2, and has real roots when

$$8P_2Q_2rx - 4V_1^2(P_2r + Q_2x) + V_1^4 - 4(P_2^2r^2 + Q_2^2x^2) \geq 0 \tag{10}$$

Which can be simplified to:

$$\frac{4[V_1^2(P_2r + Q_2r) + (P_2r - Q_2)^2]}{V_1^2} \leq 1 \tag{11}$$

Therefore the voltage stability index is given by,

$$L = \frac{4[V_1^2(P_2r + Q_2r) + (P_2r - Q_2r)^2]}{V_1^2} \tag{12}$$

Since

$$V_1V_2\sin(\theta_1 - \theta_2) = P_2r + Q_2x \tag{13}$$

And

$$V_1 V_2 \sin(\theta_1 - \theta_2) = P_2 r - Q_2 x \qquad (14)$$

Substituting equations (14) and (15) into (13) gives:

$$VSLI = \frac{4[V_1 V_2 \cos(\theta_1 - \theta_2) - V_1^2 \cos^2(\theta_1 - \theta_2)]}{V_1^2} \qquad (15)$$

The equation for the voltage stability L-index is applied to the Thevenin equivalent circuit looking at the load bus as shown in Figure 2.

The circuit shows the system equivalent Thevenin voltage and impedance. The steps used in obtaining the Thevenin equivalent are as follows:

a) Load flow solutions are used to determine the voltage profile of the system at a given load condition

b) Thevenin voltage is obtained by load flow of the system with the load at the concerned bus removed
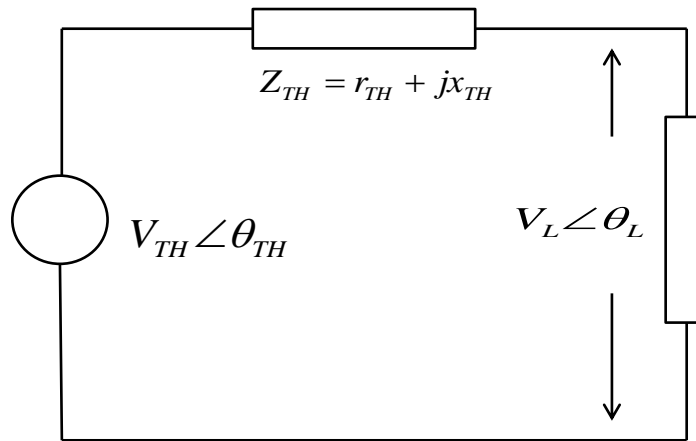
Fig. 2 Thevenin equivalent network

Applying equation (15) to the Thevenin equivalent circuit gives the equation for *L*-index as:

$$VSLI = \frac{4[V_0 V_L \cos(\theta_0 - \theta_L) - V_L^2 \cos^2(\theta_0 - \theta_L)]}{V_0^2} \tag{16}$$

APPENDIX B.

VOLTAGE STABILITY LOAD INDEX TRAINING DATA

10 Bus test system VSLI training data

Bus11P	Bus10P	Bus9P	Bus8P	Bus7P	Bus11Q	Bus10Q	Bus9Q	Bus8Q	Bus7Q	L-bus8	L-bus11
2.942	2.961	3.041	2.936	5.976	-0.8833	-0.7984	-0.8605	0.2421	-0.08654	0.63198	0.45024
2.748	2.767	2.834	2.84	5.674	-0.8985	-0.8282	-0.9477	0.1044	-0.3813	0.579398	0.428892
2.756	2.775	2.843	2.848	5.691	-0.8956	-0.8247	-0.9414	0.1148	-0.3608	0.582931	0.433251
2.685	2.704	2.768	2.808	5.576	-0.901	-0.8348	-0.9706	0.06234	-0.4662	0.563789	0.425553
3.027	3.046	3.133	3.023	6.156	-0.843	-0.7499	-0.7734	0.3628	0.1754	0.674994	0.508342
2.98	2.999	3.082	2.975	6.057	-0.8659	-0.7775	-0.8232	0.295	0.0267	0.650732	0.475479
2.942	2.961	3.041	2.936	5.976	-0.8833	-0.7984	-0.8605	0.2421	-0.08654	0.63198	0.45024
2.817	2.836	2.907	2.877	5.785	-0.8928	-0.8176	-0.9175	0.1554	-0.2761	0.598321	0.437015
2.712	2.732	2.797	2.837	5.634	-0.8916	-0.8236	-0.9504	0.09674	-0.3993	0.575412	0.439524
2.959	2.978	3.059	2.953	6.012	-0.8757	-0.7893	-0.8442	0.2654	-0.037	0.640212	0.461303
3.072	3.09	3.181	3.033	6.213	-0.8426	-0.7453	-0.754	0.3852	0.234	0.685149	0.508474
2.715	2.734	2.799	2.839	5.638	-0.8908	-0.8227	-0.9489	0.09934	-0.3941	0.5763	0.440594
2.77	2.789	2.858	2.863	5.721	-0.8904	-0.8185	-0.9304	0.1328	-0.3251	0.589069	0.440836
2.869	2.889	2.963	2.896	5.859	-0.8927	-0.8137	-0.8992	0.1849	-0.2115	0.610157	0.436744
2.685	2.704	2.768	2.808	5.576	-0.901	-0.8348	-0.9706	0.06234	-0.4662	0.563789	0.425553
2.974	2.993	3.075	2.968	6.043	-0.8689	-0.7811	-0.8296	0.2859	0.00718	0.647517	0.471142
2.871	2.89	2.965	2.898	5.863	-0.8919	-0.8128	-0.8976	0.1873	-0.2064	0.611011	0.437858
3.07	3.089	3.179	3.031	6.21	-0.8434	-0.7462	-0.7556	0.3831	0.2293	0.684396	0.507422
2.871	2.89	2.965	2.898	5.863	-0.8919	-0.8128	-0.8976	0.1873	-0.2064	0.611011	0.437858
2.959	2.978	3.059	2.953	6.012	-0.8757	-0.7893	-0.8442	0.2654	-0.037	0.640212	0.461303
2.71	2.73	2.795	2.835	5.63	-0.8923	-0.8244	-0.952	0.09412	-0.4044	0.574524	0.438456
2.866	2.885	2.959	2.893	5.852	-0.8942	-0.8155	-0.9024	0.18	-0.2216	0.608444	0.434513
2.712	2.732	2.797	2.837	5.634	-0.8916	-0.8236	-0.9504	0.09674	-0.3993	0.575412	0.439524
2.991	3.01	3.094	2.986	6.08	-0.8607	-0.7712	-0.8119	0.3106	0.06067	0.656312	0.483016
3.017	3.036	3.122	3.012	6.134	-0.8482	-0.7561	-0.7846	0.3478	0.1422	0.669616	0.501038
2.856	2.875	2.949	2.883	5.832	-0.898	-0.82	-0.9105	0.1676	-0.247	0.604142	0.428913
2.974	2.993	3.075	2.968	6.043	-0.8689	-0.7811	-0.8296	0.2859	0.00718	0.647517	0.471142
2.811	2.83	2.901	2.871	5.772	-0.895	-0.8203	-0.9223	0.1478	-0.2913	0.595718	0.433713
2.935	2.954	3.033	2.929	5.962	-0.8863	-0.802	-0.867	0.2327	-0.1065	0.628653	0.445777
3.008	3.027	3.112	3.003	6.115	-0.8526	-0.7614	-0.7942	0.3348	0.1136	0.66496	0.494723
2.952	2.971	3.052	2.946	5.998	-0.8787	-0.7929	-0.8507	0.2561	-0.05676	0.636933	0.456894
2.823	2.842	2.914	2.883	5.797	-0.8905	-0.8149	-0.9127	0.1629	-0.2609	0.600915	0.440307
2.811	2.83	2.901	2.871	5.772	-0.895	-0.8203	-0.9223	0.1478	-0.2913	0.595718	0.433713
2.914	2.933	3.01	2.907	5.917	-0.8955	-0.8131	-0.8867	0.204	-0.1667	0.618558	0.432259
2.877	2.896	2.971	2.904	5.875	-0.8897	-0.81	-0.8927	0.1947	-0.1913	0.613568	0.441191
2.858	2.877	2.951	2.885	5.836	-0.8972	-0.8191	-0.9089	0.1701	-0.2419	0.605005	0.430035
2.942	2.961	3.041	2.936	5.976	-0.8833	-0.7984	-0.8605	0.2421	-0.08654	0.63198	0.45024
2.988	3.007	3.09	2.983	6.073	-0.8622	-0.773	-0.8151	0.3062	0.05099	0.654724	0.48087
2.877	2.896	2.971	2.904	5.875	-0.8897	-0.81	-0.8927	0.1947	-0.1913	0.613568	0.441191
2.908	2.928	3.004	2.901	5.906	-0.8978	-0.8158	-0.8916	0.1968	-0.1819	0.616007	0.428849

Bus11P	Bus10P	Bus9P	Bus8P	Bus7P	Bus11Q	Bus10Q	Bus9Q	Bus8Q	Bus7Q	L-bus8	L-bus11
2.667	2.687	2.749	2.79	5.54	-0.9068	-0.8418	-0.9831	0.04084	-0.5078	0.556538	0.416857
2.809	2.828	2.899	2.869	5.768	-0.8958	-0.8212	-0.9239	0.1453	-0.2964	0.594848	0.43261
2.817	2.836	2.907	2.877	5.785	-0.8928	-0.8176	-0.9175	0.1554	-0.2761	0.598321	0.437015
2.967	2.986	3.068	2.961	6.029	-0.8719	-0.7848	-0.8361	0.2768	-0.01241	0.644282	0.466783
3.065	3.083	3.173	3.025	6.199	-0.8463	-0.7498	-0.7621	0.3748	0.2105	0.681372	0.503202
3.061	3.079	3.169	3.021	6.19	-0.8486	-0.7525	-0.7669	0.3685	0.1963	0.67909	0.500021
2.916	2.935	3.012	2.909	5.921	-0.8947	-0.8121	-0.8851	0.2065	-0.1617	0.619406	0.433393
2.766	2.785	2.853	2.859	5.712	-0.8919	-0.8203	-0.9335	0.1277	-0.3353	0.587322	0.438675
2.993	3.012	3.095	2.988	6.083	-0.86	-0.7703	-0.8103	0.3129	0.06551	0.657104	0.484087
2.991	3.01	3.094	2.986	6.08	-0.8607	-0.7712	-0.8119	0.3106	0.06067	0.656312	0.483016
2.988	3.007	3.09	2.983	6.073	-0.8622	-0.773	-0.8151	0.3062	0.05099	0.654724	0.48087
2.988	3.007	3.09	2.983	6.073	-0.8622	-0.773	-0.8151	0.3062	0.05099	0.654724	0.48087
2.693	2.713	2.777	2.817	5.594	-0.8981	-0.8314	-0.9644	0.07301	-0.4455	0.567388	0.429874
2.974	2.993	3.075	2.968	6.043	-0.8689	-0.7811	-0.8296	0.2859	0.00718	0.647517	0.471142
2.917	2.937	3.014	2.91	5.925	-0.8939	-0.8112	-0.8834	0.2089	-0.1567	0.620253	0.434525
2.756	2.775	2.843	2.848	5.691	-0.8956	-0.8247	-0.9414	0.1148	-0.3608	0.582931	0.433251
2.691	2.711	2.774	2.815	5.59	-0.8988	-0.8322	-0.9659	0.07035	-0.4507	0.56649	0.428796
3.007	3.025	3.11	3.002	6.112	-0.8533	-0.7623	-0.7958	0.3327	0.1088	0.66418	0.493666
2.717	2.736	2.801	2.841	5.642	-0.8901	-0.8218	-0.9473	0.102	-0.389	0.577187	0.441662
2.712	2.732	2.797	2.837	5.634	-0.8916	-0.8236	-0.9504	0.09674	-0.3993	0.575412	0.439524
2.969	2.988	3.07	2.963	6.033	-0.8712	-0.7838	-0.8345	0.2791	-0.00751	0.645092	0.467875
3.023	3.041	3.128	3.018	6.147	-0.8452	-0.7525	-0.7782	0.3564	0.1612	0.672696	0.50522
2.932	2.951	3.029	2.925	5.955	-0.8878	-0.8039	-0.8703	0.228	-0.1165	0.626983	0.443538
2.979	2.998	3.08	2.973	6.053	-0.8667	-0.7784	-0.8248	0.2927	0.02182	0.64993	0.474397
2.71	2.73	2.795	2.835	5.63	-0.8923	-0.8244	-0.952	0.09412	-0.4044	0.574524	0.438456
3.065	3.083	3.173	3.025	6.199	-0.8463	-0.7498	-0.7621	0.3748	0.2105	0.681372	0.503202
2.939	2.958	3.037	2.932	5.969	-0.8848	-0.8002	-0.8638	0.2374	-0.0965	0.630319	0.448012
2.972	2.991	3.073	2.966	6.04	-0.8697	-0.782	-0.8312	0.2837	0.002289	0.64671	0.470054
2.672	2.691	2.754	2.795	5.549	-0.9053	-0.84	-0.98	0.04622	-0.4973	0.558359	0.419039
3.004	3.022	3.107	2.999	6.106	-0.8548	-0.7641	-0.799	0.3283	0.09923	0.662616	0.491547
2.99	3.008	3.092	2.984	6.076	-0.8615	-0.7721	-0.8135	0.3084	0.05583	0.655518	0.481944
2.7	2.719	2.783	2.824	5.608	-0.8959	-0.8288	-0.9597	0.08096	-0.43	0.570074	0.433103
2.933	2.953	3.031	2.927	5.958	-0.8871	-0.803	-0.8687	0.2303	-0.1115	0.627819	0.444659
2.819	2.838	2.909	2.879	5.789	-0.892	-0.8167	-0.9159	0.1579	-0.271	0.599187	0.438114
2.939	2.958	3.037	2.932	5.969	-0.8848	-0.8002	-0.8638	0.2374	-0.0965	0.630319	0.448012
2.869	2.889	2.963	2.896	5.859	-0.8927	-0.8137	-0.8992	0.1849	-0.2115	0.610157	0.436744
2.875	2.894	2.969	2.902	5.871	-0.8904	-0.8109	-0.8943	0.1922	-0.1963	0.612717	0.440081
2.748	2.767	2.834	2.84	5.674	-0.8985	-0.8282	-0.9477	0.1044	-0.3813	0.579398	0.428892
2.77	2.789	2.858	2.863	5.721	-0.8904	-0.8185	-0.9304	0.1328	-0.3251	0.589069	0.440836
2.667	2.687	2.749	2.79	5.54	-0.9068	-0.8418	-0.9831	0.04084	-0.5078	0.556538	0.416857
3.058	3.076	3.165	3.018	6.184	-0.85	-0.7543	-0.7702	0.3642	0.1868	0.677562	0.497891
2.967	2.986	3.068	2.961	6.029	-0.8719	-0.7848	-0.8361	0.2768	-0.01241	0.644282	0.466783

Bus11P	Bus10P	Bus9P	Bus8P	Bus7P	Bus11Q	Bus10Q	Bus9Q	Bus8Q	Bus7Q	L-bus8	L-bus11
2.712	2.732	2.797	2.837	5.634	-0.8916	-0.8236	-0.9504	0.09674	-0.3993	0.575412	0.439524
3.058	3.076	3.165	3.018	6.184	-0.85	-0.7543	-0.7702	0.3642	0.1868	0.677562	0.497891
3.001	3.019	3.104	2.995	6.099	-0.8563	-0.7659	-0.8022	0.3239	0.08962	0.661047	0.489423
2.947	2.966	3.046	2.941	5.987	-0.881	-0.7957	-0.8556	0.2491	-0.07163	0.634462	0.453573
2.912	2.931	3.008	2.905	5.913	-0.8962	-0.814	-0.8883	0.2016	-0.1718	0.617709	0.431123
2.77	2.789	2.858	2.863	5.721	-0.8904	-0.8185	-0.9304	0.1328	-0.3251	0.589069	0.440836
2.99	3.008	3.092	2.984	6.076	-0.8615	-0.7721	-0.8135	0.3084	0.05583	0.655518	0.481944
2.762	2.781	2.849	2.855	5.704	-0.8934	-0.8221	-0.9367	0.1225	-0.3455	0.585569	0.436509
2.68	2.7	2.763	2.804	5.567	-0.9024	-0.8366	-0.9737	0.05699	-0.4765	0.561984	0.423386
2.995	3.013	3.097	2.989	6.086	-0.8592	-0.7694	-0.8086	0.3151	0.07034	0.657895	0.485157
2.971	2.989	3.071	2.965	6.036	-0.8704	-0.7829	-0.8329	0.2814	-0.00261	0.645902	0.468965
2.982	3.001	3.084	2.976	6.06	-0.8652	-0.7766	-0.8215	0.2972	0.03156	0.651532	0.47656
2.964	2.983	3.064	2.958	6.022	-0.8734	-0.7866	-0.8393	0.2723	-0.02223	0.642657	0.464595
2.875	2.894	2.969	2.902	5.871	-0.8904	-0.8109	-0.8943	0.1922	-0.1963	0.612717	0.440081
2.867	2.887	2.961	2.894	5.856	-0.8935	-0.8146	-0.9008	0.1824	-0.2165	0.609301	0.435629
3.005	3.024	3.109	3	6.109	-0.854	-0.7632	-0.7974	0.3305	0.104	0.663399	0.492607
2.817	2.836	2.907	2.877	5.785	-0.8928	-0.8176	-0.9175	0.1554	-0.2761	0.598321	0.437015
3.005	3.024	3.109	3	6.109	-0.854	-0.7632	-0.7974	0.3305	0.104	0.663399	0.492607
2.999	3.018	3.102	2.994	6.096	-0.857	-0.7668	-0.8038	0.3217	0.0848	0.660261	0.488358
3.013	3.031	3.117	3.008	6.125	-0.8504	-0.7587	-0.7894	0.3414	0.1279	0.667294	0.497887
2.928	2.947	3.026	2.921	5.947	-0.8893	-0.8057	-0.8736	0.2232	-0.1265	0.625308	0.441293
2.962	2.981	3.063	2.956	6.019	-0.8742	-0.7875	-0.841	0.27	-0.02715	0.641843	0.463499
3.064	3.082	3.172	3.024	6.196	-0.8471	-0.7507	-0.7637	0.3727	0.2057	0.680613	0.502143
2.912	2.931	3.008	2.905	5.913	-0.8962	-0.814	-0.8883	0.2016	-0.1718	0.617709	0.431123
2.68	2.7	2.763	2.804	5.567	-0.9024	-0.8366	-0.9737	0.05699	-0.4765	0.561984	0.423386
3.017	3.036	3.122	3.012	6.134	-0.8482	-0.7561	-0.7846	0.3478	0.1422	0.669616	0.501038
2.961	2.98	3.061	2.955	6.015	-0.8749	-0.7884	-0.8426	0.2677	-0.03208	0.641028	0.462402
2.858	2.877	2.951	2.885	5.836	-0.8972	-0.8191	-0.9089	0.1701	-0.2419	0.605005	0.430035
3.103	3.121	3.214	3.028	6.241	-0.8495	-0.7496	-0.7503	0.3865	0.2459	0.687768	0.49817
2.76	2.779	2.847	2.853	5.7	-0.8941	-0.8229	-0.9382	0.12	-0.3506	0.584691	0.435424
2.966	2.985	3.066	2.96	6.026	-0.8727	-0.7857	-0.8377	0.2746	-0.01732	0.64347	0.46569
2.954	2.973	3.054	2.948	6.001	-0.878	-0.792	-0.8491	0.2584	-0.05181	0.637755	0.457998
2.867	2.887	2.961	2.894	5.856	-0.8935	-0.8146	-0.9008	0.1824	-0.2165	0.609301	0.435629
2.706	2.726	2.79	2.83	5.621	-0.8937	-0.8262	-0.9551	0.08887	-0.4146	0.572747	0.436318
2.667	2.687	2.749	2.79	5.54	-0.9068	-0.8418	-0.9831	0.04084	-0.5078	0.556538	0.416857
2.877	2.896	2.971	2.904	5.875	-0.8897	-0.81	-0.8927	0.1947	-0.1913	0.613568	0.441191
2.748	2.767	2.834	2.84	5.674	-0.8985	-0.8282	-0.9477	0.1044	-0.3813	0.579398	0.428892
2.984	3.002	3.085	2.978	6.063	-0.8644	-0.7757	-0.8199	0.2995	0.03643	0.652332	0.47764
2.862	2.881	2.955	2.889	5.844	-0.8957	-0.8173	-0.9057	0.175	-0.2317	0.606727	0.432277
3.011	3.03	3.115	3.006	6.122	-0.8511	-0.7596	-0.791	0.3392	0.1232	0.666517	0.496834
2.987	3.005	3.089	2.981	6.07	-0.863	-0.7739	-0.8167	0.304	0.04614	0.653927	0.479794
2.946	2.965	3.044	2.939	5.984	-0.8817	-0.7966	-0.8572	0.2468	-0.07659	0.633636	0.452464

Bus11P	Bus10P	Bus9P	Bus8P	Bus7P	Bus11Q	Bus10Q	Bus9Q	Bus8Q	Bus7Q	L-bus8	L-bus11
3.065	3.083	3.173	3.025	6.199	-0.8463	-0.7498	-0.7621	0.3748	0.2105	0.681372	0.503202
2.772	2.791	2.86	2.865	5.725	-0.8897	-0.8177	-0.9288	0.1353	-0.32	0.589942	0.441915
3.058	3.076	3.165	3.018	6.184	-0.85	-0.7543	-0.7702	0.3642	0.1868	0.677562	0.497891
2.76	2.779	2.847	2.853	5.7	-0.8941	-0.8229	-0.9382	0.12	-0.3506	0.584691	0.435424
2.864	2.883	2.957	2.891	5.848	-0.895	-0.8164	-0.904	0.1775	-0.2267	0.607586	0.433395
2.689	2.709	2.772	2.813	5.585	-0.8995	-0.8331	-0.9675	0.06768	-0.4558	0.565591	0.427716
2.964	2.983	3.064	2.958	6.022	-0.8734	-0.7866	-0.8393	0.2723	-0.02223	0.642657	0.464595
2.748	2.767	2.834	2.84	5.674	-0.8985	-0.8282	-0.9477	0.1044	-0.3813	0.579398	0.428892
2.674	2.694	2.756	2.797	5.554	-0.9046	-0.8392	-0.9784	0.04892	-0.4921	0.559267	0.420127
2.984	3.002	3.085	2.978	6.063	-0.8644	-0.7757	-0.8199	0.2995	0.03643	0.652332	0.47764
2.856	2.875	2.949	2.883	5.832	-0.898	-0.82	-0.9105	0.1676	-0.247	0.604142	0.428913
2.969	2.988	3.07	2.963	6.033	-0.8712	-0.7838	-0.8345	0.2791	-0.00751	0.645092	0.467875
2.866	2.885	2.959	2.893	5.852	-0.8942	-0.8155	-0.9024	0.18	-0.2216	0.608444	0.434513
2.961	2.98	3.061	2.955	6.015	-0.8749	-0.7884	-0.8426	0.2677	-0.03208	0.641028	0.462402
2.667	2.687	2.749	2.79	5.54	-0.9068	-0.8418	-0.9831	0.04084	-0.5078	0.556538	0.416857
3.026	3.044	3.131	3.021	6.153	-0.8438	-0.7507	-0.775	0.3607	0.1707	0.674229	0.507303
3.002	3.021	3.105	2.997	6.103	-0.8555	-0.765	-0.8006	0.3261	0.09442	0.661832	0.490485
2.988	3.007	3.09	2.983	6.073	-0.8622	-0.773	-0.8151	0.3062	0.05099	0.654724	0.48087
3.004	3.022	3.107	2.999	6.106	-0.8548	-0.7641	-0.799	0.3283	0.09923	0.662616	0.491547
2.866	2.885	2.959	2.893	5.852	-0.8942	-0.8155	-0.9024	0.18	-0.2216	0.608444	0.434513
2.957	2.976	3.057	2.951	6.008	-0.8764	-0.7902	-0.8458	0.2631	-0.04194	0.639394	0.460203
2.947	2.966	3.046	2.941	5.987	-0.881	-0.7957	-0.8556	0.2491	-0.07163	0.634462	0.453573
2.935	2.954	3.033	2.929	5.962	-0.8863	-0.802	-0.867	0.2327	-0.1065	0.628653	0.445777

APPENDIX C.

UTILITY FUNCTION

QV SENSITIVITY ANALYSIS

Eigenvalue #	Most associate bus	Real part	Imaginary part
Eig#1	Bus67	4611.8585	0
Eig#2	Bus66	4579.6828	0
Eig#3	Bus65	4381.8966	0
Eig#4	Bus68	3982.0472	0
Eig#5	Bus35	1965.2625	0
Eig#5	Bus44	1846.6413	0
Eig#6	Bus6	1033.0611	0
Eig#7	Bus64	1013.79	0
Eig#8	Bus10	784.6738	0
Eig#10	Bus37	736.5289	0
Eig#11	Bus63	700.2959	0
Eig#12	Bus16	654.1467	0
Eig#13	Bus42	604.6813	0
Eig#14	Bus53	587.9127	0
Eig#15	Bus41	551.2881	0
Eig#16	Bus8	528.9415	0
Eig#17	Bus61	509.1374	0
Eig#18	Bus30	489.7563	0
Eig#19	Bus62	424.1716	0
Eig#20	Bus58	419.7676	0
Eig#21	Bus13	408.4726	0
Eig#22	Bus56	405.3253	0
Eig#23	Bus34	390.6953	0
Eig#24	Bus60	387.8334	0
Eig#25	Bus60	374.4689	0
Eig#26	Bus52	352.7511	0
Eig#27	Bus55	345.1241	0
Eig#28	Bus60	336.3313	0
Eig#29	Bus55	319.6573	0
Eig#30	Bus55	326.6141	0
Eig#31	Bus59	326.894	0
Eig#32	Bus31	301.9073	0
Eig#33	Bus57	300.8495	0
Eig#34	Bus59	287.3564	0
Eig#35	Bus54	275.1794	0
Eig#36	Bus45	272.0482	0
Eig#37	Bus34	253.9617	0
Eig#38	Bus3	227.0402	0

Eigenvalue #	Most associate bus	Real part	Imaginary part
Eig#39	Bus47	219.959	0
Eig#40	Bus14	216.5113	0
Eig#41	Bus26	203.493	0
Eig#42	Bus19	204.6067	0
Eig#43	Bus9	187.6103	0
Eig#44	Bus29	181.6364	0
Eig#45	Bus24	171.8244	0
Eig#46	Bus12	9.5199	0
Eig#47	Bus40	11.62	0
Eig#48	Bus49	14.6342	0
Eig#49	Bus21	145.7387	0
Eig#50	Bus4	134.1794	0
Eig#51	Bus38	132.0284	0
Eig#52	Bus50	129.8033	0
Eig#53	Bus28	19.7842	0
Eig#54	Bus44	24.8402	0
Eig#55	Bus28	29.8713	0
Eig#56	Bus43	36.7316	0
Eig#57	Bus12	40.2305	0
Eig#58	Bus12	44.7102	0
Eig#59	Bus28	50.1306	0
Eig#60	Bus20	64.3044	0
Eig#61	Bus70	65.6708	0
Eig#62	Bus15	108.0808	0
Eig#63	Bus33	102.447	0
Eig#64	Bus39	99.5449	0
Eig#65	Bus14	72.5249	0
Eig#66	Bus40	76.2263	0
Eig#67	Bus46	92.0915	0
Eig#68	Bus27	81.1111	0
Eig#69	Bus25	88.3988	0
Eig#70	Bus69	999	0

BUS PARTICIPATION FACTORS

Eigenvalue #	Bus 31	Bus 32	Bus 33	Bus 34	Bus 35	Bus 39	Bus 50
Eig#1	0.000000	0.000000	0.000000	0.000000	0.000000	0.000000	0.000000
Eig#2	0.000000	0.000000	0.000000	0.000000	0.000000	0.000000	0.000000
Eig#3	0.000000	0.000000	0.000000	0.000000	0.000000	0.000000	0.000000
Eig#4	0.000000	0.000000	0.000000	0.000000	0.000000	0.000000	0.000000
Eig#5	0.000000	0.000000	0.000040	0.003390	0.539640	0.000000	0.000000
Eig#5	0.000000	0.000000	0.000000	0.000000	0.000000	0.000090	0.000000
Eig#6	0.000000	0.000000	0.000000	0.000000	0.000000	0.000000	0.000000
Eig#7	0.000000	0.000000	0.000010	0.001870	0.000000	0.000000	0.000000
Eig#8	0.000000	0.000000	0.000000	0.000000	0.000000	0.000000	0.000000
Eig#10	0.000010	0.000050	0.000120	0.013650	0.000020	0.000000	0.000010
Eig#11	0.000000	0.027230	0.001160	0.000060	0.000000	0.000000	0.000000
Eig#12	0.000000	0.000000	0.000000	0.000000	0.000000	0.000000	0.000000
Eig#13	0.000000	0.000000	0.000000	0.000040	0.000000	0.000000	0.000040
Eig#14	0.000000	0.000000	0.000000	0.000000	0.000000	0.000000	0.000000
Eig#15	0.000010	0.000050	0.000060	0.000420	0.000000	0.000000	0.000020
Eig#16	0.000060	0.000170	0.000020	0.000020	0.000000	0.000000	0.000000
Eig#17	0.000000	0.000000	0.000000	0.000000	0.000000	0.000000	0.000000
Eig#18	0.001160	0.009230	0.001610	0.001310	0.000020	0.000000	0.000000
Eig#19	0.061480	0.000010	0.000000	0.000090	0.000000	0.000000	0.000000
Eig#20	0.000000	0.000000	0.000000	0.000010	0.000000	0.000000	0.000000
Eig#21	0.000000	0.000000	0.000000	0.000010	0.000000	0.000000	0.000000
Eig#22	0.000000	0.000010	0.000060	0.000430	0.000010	0.000000	0.000000
Eig#23	0.000120	0.008390	0.049320	0.304880	0.010280	0.000020	0.000160
Eig#24	0.000640	0.002110	0.010600	0.059760	0.001990	0.000000	0.000130
Eig#25	0.000120	0.000090	0.000460	0.002160	0.000080	0.000000	0.000000
Eig#26	0.000020	0.001340	0.001840	0.004720	0.000030	0.000010	0.028430
Eig#27	0.000080	0.000230	0.000190	0.000110	0.000010	0.000000	0.000150
Eig#28	0.037720	0.003240	0.014910	0.028380	0.001900	0.000000	0.000060
Eig#29	0.036890	0.060260	0.093180	0.046320	0.004080	0.000000	0.000560
Eig#30	0.034800	0.025120	0.048200	0.040820	0.003180	0.000000	0.001210
Eig#31	0.001160	0.000880	0.001230	0.000910	0.000070	0.000000	0.000350
Eig#32	0.251010	0.154670	0.112500	0.002240	0.000330	0.000000	0.000200
Eig#33	0.016500	0.009680	0.006910	0.000100	0.000020	0.000000	0.000010
Eig#34	0.000000	0.000000	0.000000	0.000000	0.000000	0.000000	0.000000
Eig#35	0.000230	0.000020	0.000010	0.000030	0.000010	0.000000	0.000030
Eig#36	0.028260	0.078440	0.053800	0.030750	0.026280	0.001410	0.019200
Eig#37	0.111280	0.134480	0.055340	0.174320	0.011810	0.000800	0.008620
Eig#38	0.000040	0.001610	0.000060	0.003400	0.000720	0.000010	0.000060
Eig#39	0.065750	0.034810	0.008120	0.032720	0.008180	0.000100	0.000190

Eig#40	0.001920	0.000150	0.000260	0.000000	0.000000	0.000000	0.000010
Eigenvalue#	*Bus 31*	*Bus 32*	*Bus 33*	*Bus 34*	*Bus 35*	*Bus 39*	*Bus 50*
Eig#41	0.001080	0.000420	0.000060	0.000360	0.000140	0.000000	0.000000
Eig#42	0.000000	0.000000	0.000000	0.000000	0.000000	0.000000	0.000010
Eig#43	0.036670	0.023940	0.000020	0.021210	0.014350	0.000170	0.000160
Eig#44	0.000010	0.000010	0.000000	0.000000	0.000010	0.000000	0.000010
Eig#45	0.000500	0.000230	0.000030	0.000060	0.000070	0.000000	0.000000
Eig#46	0.006120	0.001430	0.001820	0.000540	0.000050	0.000050	0.000150
Eig#47	0.024860	0.004160	0.006050	0.000850	0.000010	0.000210	0.000050
Eig#48	0.001270	0.000490	0.002250	0.000730	0.000710	0.000160	0.000520
Eig#49	0.000000	0.000000	0.000000	0.000000	0.000000	0.000000	0.000010
Eig#50	0.000050	0.000090	0.000020	0.000060	0.000010	0.000050	0.001910
Eig#51	0.037840	0.030050	0.001470	0.003590	0.026440	0.003690	0.139680
Eig#52	0.010190	0.003760	0.008680	0.018780	0.013410	0.021000	0.428510
Eig#53	0.000000	0.000050	0.000070	0.000030	0.000020	0.000030	0.000170
Eig#54	0.001840	0.006150	0.013620	0.026040	0.044720	0.047130	0.022470
Eig#55	0.000210	0.000080	0.000070	0.000010	0.000000	0.000200	0.000010
Eig#56	0.024480	0.032090	0.055210	0.043180	0.053340	0.016510	0.021610
Eig#57	0.027740	0.008410	0.007360	0.000090	0.008770	0.000810	0.059470
Eig#58	0.044360	0.028640	0.039880	0.007450	0.000370	0.000040	0.031400
Eig#59	0.000120	0.001820	0.003350	0.001770	0.000870	0.000030	0.001950
Eig#60	0.002960	0.002580	0.007120	0.008470	0.009250	0.000050	0.008010
Eig#61	0.039230	0.031630	0.082570	0.098520	0.107170	0.000790	0.090700
Eig#62	0.024190	0.020800	0.031080	0.000020	0.003020	0.000700	0.005330
Eig#63	0.045840	0.127970	0.179850	0.000130	0.025170	0.030380	0.026350
Eig#64	0.003770	0.000430	0.000110	0.001460	0.002070	0.851750	0.015400
Eig#65	0.002590	0.000210	0.000760	0.000480	0.000880	0.000030	0.000510
Eig#66	0.010380	0.000700	0.003470	0.006470	0.014490	0.000030	0.009320
Eig#67	0.004150	0.123620	0.098300	0.003980	0.064880	0.023650	0.080580
Eig#68	0.000010	0.000040	0.000030	0.000020	0.000010	0.000010	0.000000
Eig#69	0.000010	0.000050	0.000010	0.000100	0.000610	0.000080	0.000570
Eig#70	0.000000	0.000000	0.000000	0.000000	0.000000	0.000000	0.000000

Utility function design:

The objective of the adaptive dynamic programming controller developed in this dissertation is to minimize Voltage Stability Load Index (VSLI) deviations at buses 35, 39, and 50. There for the utility function is defined as:

$$U(t) = A_1 (VSLI_{35SS} - VSLI_{35}(t))^2 + A_2 (VSLI_{39SS} - VSLI_{39}(t))^2$$
$$+ A_3 (VSLI_{50SS} - VSLI_{50}(t))^2$$

The subscripts '*ss*' represent steady state values of VSLI. The coefficients A_1, A_2, and A_3 are weighting factors with a total sum of 1 such that VSLI deviations at each bus contribute to the utility function proportionally to the voltage stability sensitivity of each bus. QV sensitivity analysis of the system is performed to determine bus participation at each of three buses.

Eigenvalue #	Eigenvalue	Bus #	Participation Factor	VSLI coefficient
31	152.77	35	0.13237	0.36
36	126.34	50	0.17925	0.4
49	100.49	39	0.13543	0.24

Bus 39 has the highest Q-V sensitivity since its participation is higher in the smallest of the three eigenvalues. The second most sensitive is bus 50 then followed by bus 35. The coefficients of the utility function A_1, A_2, and A_3 are chosen to give weighting factors of VSLI values at the three buses according to take into account the eigenvalues and participation factors. The eigenvalue is multiplied by the participation factor and each coefficient is a fraction of the total of the three products.

REFERENCES

[1]   A. Y. Saber, G. K. Venayagamoorthy, "Efficient Utilization of Renewable Energy Sources by Gridable Vehicles in Cyber-Physical Energy Systems," *Systems Journal, IEEE*, vol.4, no.3, pp.285-294, Sept. 2010.

[2]   Huang, A.Q.; Crow, M.L.; Heydt, G.T.; Zheng, J.P.; Dale, S.J.;, "The Future Renewable Electric Energy Delivery and Management (FREEDM) System: The Energy Internet," *Proceedings of the IEEE*, vol.99, no.1, pp.133-148, Jan. 2011

[3]   NIST Framework and Roadmap for Smart Grid Interoperability Standards, Release 1.0.

[4]   G. K. Venayagamoorthy, "Potentials and promises of computational intelligence for smart grids," Power & Energy Society General Meeting, 2009. PES '09. IEEE, vol., no., pp.1-6, 26-30 July 2009.

[5]   K. J. Makasa, G. K. Venayagamoorthy, "Estimation of voltage stability index in a power system with Plug-in Electric Vehicles," Bulk Power System Dynamics and Control (iREP) - VIII (iREP), 2010 iREP Symposium, vol., no., pp.1-7, 1-6 Aug. 2010.

[6]   K. J. Makasa, G. K. Venayagamoorthy, "On-line voltage stability load index estimation based on PMU measurements," Power and Energy Society General Meeting, 2011 IEEE, vol., no., pp.1-6, 24-29 July 2011.

[7]   C. W. Taylor, D.C. Erickson, K.E. Martin R. E. Wilson, V. Venkatasubramanian, "WACS-Wide-Area Stability and Voltage Control System: R&D and Online Demonstration," Proceedings of the IEEE, vol.93, no.5, pp.892-906, May 2005.

[8]   P. Kundur, J. Paserba, V. Ajjarapu G. Andersson, A. Bose, C. Canizares, N. Hatziargyriou, D. Hill, A. Stankovic, C. Taylor, T. Van Cutsem, V. Vittal, "Definition and classification of power system stability IEEE/CIGRE joint task force on stability".

[9]   C. W. Taylor, "Power System Voltage Stability", EPRI Power System Engineering Series, McGraw-Hill, 1993. ISBN 0-07-063164-0.

[10]   E. Vittal, M. O'Malley, A. Keane, "A Steady-State Voltage Stability Analysis of Power Systems With High Penetrations of Wind," Power Systems, IEEE Transactions on, vol.25, no.1, pp.433-442, Feb. 2010.

[11]   Tamimi, Behnam; Canizares, Claudio; Bhattacharya, Kankar;, "Modeling and performance analysis of large solar photo-voltaic generation on voltage stability and inter-area oscillations," Power and Energy Society General Meeting, 2011 IEEE, vol., no., pp.1-6, 24-29 July 2011.

[12]   R. Kumar, "Assuring voltage stability in the smart grid," Innovative Smart Grid Technologies (ISGT), 2011 IEEE PES, vol., no., pp.1-4, 17-19 Jan. 2011.

[13]   Libao Shi; Zheng Xu; Yixin Ni; Liangzhong Yao; Bazargan, M.;, "Challenges of large wind generation intermittence and fluctuation for future smart grids," Electric Utility Deregulation and Restructuring and Power Technologies (DRPT), 2011 4th International Conference on, pp.1325-1328, 6-9 July 2011.

[14]   A. G. Phadke, J. S. Thorp, "Synchronized Phasor Measurements and Their Applications", Power Electronics and Power Systems, Springer Science + Business Media, LLC, 2008. ISBN 978-0-378-76535-8.

[15] G. K. Morison, B. Gao, P. Kundur, "Voltage Stability Analysis using Static and Dynamic Approaches", IEEE Transactions on Power Systems, Vol.8 No.3, August 1993, pp 1159-1171.

[16] O. Samuelsson, "Minicourse on Power System Stability", Industrial Electrical Engineering and Automation, Seminar 5, summer 2000, http://www.iea.lth.se/~ielolof/Stability/Seminar5.pdf.

[17] Li Wei; Wang Jian; Cai Zhiyuan; Ma Shaohua; Gong Yishan; Lu Chuan;, "An intellectualized voltage-regulator controlling load tap switch for changing primary winding tap location of power transformer," Electrical Machines and Systems, 2001. ICEMS 2001. Proceedings of the Fifth International Conference on, vol.1, no., pp.224-226 vol.1, 2001.

[18] Wijnbergen, S.; de Haan, S.W.H.; Slootweg, J.G.;, "A System for Dispersed Generator Participation in Voltage Control and Primary Frequency Control of the grid," Power Electronics Specialists Conference, 2005. PESC '05. IEEE 36th, vol., no., pp.2918-2924, 16-16 June 2005.

[19] Le Fu; Pal, B.; Cory, B.;, "Voltage regulation for primary level power networks by virtual voltage coordinated control," Power Engineering Society General Meeting, 2006.

[20] Wong, T.K., Mak, C.M., Chung, T.S., "Co-ordination of transformer tap and capacitor operation for reactive power voltage control in a distribution primary substation," International Conference on Advances in Power System Control, Operation and Management, 2000. APSCOM-00. 2000, vol.2, no., pp. 479- 485 vol.2, 30 Oct.-1 Nov. 2000.

[21] Al-Majed, S.I., "Secondary Voltage Control: Enhancing power system voltage profile," Power and Energy Conference, 2008. PECon 2008. IEEE 2nd International, vol., no., pp.1218-1221, 1-3 Dec. 2008.

[22] Corsi, S.; De Villiers, F.; Vajeth, R.;, "Power system stability increase by secondary voltage regulation applied to the South Africa transmission grid," Bulk Power System Dynamics and Control (iREP) - VIII (iREP), 2010 iREP Symposium, vol., no., pp.1-18, 1-6 Aug. 2010.

[23] Guangyue Xu; Vittal, V.; Meklin, A.; Thalman, J.E.;, "Controlled Islanding Demonstrations on the WECC System," *Power Systems, IEEE Transactions on*, vol.26, no.1, pp.334-343, Feb. 2011.

[24] Senroy, N.; Heydt, G.T.; Vittal, V.;, "Decision Tree Assisted Controlled Islanding," Power Systems, IEEE Transactions on, vol.21, no.4, pp.1790-1797, Nov. 2006.

[25] Vittal, V.; Heydt, G.T.;, "The problem of initiating controlled islanding of a large interconnected power system solved as a Pareto optimization," Power Systems Conference and Exposition, 2009. PSCE '09. IEEE/PES, vol., no., pp.1-7, 15-18 March 2009.

[26] You, H.; Vittal, V.; Xiaoming Wang;, "Slow coherency-based islanding," Power Systems, IEEE Transactions on, vol.19, no.1, pp. 483-491, Feb. 2004.

[27] Chakrabarti, S.; Kyriakides, E.;, "Optimal Placement of Phasor Measurement Units for Power System Observability," Power Systems, IEEE Transactions on, vol.23, no.3, pp.1433-1440, Aug. 2008.

[28] Mohammadi, M.; Gitizadeh, M.; Roosta, A.;, "Dynamic stability improvement of a power system incorporating DFIG wind power plant using optimized control parameters of a SVC," Power Engineering and Optimization Conference (PEDCO) Melaka, Malaysia, 2012 Ieee International, vol., no., pp.416-421, 6-7 June 2012.

[29] Ntshangase, M.; Kariuki, S.K.; Chowdhury, S.; Chowdhury, S.P.;, "Voltage stability analysis of electricity networks with DFIG-based wind power plants," Power and Energy Society General Meeting, 2012 IEEE, vol., no., pp.1-8, 22-26 July 2012.

[30] Pereira, R. M. Monteiro; Ferreira, C. M. Machado; Ferreira, C. M. Machado; Barbosa, F. P. Maciel;, "DFIG Performance Assessment during Low Voltage Ride through in the Dynamic Voltage Stability of an Electric Power System," Universities' Power Engineering Conference (UPEC), Proceedings of 2011 46th International, vol., no., pp.1-6, 5-8 Sept. 2011.

[31] P. Kundur, Power System Stability and Control, EPRI Power System Engineering Series, McGraw-Hill, 1994. ISBN 0-07-035958-X.

[32] O. Samuelsson, "Minicourse on Power System Stability", Industrial Electrical Engineering and Automation, Seminar 5, summer 2000, http://www.iea.lth.se/~ielolof/Stability/Seminar5.pdf.

[33] M. Glavic, "Power System Voltage Stability: A Short Tutorial", University of Liege, Electrical, Electronic and Computer Science Department, http://www.montefiore.ulg.ac.be/~glavic/REE-Seminar.pdf.

[34] Venayagamoorthy, G.K.;, "A successful interdisciplinary course on computational intelligence," Computational Intelligence Magazine, IEEE, vol.4, no.1, pp.14-23, February 2009.

[35] Jaeger H.; "Tutorial on training recurrent neural networks, covering BPPT, RTRL, EKF and the echo state network approach," GMD Report 159, Fraunhofer Institute AIS.

[36] Prokhorov, D.V.; Wunsch, D.C., II;, "Adaptive critic designs," Neural Networks, IEEE Transactions on, vol.8, no.5, pp.997-1007, Sep 1997.

[37] Wei Qiao; Harley, R.G.; Venayagamoorthy, G.K.;, "Coordinated Reactive Power Control of a Large Wind Farm and a STATCOM Using Heuristic Dynamic Programming," Energy Conversion, IEEE Transactions on, vol.24, no.2, pp.493-503, June 2009.

[38] G.L. Lendaris, J.C. Neidhoefer, "Guidance in the use of adaptive critics for control," in Handbook of learning and Approximate Dynamic Programming, J. Si, A.G. Barto, W.B. Powell, D.C. Wusnch II, Eds.

[39] A. K. Sinha, D. Hazarika, "A Comparative Study of Voltage Stability Indices in a Power System", International Journal of Electrical Power & Energy Systems, vol. 22, issue 8, November 2000, pp. 589-596.

[40]   M. V. Suganyadevia, C. K. Babulal, "Estimating of Loadability Margin of a Power System by Comparing Voltage Stability Indices", International Conference on Control, Automation, Communication and Energy Conservation, INCACEC, 4-6 June 2009, pp. 1 – 4.

[41]   J. Hongjie, Y. Xiaodan, Y. Yixin.: "An Improved Voltage Stability Index and its Application", International Journal of Electrical Power & Energy Systems, vol. 27, Issue 8, October 2005, pp. 567-574.

[42]   P. Mitra, G. K. Venayagamoorthy, "Wide area Control for Improving Stability of a Power System with Plug-in Electric Vehicles", IET Proceedings Generation Transmission and Distribution [In press].

[43]   Momoh, J.A.; Yan Xia; Boswell, G.; "Voltage stability enhancement using Phasor Measurement Unit (PMU) technology," Power Symposium, 2008. NAPS '08. 40th North American, vol., no., pp.1-6, 28-30 Sept. 2008.

[44]   Chakrabarti, S.; Kyriakides, E.;, "Optimal Placement of Phasor Measurement Units for Power System Observability," Power Systems, IEEE Transactions on, vol.23, no.3, pp.1433-1440, Aug. 2008.

[45]   T. K. Rahman, G. B. Jasmon, "A New Technique for Voltage Stability Analysis in a Power System and Improved Loadflow Algorithm for Distribution Network", Proceedings of 1995 International Conference on Energy Management and Power Delivery, 1995. EMPD '95, Vol. 2, pp. 71 4 – 719.

[46]   http://www.faculty.iu-bremen.de/hjaeger/pubs/ESNTutorial.pdf.

[47]   T. K. Rahman, G. B. Jasmon, "A New Technique for Voltage Stability Analysis in a Power System and Improved Loadflow Algorithm for Distribution Network", Proceedings of 1995 International Conference on Energy Management and Power Delivery, 1995. EMPD '95, Vol. 2, pp. 71 4 – 719.

[48]   Y. Kataoka, M. Watanabe, S. Iwamoto, "A New Voltage Stability Index Considering Voltage Limits", Proceedings of the Power Systems Conference and Exposition, PSCE '06, Atlanta, GA, USA.

[49]   Milosevic, B.; Begovic, M.;, "Voltage-stability protection and control using a wide-area network of phasor measurements," Power Systems, IEEE Transactions on, vol.18, no.1, pp. 121- 127, Feb 2003.

[50]   Zhou, D.Q.; Annakkage, U.D.; Rajapakse, A.D.;, "Online Monitoring of Voltage Stability Margin Using an Artificial Neural Network," Power Systems, IEEE Transactions on, vol.25, no.3, pp.1566-1574, Aug. 2010.

[51]   Milosevic, B.; Begovic, M.;, "Voltage-stability protection and control using a wide-area network of phasor measurements," Power Systems, IEEE Transactions on, vol.18, no.1, pp. 121- 127, Feb 2003.

[52]   Wenxin Liu; Li Liu; Cartes, D.A.; "Slow Coherency and Angle Modulated Particle Swarm Optimization Based Islanding of Large Scale Power Systems," Neural Networks, 2007. IJCNN 2007. International Joint Conference on, vol., no., pp.2087-2092, 12-17 Aug. 2007.

[53]   Liu, W; Liu, L; Cartes, D.A.;, "Angle Modulated Particle Swarm Optimization Based Defensive Islanding of Large Scale Power Systems," Power Engineering Society Conference and Exposition in Africa, 2007. PowerAfrica '07. IEEE, vol., no., pp.1-8, 16-20 July 2007.

[54]   Chakrabarti, S.; Venayagamoorthy, G.K.; Kyriakides, E.; "PMU placement for power system observability using binary particle swarm optimization," Power Engineering Conference, 2008. AUPEC '08. Australasian Universities, vol., no., pp.1-5, 14-17 Dec. 2008.

[55]   You Haibo V. Vittal, Yang Zhong, "Self-healing in power systems: an approach using islanding and rate of frequency decline-based load shedding," Power Systems, IEEE Transactions on, vol.18, no.1, pp. 174- 181, Feb 2003.

[56]   Nezam-Sarmadi, S.A.; Nouri-Zadeh, S.; Ranjbar, A.M.; Pishvaie, M.R.;, "An Islanding Algorithm to Restore a PMU Installed Power System," Power and Energy Engineering Conference (APPEEC), 2010 Asia-Pacific, vol., no., pp.1-4, 28-31 March 2010.

[57]   Kodsi, S.K., Canizares C.A.;"Modeling and Simulation of IEEE 14 bus System with FACTS Controllers", Technical Report #2003-3.

[58]   Lopes, J.A.P.; Soares, F.J.; Almeida, P.M.R.;, "Integration of Electric Vehicles in the Electric Power System," Proceedings of the IEEE, vol.99, no.1, pp.168-183, Jan. 2011.

[59]   Nguyen, M.H.; Saha, T.K.;, "Dynamic simulation for wind farm in a large power system," Power Engineering Conference, 2008. AUPEC '08. Australasian Universities, vol., no., pp.1-6, 14-17 Dec. 2008.

[60]   Zhou, D.Q., Annakkage, U.D., Rajapakse, A.D., "Online Monitoring of Voltage Stability Margin Using an Artificial Neural Network," Power Systems, IEEE Transactions on, vol.25, no.3, pp.1566-1574, Aug. 2010.

[61]   Podmore, R.; Robinson, M.R.;, "The Role of Simulators for Smart Grid Development," Smart Grid, IEEE Transactions on, vol.1, no.2, pp.205-212, Sept. 2010.

[62]   Kayikci, M.; Milanovic, J.V.;, "Reactive Power Control Strategies for DFIG-Based Plants," Energy Conversion, IEEE Transactions on, vol.22, no.2, pp.389-396, June 2007.

[63]   S. Sahari, A. F. Abidin, T. K. Rahman, "Development of Artificial Neural Network for Voltage Stability Monitoring", Proceedings of the 2003 Power Engineering Conference, PECon.

[64]   V. G. Gudise, G. K. Venayagamoorthy, "Comparison of Particle Swarm Optimization and Backpropagation as Training Algorithms for Neural Networks", Proceedings of the 2003 IEEE Swarm Intelligence Symposium, 24-26 April 2003, pp. 110 – 117.

[65]   Tare R. S., Bijwe.P. R.: "A new index for voltage stability monitoring and enhancement", International Journal of Electrical Power & Energy Systems, Volume 20, Issue 5, June 1998, Pages 45-351.

[66]   Kamalasadan S., Thukaram D., A.K. Srivastava, "A new intelligent algorithm for online voltage stability assessment and monitoring", International Journal of Electrical Power & Energy Systems, Volume 31, Issues 2-3, February-March 2009, Pages 100-110.

[67]   del Valle, Y.; Venayagamoorthy, G.K.; Mohagheghi, S.; Hernandez, J.-C.; Harley, R.G.;, "Particle Swarm Optimization: Basic Concepts, Variants and Applications in Power Systems," Evolutionary Computation, IEEE Transactions on, vol.12, no.2, pp.171-195, April 2008.

[68]   Y. del Valle, G.K. Venayagamoorthy, S. Mohagheghi, J.C. Hernandez, R.G. Harley, "Particle Swarm Optimization: Basic Concepts, Variants and Applications in Power Systems," Evolutionary Computation, IEEE Transactions on, vol.12, no.2, pp.171-195, April 2008.

[69]   Mathur, R., Varma, R., "Thyristor-Based FACTS Controllers for Electrical Transmission Systems". vol., no., pp.495.

[70]   Ray, S.; Venayagamoorthy, G.K.; Chaudhuri, B.; Majumder, R.; "Comparison of Adaptive Critic-Based and Classical Wide-Area Controllers for Power Systems," Systems, Man, and Cybernetics, Part B: Cybernetics, IEEE Transactions on, vol.38, no.4, pp.1002-1007, Aug. 2008.

[71]   Kanchanaharuthai, A.; Chankong, V.; Loparo, K.;, "Transient stability and voltage regulation in power systems with renewable distributed energy resources," Energytech, 2011 IEEE, vol., no., pp.1-6, 25-26 May 2011.

[72]   Tare R. S., Bijwe.P. R.: "A new index for voltage stability monitoring and enhancement", International Journal of Electrical Power & Energy Systems, Volume 20, Issue 5, June 1998, Pages 45-351.

[73]   Mohagheghi, S.; Jung-Wook Park; Harley, R.G.; Venayagamoorthy, G.K.;, "Adaptive critic design based neurocontroller for a STATCOM connected to a power system," Industry Applications Conference, 2003. 38th IAS Annual Meeting. Conference Record of the, vol.2, pp. 749- 754 vol.2, 12-16 Oct. 2003.

[74]   Mohagheghi, S.; Venayagamoorthy, G.K.; Harley, R.G.;, "Adaptive Critic Design Based Neuro-Fuzzy Controller for a Static Compensator in a Multimachine Power System," Power Systems, IEEE Transactions on, vol.21, no.4, pp.1744-1754, Nov. 2006.

[75]   Sancha, J.L.; Fernandez, J.L.; Cortes, A.; Abarca, J.T.;, "Secondary voltage control: analysis, solutions and simulation results for the Spanish transmission system," Power Systems, IEEE Transactions on, vol.11, no.2, pp.630-638, May 1996.

[76]   Popovic, D.S.; Calovic, M.S.; Levi, V.A.; "Voltage reactive security analysis in power systems with automatic secondary voltage control," Generation, Transmission and Distribution, IEE Proceedings, vol.141, no.3, pp.177-183, May 1994.

[77]   Sancha, J.L., Fernandez, J.L.; Cortes, A.; Abarca, J.T., "Secondary voltage control: analysis, solutions and simulation results for the Spanish transmission system," Power Industry Computer Application Conference, 1995. Conference Proceedings, 1995 IEEE, vol., no., pp.27-32, 7-12 May 1995.

[78]   Ranjit Kumar, A.B.; Ipakchi, A.; Brandwajn, V.; El-Sharkawi, M.; Cauley, G.;, "Neural networks for dynamic security assessment of large-scale power systems: requirements overview," Neural Networks to Power Systems, 1991., Proceedings of the First International Forum on Applications of, vol., no., pp.65-71, 23-26 Jul 1991.

[79]   Fei-Yue Wang, Huaguang Zhang, and Derong Liu.; "Adaptive Dynamic Programming: An Introduction." IEEE Computational Intelligence Magazine 4.2, pp 39-47, May 2009.

[80]   Mohagheghi, S.; Yamille, Del Valle; Venayagamoorthy, G. K.; Harley, Ronald G.: "A Proportional-Integrator Type Adaptive Critic Design-Based Neurocontroller for a Static Compensator in a Multimachine Power System." IEEE Transactions on Industrial Electronics vol.54, no. 1, pp 86-96, February 2007.

VITA

Kangombe Joseph Makasa was born September 12, 1975 in Zambia. He received his Bachelor of Engineering degree in Electrical Engineering from the University of Zambia in 2001, and his Master of Science degree in Electrical Engineering from the University of KwaZulu-Natal in South Africa in 2007. He received his PhD degree in Electrical Engineering in December 2015 from the Missouri University of Science and Technology.

Mr. Makasa worked for the Midcontinent Independent System Operator (MISO) in Carmel, IN as an EMS/SCADA Engineer from July 2012 to date. In his past employment he worked as a System Engineer for Eskom Generation in South Africa from February 2007 to July 2009 and as an Electrical Engineer-in-Training for Zambia Sugar PLC from January 2002 to February 2004.